Analytical and numerical approaches to modelling severe plastic deformation

Alexei Vinogradov[1] and Yuri Estrin[2,3,4] *

[1]Department of Mechanical and Industrial Engineering, Norwegian University of Science and Technology - NTNU, 7491 Trondheim, Norway

[2]Department of Materials Science and Engineering, Monash University, Clayton VIC3800, Australia

[3]Department of Mechanical Engineering, The University of Western Australia, Nedlands WA 6009, Australia

[4]Laboratory of Hybrid Nanostructured Materials, NUST "MISIS", 119049 Moscow, Russia

Severe plastic deformation (SPD) has established itself as a potent means of producing bulk ultrafine grained and nanostructured materials. It has given rise to burgeoning research that has become an integral part of the present day materials science. This research has received a broad coverage in literature, and several recent publications (including reviews in *Progress in Materials Science*) provide a very good introduction to the history, the current status, and the potential applications of SPD technologies. There is one aspect of SPD-related research, though, which despite its great importance has not been covered by any substantive review, *viz.* the modelling and simulation work. Due to the complexity of SPD processing and the specificity of material behaviour at the extremely large strains involved, analytical and computational studies have been indispensable for process design, parameter optimisation, and the prediction of the microstructures and properties of the ultrafine grained materials produced. They have also provided a better understanding of the physical mechanisms underlying SPD and the mechanical response of the materials that underwent this kind of processing. The pertinent literature is vast and often difficult to navigate. The present article addresses this aspect of SPD and provides a commented exposé of a modelling and numerical simulation toolkit that has been, or can potentially be, applied in the context of severe plastic deformation.

Keywords: severe plastic deformation; modelling; dislocation kinetics; finite element methods

* Corresponding author, E-mail: yuri.estrin@monash.edu

Contents

1. Introduction

Deformation-induced microstructure refinement down to submicron range has come to the fore in the past decades as a promising strategy for design of novel metallic materials with superior properties. A group of materials processing methods, which enable such extreme microstructure refinement by virtue of plastic deformation to very large strains hardly achievable with traditional metal forming operations, are commonly referred to as *severe plastic deformation* (SPD) techniques [1]. Not only do these techniques give rise to a radical improvement of the properties of metals and alloys by producing microstructures with exceptionally small grain size, but they also provide an interesting test bed for validation of models for large strains. Details of the SPD processing methods, the microstructures they produce, and the ensuing properties of the processed materials can be found in several comprehensive surveys [1-4]. The complexity of the physical mechanisms underlying the microstructure development under severe plastic deformation and the large number of the processing parameters that may affect this development and the ensuing properties of the processed materials make it necessary to rely on mathematical modelling of SPD. Given the relatively young age of the area of SPD technologies, the literature on the modelling of SPD processes is astonishingly vast and sometimes difficult to navigate. With the diversity of the arsenal of modelling approaches available for numerical simulation of severe plastic deformation in mind, we would like to take the reader on a 'guided tour' through this extensive literature. The relative advantages and weaknesses of the various modelling techniques will be considered and commented on. By no means do we see this overview as a collection of juxtaposed modelling tools for a numerical simulation practitioner. It is rather intended as an informative introduction for researchers embarking on modelling of SPD, while also providing in-depth insights into the matter for the more experienced readers.

SPD techniques, which go back to the pioneering work by Bridgman [5], combine severe shear deformation with high hydrostatic pressure, which is now known to lead to extreme grain refinement,

down to a deep submicron range. The importance of grain size as a pre-eminent characteristic of the microstructure has long been recognized [1, 4, 6, 7]. Pronounced strengthening achievable through grain refinement is commonly associated with the well-known Hall–Petch relation whose origin has been reviewed on many occasions. A recent comprehensive review by Armstrong [8, 9] and a new physical re-interpretation of this relation by Langer [10] are particularly noteworthy. Originally employed to describe the empirical scaling of the yield stress with the inverse square root of the average grain size of iron-based materials, this relation has provided a general framework for many strengthening strategies employing the increasing fraction of grain boundaries as a core element in both a 'top-down' and a 'bottom-up' approach to synthesis of novel materials [11-14]. It has also served as a touchstone in testing the soundness of models devised to rationalise the grain size dependence of the mechanical response of polycrystalline materials [15-19].

Grain refinement is undoubtedly pivotal to the enhanced mechanical performance of SPD manufactured material [1, 2, 4, 9], and understanding the various mechanisms that may give rise to the Hall-Petch relation is a formidable task. The abundance of grain boundaries in ultrafine-grained (UFG) materials is certainly one of the key features defining their mechanical behaviour, and such mechanisms as the formation of dislocation pile-ups [20] or the activation of Frank-Read dislocation sources at grain boundaries [21, 22] do give rise to the Hall-Petch relation. Such *direct* grain boundary strengthening mechanisms are not sole contributors to strength of UFG materials, though. Indirect effects entering the flow stress through the influence of grain boundaries on the dislocation density evolution (dislocation hardening) [4, 23] can be equally significant, if not even more important. This has been demonstrated in numerous publications, see e.g. [24-31]. Recently Starink [32] has re-visited this subject and summarised the findings by showing that in many SPD processed metals and alloys the dislocation strengthening is the predominant strengthening mechanism and that it gives rise to the same kind of Hall-Petch dependence, $\sigma \sim d^{-1/2}$ (where σ is the flow stress and d is the average grain size), as the direct grain

boundary strengthening. Hence, the description of strain hardening of SPD-processed ultrafine grained materials can be based on the time proven modelling approaches involving dislocation density evolution.

Although extraordinarily high strains are imparted onto a workpiece during SPD processing, the overall behaviour of the material can still be described in terms of the general laws of solid mechanics and the theory of plasticity. In a recent essay, Osakada [33] presented an overview of plasticity in relation to the analysis of metal forming. McDowell [34] also reviewed the research trends in metal plasticity in a historical retrospective. He highlighted two transformational trends which have moved and developed the subject in new directions in the not-so-remote past: (i) the use of potent high resolution characterisation tools capable of measuring attributes of microstructures directly related to plastic flow (such as crystallographic orientation and misorientation between adjacent domains, grain/phase size and shape distribution, dislocation density, etc.), and (ii) development of computational modelling and simulation tools that address inelastic deformation phenomena over a broad range of length scales - from the atomistic to the macroscopic ones. A historical overview of one of the most popular severe plastic deformation techniques, high pressure torsion, from its inception in the work by Bridgman [5] to the late 1980s was published by Edalati et al. [35].

Metal plasticity is fundamentally associated with nucleation, migration and interaction of a broad variety of crystal lattice defects with different dimensionality, such as vacancies, dislocations, grain or interphase boundaries, as well as voids and pores. With dislocations being the principal carriers of plasticity in most cases, the dislocation theory constitutes a basis for understanding the evolution of microstructure during plastic flow. The classical treatises written by such nestors of the dislocation theory as A. Cottrell, T. Mura, J.P. Hirth, J. Lothe, J. Friedel, and F.N.R. Nabarro [36-40] provide an in-depth introduction to dislocations. Contemporary work based on discrete dislocation dynamics

addresses the issue of dislocation structure formation and evolution more directly, utilising the basics of dislocation theory in a sophisticated computational framework (cf. [41]).

The picture of plasticity drawn schematically in Figure 1 is very multifaceted and requires viewing from various angles and at different length scales. So do modelling and computational simulations, as demonstrated convincingly in the "Handbook of Materials Modeling" edited by S. Yip [42]. A good introduction to the key theoretical concepts underlying multiscale modelling of materials from atomistic simulations to continuum mechanics and thermodynamics was presented by Tadmor and Miller [43, 44]. Models represented in Figure 1 operate at various length scales and microstructure levels. They involve dynamics of individual atoms (as described by *ab-initio* quantum mechanics and molecular dynamics [45-47]), linear elasticity based theory of discrete dislocations [48, 49] and disclinations [50]. Dislocations may form pile-ups at the boundaries [38] or organise themselves into spatially ordered patterns or substructures [41, 51-54] within individual grains, heterogeneous flow of aggregates of crystallites (polycrystal plasticity [55, 56]), and, finally, collective effects at large scale (macroscopic theory of plasticity [57, 58]). At an intermediate scale of continuously distributed dislocation density, dislocation patterning was considered in terms of the reaction-diffusion approach [54, 59-64].

Ideally, research into the mechanical behaviour of solids should be done by progressing from left to right in Figure 1, a model at a smaller scale informing that at the next level of the length-scale hierarchy. In practice, however, this 'hand-shake' of the models does not necessarily occur, as historically the models targeting the various scales were developed independently from each other and mostly in the opposite direction – from right to left. Current efforts are focused on multiscale modelling bridging different length scales with their distinctly different and often disparate 'languages'. Early approaches to multiscale modelling were presented in [65-67]. Excellent, more recent accounts of

computational modelling incorporating different length scales in plasticity offer a comprehensive picture of the state-of-the-art in this area [41, 68-78].

Although theories at larger length scales attempt to subjugate the smaller scale phenomena into 'effective' properties or 'constitutive rules,' macroscopic phenomena associated with large strains ultimately depend on the details of smaller scale processes. The number of degrees of freedom associated with a mathematical description at each scale decreases for the same volume of material as one progresses from left to right in Figure 1. This reduction of the number of the degrees of freedom for a given material volume with ascending level of hierarchy is a fundamental goal of multiscale modelling. Information necessary to calibrate model parameters can flow bottom–up, top–down, or in both directions. An alternative approach is the so called concurrent multiscale modelling, which is the opposite of the hierarchical one in that a larger length scale model does not subjugate a smaller scale one [71, 79]. Rather, the models (commonly just two of them) are treated in parallel and bridging occurs by using matching procedures in some overlapping domain [71]. In this way, some length scales may be skipped and, for example, continuum level simulations can be coupled directly to the atomistic scale ones. Another useful concept is quasi-continuous modelling, in which atomistic simulations are carried out in a region of interest, which is embedded in a medium modelled as a continuum [80]. A most up-to-date summary of multiscale materials modelling defining the model taxonomy and outlining the conceptual and computational challenges can be found in [81].

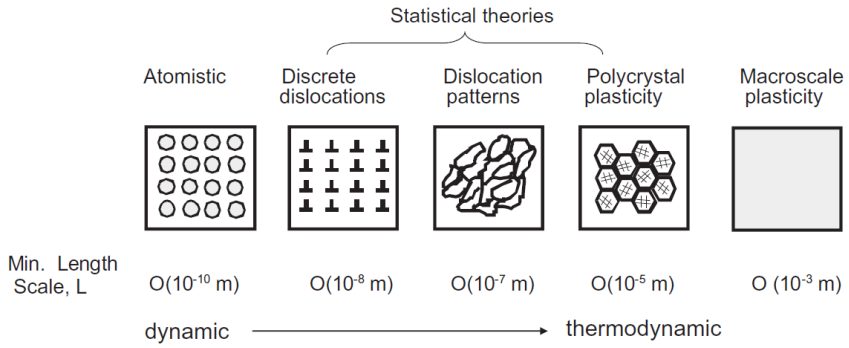

Figure 1. Hierarchy of length scales in metal plasticity ranging from atomic (dislocation cores) to dislocation patterns to multiple grains to macroscopic scale. A major gap in multiscale modelling and simulation lies between the scales of atomistic simulations and dislocation pattern modelling. Attempts to close this gap by discrete dislocation simulations play an increasingly greater role but phenomenological statistical theories are still predominant (from [34], reproduced with permission).

Representing the top of the hierarchical pyramid, solid mechanics is the most popular instrument for obtaining both analytical and numerical solutions for the mechanical behaviour of a workpiece subjected to SPD processing. Solid mechanics nowadays is a mature theory comprising the governing physical laws, sets of computational techniques, and numerical methods for virtually all scales shown in Figure 1 that can be used to predict the response of a solid to mechanical loading. Fundamentals of solid mechanics can be found in many excellent textbooks, e.g. [56, 82-86], systematically covering all aspects of modern approaches from theoretical background and basic mathematical principles to practical implementation of finite element codes.

Choosing the right modelling approach, which determines the governing equations to describe the material behaviour under specific loading conditions, is crucial for setting up a solid mechanics calculation. The toolbox developed in solid mechanics includes a variety of conceptual models with specific applications listed below, and this is by no means an exhaustive list.

1. Linear elasticity [87] is an important tool for describing small deformations of a polycrystalline material subjected to loads that are much smaller than the material's macroscopic yield stress, e.g. during very high cycle fatigue. Mechanics of elasticity is of crucial significance for the theory of defects

such as dislocations or disclinations in solids [88]. Despite its fundamental importance, it is often neglected in simulations of metal forming and large deformations at macroscopic scale [89]. It is, however, an appreciated instrument in discrete dislocation dynamics simulations owing to the applicability of the elasticity theory to describing the dislocation stress and strain fields outside of the dislocation core.

2. Viscoelastic models [90], which include the Maxwell model, the Kelvin-Voigt model, and the Standard Linear Solid Model, are widely used to predict the response of materials that exhibit both viscous and elastic behaviour under different loading conditions. Elastic and viscous components are represented by linear combinations of springs and dashpots, respectively. Depending on the arrangements of these elements resulting in different rheological equations, these models have enabled a description of the behaviour of materials under creep or stress relaxation conditions. Such models are well suited for materials which exhibit a strongly rate dependent behaviour and are therefore most widely used in simulation of the mechanical response of polymers. For example, Zaïri et al. [91] have calculated the plastic response of a polymer during equal channel angular pressing at room temperature with different extrusion velocities, friction conditions and die geometry. This group of models has limited applicability to metals and will not be considered in the present review. Interested readers are referred to [90].

3. Rate independent plasticity represents a wide class of models describing the deformation response of solids loaded above their yield point up to large strains. The simplest model is that of a rigid elastic-perfectly plastic solid that deforms elastically at stresses below the yield point and then flows plastically at a constant stress if a constant strain rate is applied. An elastic-perfectly plastic solid thus exhibits a sharp transition from perfectly elastic to perfectly plastic deformation when the yield stress is reached. Such models are often used to calculate the forces on tools in metal forming, for example during equal channel angular pressing (ECAP) or high pressure torsion (HPT), cf. [92]. More realistic

models involve strain hardening in some way [93]. The models of this kind are used in simulation of plasticity at large strains and of low cycle fatigue behaviour under fairly large strain amplitudes. Finally, the most sophisticated plasticity models attempt to track the microstructure development in the plastically deforming metal. This group of models are popular in metal forming simulations, particularly simulations of SPD, as will be discussed in the next sections.

4. Viscoplasticity is similar in structure to rate independent plasticity, but it accounts for the strain rate dependence of the flow stress, which commonly tends to increase with increasing strain rate, particularly under dynamic loading [94]. For example, Anand [95] developed a model for the elastic–viscoplastic response of ductile single crystals deforming by crystallographic slip. Numerical simulation of the deformation response of face centred cubic (FCC) polycrystalline materials was conducted by assigning a finite element to each crystallite under the assumption of initially isotropic crystallographic texture. The simulation results were shown to be in good agreement with experiment on copper. This refers both to the strain hardening behaviour, which was found to be anisotropic, and to the evolution of crystallographic texture. An example illustrating an excellent agreement between experimental observations of texture evolution during deformation to large strains by simple shear and theoretical predictions [96] provided by the self-consistent viscoplastic polycrystal plasticity model backed by a dislocation density based strain hardening model is shown in Figure 2. The details of these modelling efforts will be considered in the following sections.

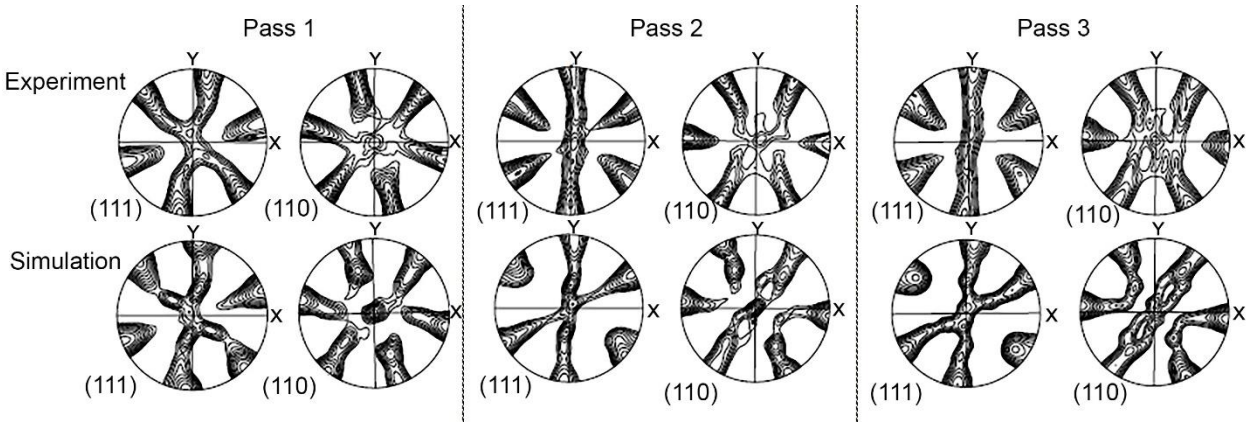

Figure 2. Comparison of simulated crystallographic texture for simple shear during ECAP processing of pure copper to different numbers of passes (from 1 to 3) via Route A assuming no rotation of the billet between the passes (adapted from [96], reproduced with permission).

In their finite element computations, Acharya and Beaudoin [97] predicted grain size dependent strain hardening behaviour of FCC and BCC polycrystals at relatively small strains of 2–30% by applying a viscoplasticity model (see also [98, 99]). At the individual grain level, isotropic Voce-type hardening was assumed. To account for the material's resistance to plastic flow, lattice incompatibility associated with the presence of lattice dislocations was introduced in a continuum description. Although the constitutive model for dislocation density evolution did not include the grain size explicitly, its effect on the plastic flow was considered by analysing the results of modelling of the mechanical response of FCC nickel and BCC HY-100 steel. An inverse relationship between the flow stress and the grain diameter was found. The predicted strain hardening behaviour of polycrystalline nickel with a grain size below 100 μm agreed well with the experimental data of Narutani and Takamura [100]. A transition to Stage IV hardening following saturation of the Voce-type response inherent in Stage III hardening was found to be governed by a build-up of crystal lattice incompatibility due to dislocation storage. This constitutive model was further extended to include temperature and strain rate effects [101, 102].

7. The crystal plasticity method has evolved recently as a framework integrating the extensive knowledge gained from experimental and theoretical studies of single crystal deformation, atomistic fundamentals of dislocations, and continuum mechanics of deforming solids. In crystal plasticity models, this knowledge of the physics of the deformation processes at different length scales [69, 103] is incorporated in the computational tools of continuum mechanics [84, 85, 104]. This approach was reviewed by Roters et al. [78] in a comprehensive monograph dedicated to diverse aspects of the plastic behaviour of crystalline solids. Crystal plasticity starts with a premise that crystals are mechanically anisotropic and therefore the instantaneous and time-dependent deformation of crystalline aggregates is an innately non-homogeneous process, which depends on the direction of the mechanical loads and geometrical constraints imposed. Macroscopically directional properties of a polycrystal arise when the orientation distribution of the grains, which is commonly characterised by crystallographic texture, is non-random. Quantitative prediction of crystallographic texture evolution during SPD that would account for concurrent grain refinement is therefore one of the major tasks for crystal plasticity implementations in simulations of SPD processes [94, 105, 106]. Most current models of texture evolution under severe plastic deformation do not consider this continual variation of the grain population – with some exceptions ([107, 108]) that will be discussed below.

8. Strain Gradient Plasticity is a kind of hybrid approach motivated by advances in dislocation mechanics since the 1990s. Classical plasticity theories do not account for non-local effects and fail to predict strain localisation or deformation microstructures with a distinct pattern of spatially arranged dislocations with a well-defined length scale [109]. Unlike conventional constitutive models, strain gradient plasticity is capable of accounting for non-local effects on the deformation behaviour and strength of polycrystalline aggregates [17, 110, 111]. The approach by Fleck and Hutchinson [112, 113] has advanced the concept in which an explicit distinction is made between dislocations stored during uniform straining (statistically stored dislocations) and those necessitated by gradients of strain. The

latter are referred to as geometrically-necessary dislocations (GNDs) first introduced by Nye [114]. GNDs develop from inhomogeneities of plastic flow due to loading conditions, texture, second phases, etc. to accommodate lattice misorientations. A main drawback of most strain gradient plasticity theories is that the so-called *internal length scale* entering gradient plasticity formulations is vaguely defined. Being introduced as a phenomenological variable, it serves as a 'free' parameter that is to be determined from experimental data by appropriate fitting procedures. Numerous attempts to establish a relationship between the internal length scale and the microstructure were reviewed by Zhang and Aifantis [115]. In the studies referenced therein, this parameter has been associated with the dislocation source length, average dislocation spacing, size of pile-ups at grain boundaries or interfaces, grain size, width of slip zones, or specimen size. Despite all efforts, the physical origin of the internal length scale is still a matter of debate, however.

9. Discrete Dislocation Plasticity (DDP) is a theory originating from the recognition that plastic flow in crystalline metals arises primarily from the collective motion of large numbers of dislocations. It emerged as a computational technique tracking the nucleation, motion and annihilation of individual dislocations interacting with each other in a solid under load [41, 48, 52, 116-119].

10. Atomistic models are seeing a booming development owing to a rise in the available computation power on one hand and the advancement of fundamental quantum-mechanical concepts enabling *ab-initio* calculations of realistic interatomic potentials and elastic constants on the other hand. In this approach phenomenological stress-strain relations are replaced with a direct calculation of the stress-strain response using atomic scale simulations. A most recent example of such fully dynamic atomistic simulations of single-crystal plasticity was provided by Zepeda-Ruiz et al. [120] for a specific case of a BCC metal tantalum. Macroscopic stress-strain curves were calculated from these atomistic simulations directly, avoiding multiscale modelling.

In what follows, we shall give an overview of the available modelling techniques – both analytical and numerical. On that basis we shall discuss the salient results they have delivered and eventually single out the approaches that in our view are most suitable in the context of modelling of severe plastic deformation.

2. Modelling severe plastic deformation

Great expectations are being put in achieving superior mechanical properties of bulk nanostructured and ultrafine-grained materials manufactured by SPD. Despite a steady growth of the research area of SPD and the promise it offers, an overly cautious attitude towards this group of processing techniques prevailed in metal forming industry until recently. Various barriers on the way of SPD processing from laboratory to shop floor include real technological challenges, such as the need for upscaling the processes and making them continuous or semi-continuous. Some examples of processing routes of this kind, which promise successful transfer to industry scale manufacturing [121-125] were given in the recent reviews [1, 4, 126].

Regardless of the specifics of the processing schedule used, the microstructures and the mechanical properties of the deformed materials are governed by the degree of plastic deformation (although not by it alone). Therefore, understanding the stress and strain development in a workpiece is pivotal for efficient and sound SPD process design. The primary factors governing the efficacy of SPD processing for microstructure refinement have long been understood and highlighted in many publications. In the case of ECAP, which is illustrated schematically in Figure 3, these include the die channel shape and dimensions, the angle between the entrance and exit channels, the inner and outer corner radii, the coefficient of friction, the strain path (or processing route), and the processing parameters, such as back pressure, ram speed, and temperature. The intrinsic material properties of the billet have, of course, a decisive influence on the processability by ECAP and the ensuing material

properties, as well. The significance of all these process and material variables cannot be overestimated. A huge body of experimental data was summarised in recent reviews [4, 126, 127]. Medeiros et al. [128] performed a variance analysis based on the central composite factorial design to quantify the relevance of processing parameters to the ECAP load and the effective plastic strain. From the statistical analysis of variance (ANOVA), the ECAP parameters affecting the load the most can be ranked in the following order of importance: (1) the coefficient of friction, (2) the die channel angle, (3) the outer fillet radius, (4) the inner fillet radius, and (5) the ram velocity. Also, with regard to the equivalent plastic strain the ranked order of significance of the affecting parameters was determined to be as follows: (1) the die channel angle, (2) the inner fillet radius, and (3) the outer fillet radius. However, despite substantial efforts none of the experimental research aiming at characterising the processing factors and their roles in the properties of a final product can claim to be comprehensive. As a matter of fact, the assessment of all these factors in their entirety requires enormous experimental efforts. Indeed, if one were to limit oneself to just the most important factors and to aim at characterising the effect of, say, two channel shapes, two different cross-section sizes, five different friction conditions (corresponding, for example, to different lubricants, the quality of the die wall machining, or the die design), five different materials, four most common strain paths (A, B, C and Bc, see [2] for the definition of the ECAP routes), three different pressing velocities, three levels of back pressure, and three different temperatures, one would need to perform over 10,000 pressings followed by microstructure characterisation and mechanical testing. Therefore, the use of modelling tools in either mechanistic analytical formulations, cf. [129-133], or finite element analysis [84-86, 134] is indispensable for optimisation of the processing schemes and conditions for a given material in a cost- and time-effective way. Of course, the mathematical models discussed in the previous section, particularly the analytical models, provide useful insights in the deformation behaviour. However, while providing the analytically tractable and elegant solutions, these models commonly oversimplify the processing conditions and provide estimates of *average*

equivalent strains across the workpiece. As such, they do not account for strain and stress inhomogeneity, which inevitably occurs during SPD processing. Therefore, the analytical solutions are not capable of simulating a real SPD process in sufficient detail. Nowadays, it is the finite element method (FEM) based modelling that plays a crucial role in understanding, critical assessment and optimisation of the existing SPD processes, visualisation of strain distributions across the sample, and prediction of the mechanical properties of the processed material. They are also invaluable in developing new SPD processes by enabling virtual process simulations prior to committing to the use of expensive tooling and machinery.

In this section we look at the ways in which FEM was applied to the simulations of an archetypal SPD process – equal channel angular pressing (Figure 3) – arguably the most commonly used technique in the context of SPD processing. Further SPD methods will be considered in subsequent sections, particularly in Section 5.

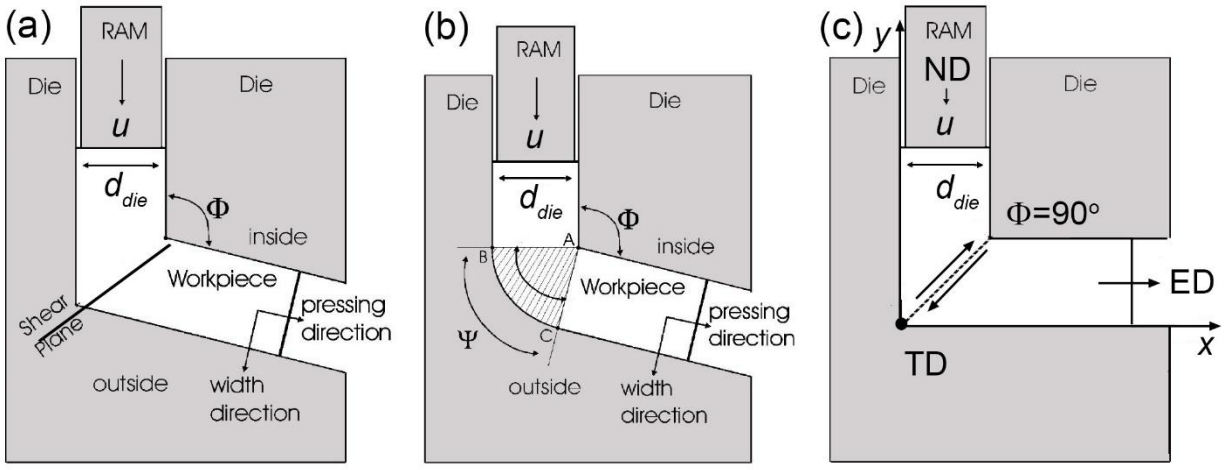

Figure 3. Schematic illustration of ECAP showing the channel angle Φ and the corner angle Ψ: (a) corner angle Ψ = 0, (b) corner angle Ψ > 0 and (c) Φ =90° , ED, TD and ND denote extrusion, transverse and normal directions , respectively (Adapted from [135], reproduced with permission)

2.1 Estimates of equivalent strain during ECAP

Various analytical calculations [131, 136-142] and numerical finite element simulations were used for modelling and prediction of strains induced by ECAP. The models differ in the die geometry represented in Figure 3, incorporation of frictional effects, and the techniques used to calculate the strain distribution. Sharp corner dies, dies with an external arc of curvature, and round corner dies are some of the various geometries employed for ECAP. In the dies with an external arc of curvature, the centre of curvature is located at the inner corner of the die. The round corner dies have a fillet at the outer corner whose centre of curvature does not lie at the inner corner. Detailed understanding of the kinematics of deformation and the effects the die geometry plays in it is crucial for rationalising the basic mechanisms that control the grain refinement in the ECAP process. Eivani and Taheri [141, 142] presented the upper-bound solution in which both the friction conditions and the nonlinear strain hardening behaviour were considered for a die geometry where only the outer die had a corner curvature. The consideration of nonlinear strain hardening of the material in the calculations of the ECAP pressure, assuming a frictionless condition, with an outer die corner curvature, was first proposed by Alkorta and Gil Sevillano [137]. Their analytical solution was based upon the upper bound theorem and provided a good agreement with numerical predictions determined from a plane-strain finite element model. Paydar et al. [138] also exploited the upper bound approach to analyse the equal channel angular pressing with circular cross-sections of the die and the billet. The expressions for the total dissipated power and the applied pressure required for processing were established by considering velocity discontinuities and non-zero friction at all surfaces. The model developed predicted an increase in size of the deformation zone with increasing friction, similar to Segal's original model [131]. In a series of publications Pérez and Luri [140, 143-148] obtained theoretical expressions for the shear strain accounting for all the possible die configurations and including the friction effects for perfectly plastic materials. Aiming at optimisation of the die geometry, these authors showed a gain close to 11% in the

equivalent plastic strain per pass when the inner radius was 2.67 times larger than the fillet radius of the outer die. They also demonstrated that an increase of the inner fillet radius led to a greater equivalent plastic strain and higher pressure levels. Building on the recognition that an extended arc curvature has a detrimental effect on strain homogeneity in the workpiece during ECAP, Şimşir et al. [149] performed an upper bound analysis by FEM and showed that the process performance in terms of the magnitude and uniformity of strain can be improved by modifying the shape of the die corner.

Segal [129, 150, 151] was the first to exploit a widely known slip line field theory for solutions of the boundary value problems in mechanics of ECAP. The slip line kinematic approach simplifies the governing equations for plastic solids by making several restrictive assumptions including [83]: (1) plane-strain deformation, (2) quasi-static loading, (3) isothermal conditions, (4) absence of body forces, and (5) idealisation of the material as a rigid-ideally plastic von Mises solid whose mechanical properties are characterised by the yield stress in uniaxial tension. With these assumptions Segal obtained slip line field solutions for different ECAP die geometries and friction conditions. For a simple die with sharp corners and an angle Φ between the channels, Figure 3a, the von Mises equivalent strain ε_{eq} imposed onto a billet per each ECAP pass is given by [129]

$$\varepsilon_{eq} = \frac{2}{\sqrt{3}} cot\left(\frac{\Phi}{2}\right) \tag{1}$$

In the case of a die with a round outer corner geometry, Figure 3b, which owes its great popularity to the simplicity of design and manufacture, the strain is given by the following relation proposed by Iwahashi et al. for the frictionless conditions [152]

$$\varepsilon_{eq} = \frac{1}{\sqrt{3}}\left[2cot\left(\frac{\Phi}{2}+\frac{\Psi}{2}\right)+\Psi cosec\left(\frac{\Phi}{2}+\frac{\Psi}{2}\right)\right] \tag{2}$$

Goforth et al. [153] proposed an alternative formula for the equivalent plastic strain:

$$\varepsilon_{eq} = \frac{1}{\sqrt{3}}\left[2cot\left(\frac{\Phi}{2}+\frac{\Psi}{2}\right)+\Psi\right] \quad (3)$$

Alkorta and Gil Sevillano [137] derived the same expression in the upper bound approximation for the frictionless die with a curved outer corner, while Milind and Date [154] arrived at Eq. (3) using a kinematics based approach. Aida et al. [155] reconciled the latter two equations and showed that both yield the same results at the upper and the lower bounds for the arc angle $\Psi = \Phi - \pi$ and $\Psi = 0$, respectively, and that they differ by less than 5% under all other conditions for the channel angle Φ equal to or exceeding 90˚. Segal's slip line model assumes that plastic flow in simple shear deformation in the 90° sharp corner dies is confined to the plane of intersection between the channels. To avoid this limitation, Tóth et al. [105, 156] developed an analytical flow line model which they applied – with considerable success - to calculating texture evolution under ECAP [96]. In this model a flow line is described by the following equation:

$$\left(d_{die}-x\right)^{n_{fl}}+\left(d_{die}-y\right)^{n_{fl}}=\left(d_{die}-x_0\right)^{n_{fl}} \quad (4)$$

where d_{die} is the diameter of the die, x_0 denotes the current position on the flow line, and n_{fl} is a free parameter describing the flow line shape in Cartesian (x, y) coordinates corresponding to the rectangular die as illustrated schematically in Figure 3c. The condition $n_{fl}=2$ defines an idealised circular flow line; higher n_{fl} values approximate well the flow pattern arising under different friction conditions; in the limiting case of $n_{fl}\to\infty$, the flow line is simply represented by two straight intercepts connected at the shear plane of the die, as in Segal's model. The experimentally observed flow patterns can be approximated by the proposed model very well, as shown in Figure 4. A generalised expression for the equivalent von Mises strain per ECAP pass in the $\Phi = 90^o$ die derived from the model reads

$$\varepsilon_{eq} = \frac{2}{\sqrt{3}} \frac{\pi\left(n_{fl} - 1\right)}{n_{fl}^2 \sin\left(\pi / n_{fl}\right)} \tag{5}$$

This equation yields the same total strain, $\varepsilon_{eq} = 2/\sqrt{3}$, as Segal' model for the limit case of $n_{fl} \to \infty$. Equation (5) implies that the accumulated strain is uniform across a section of the die, provided n_{fl} is constant. The latter assumption is quite restrictive and does not have general validity. The flow line model proposed by Tóth et al. predicts a varying deformation field along the flow line in good agreement with FE simulations [156]. Using a large 50×50 mm^2 ECAP die set-up, Panigrahi et al. [157] demonstrated experimentally that the flow line exponent n_{fl} increases significantly and almost linearly from about 6 at the top to about 20 at the bottom side of a billet. This behaviour of n_{fl} reflects the occurrence of a strain gradient in the extended plastic deformation zone, Figure 4. Using the experimentally determined n_{fl} values, the flow line model [156] correctly predicts the distribution of texture components in a billet's cross-section from top to bottom. A further generalisation of this analytical model was provided by Hasani et al. [158], who considered the elliptical modification of the flow line equation, Eq. (4), and used it for modelling the plastic flow and texture evolution in the *nonequa*l channel angular pressing, in which process the exit channel has smaller dimensions than the entrance channel.

Motivated by the same desire to avoid the simplistic representation of the ECAP process as sharply localised shear and to account for inhomogeneity of plastic flow in a spread plastic deformation zone, Beyerlein and Tomé [159] proposed another form of analytical solutions for the strain and velocity gradients tensors as functions of the position in the die and deformation time for three typical deformation situations, including ideal localised simple shear, a central fan-shaped plastic deformation zone, and a central deformation fan combined with an outer region of rigid rotation. Not only is this

analytical model capable of successfully describing texture evolution in the multipass ECAP processing, but it also enables a thorough analysis of the deformation kinematics.

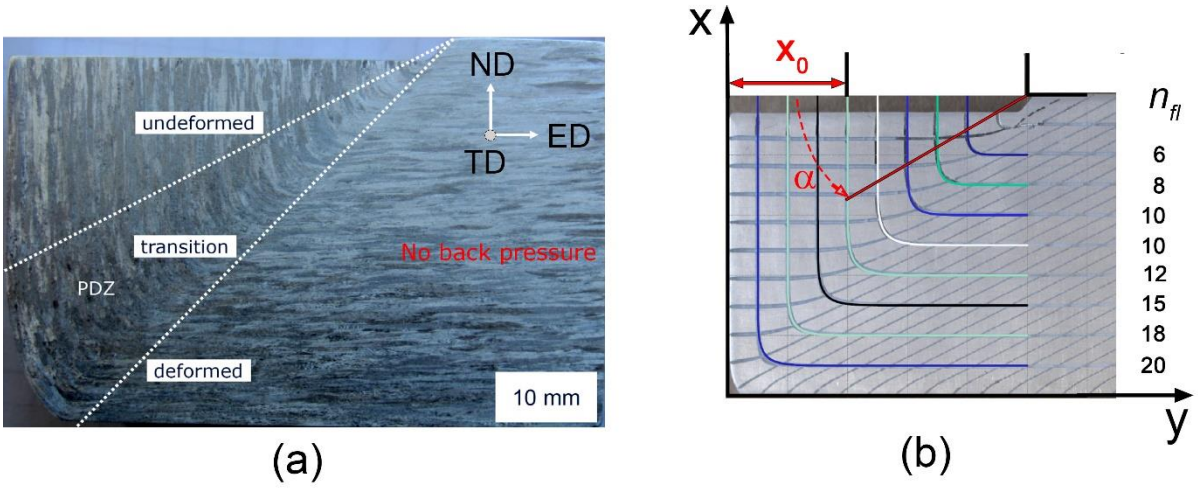

Figure 4. Flow pattern in a cross-section of commercially pure aluminum AA 1050 billet deformed by ECAP (a). Etching reveals a fan-shaped plastic deformation zone (PDZ) between undeformed and deformed parts in the entrance and exit channels, respectively. The experimentally observed flow lines on the TD plane are shown in (b); the flow line shape parameter n_{fl} entering the model due to Tóth et al. [156] calculated for individual flow lines is shown on the right. (Adapted from [157], reprinted with permission).

Analytical modelling was also used to describe HPT processing. The approach goes back to Bridgman [35, 160, 161] who, in an idealised way, expressed the velocity field in the specimen (which is independent of the torsion angle of the anvil, β) as

$$V_z = V_r = 0, \quad V_\theta = \frac{r\omega z}{H} \tag{6}$$

with ω the angular velocity, and the von Mises equivalent strain as

$$\varepsilon_{eq} = \frac{r\beta}{\sqrt{3}H} \tag{7}$$

In the cylindrical coordinate system (r, θ, z) used, r is the distance from the specimen axis; H denotes the specimen thickness [162, 163]. This type of kinematic model was also used by Khoddam et al. [132]. Beygelzimer et al. [164] provided a strict mathematical analysis to identify conditions under which the simplified description given by the above equations is valid. Their conclusion was that in the rigid plastic formulation, a power-law hardening in a rotation angle interval would lead to self-similar regimes of HPT

if the friction with the lateral wall of the die is not too high. In such an interval, the above mathematical description holds. Outside of this interval they break down, and the plasticity problem needs to be solved for each value of β. This is an important message that should be considered in calculations of the HPT process.

It should be noted that it is customary in the SPD community to use the von Mises equivalent strain as a measure of strain, as was also done in deriving the above equations. The ongoing discussion in literature on whether it is the von Mises or the Hencky strain [165, 166] that provides the appropriate measure of deformation involving simple shear, of which SPD processes are typical examples, was reviewed in a recent publication [167]. Based on group theory analysis, it was demonstrated that the Hencky equivalent strain does not satisfy group theory properties for simple shear, while the von Mises equivalent strain does. This analysis provides a theoretical underpinning for the use of the von Mises platform, which is adopted here.

2.2 Constitutive modelling approaches to simulations of ECAP

As was emphasised above, the microstructure and the concomitant mechanical properties of SPD-manufactured materials show a strong dependence not only on the amount of plastic strain imparted to the material but also on the strain path. This is particularly the case for multi-step processing schedules where the results depend on the sequence of strain increments associated with the processing steps. Substantial modelling efforts have been invested in understanding the strain development during various SPD processes.

ECAP has received most attention in finite element modelling, which has finally led from laboratory investigations to technologically relevant ideas of possible upscaling of SPD techniques, and we shall dwell on this process in some detail. When a rectangular workpiece is subjected to ECAP under isothermal conditions with ideal lubrication, the strain along the direction normal to the flow plane is

zero, i.e. plane strain deformation dominates the plastic flow. This justifies a two-dimensional treatment of plastic strain distribution over a rectangular billet during ECAP as a first approximation [168]. Owing to its simplicity, 2D finite element modelling enjoys the greatest popularity even though the significance of boundary conditions at the side walls is admittedly disregarded in the 2D approach. Experimental arguments in favour of nearly isothermal condition during ECAP at low processing speed were provided by Yamaguchi et al. [169, 170] and Berbon et al. [171], at least for the relatively slow ram velocity of 0.18 mm/s. An essential input in any FEM simulation that strongly influences the results is a constitutive model specifying the response of the material to an applied stress under given conditions, i.e. a functional dependence of the flow stress on strain and further variables such as strain rate $\dot{\varepsilon}$ and temperature T, $\sigma = \sigma(\varepsilon, \dot{\varepsilon}, T)$. For this purpose, when strain hardening is considered, a Ludwik type dependence of the flow stress σ on plastic strain ε_{pl} is assumed, most commonly in the form:

$$\sigma = K\varepsilon_{pl}^{n} \tag{8}$$

where K and n are material parameters, which may generally be strain rate and temperature dependent and are supposed to be known from a set of experiments, e.g. from uniaxial tensile tests performed at different strain rates and temperatures. A variant of this constitutive equation, which takes into account the strain rate dependence of stress in a power-law form, is the Ludwik-Hollomon equation

$$\sigma = K\varepsilon_{pl}^{n}\dot{\varepsilon}_{pl}^{m^*} \tag{9}$$

Here the exponent m^* characterises the strain rate sensitivity of the flow stress and may be temperature dependent. Obviously, the validity of the Ludwik or the Ludwik-Hollomon equation implies continual increase of stress with strain. Assuming a Ludwik type strain hardening, the Considère instability criterion predicts the onset of strain localisation (necking) at a critical strain $\varepsilon_n = n$ under uniaxial tensile deformation. An excellent critical review on plastic strain localisation in materials has

been provided recently by Antolovich and Armstrong [172] with the focus on the influence of the microstructure on different scales and loading conditions – temperature and strain rate – on the strain hardening behaviour and the appearance of plastic instabilities. The onset of necking limits the validity of Eq. (8) to a relatively small strain range below the necking point. Although this type of strain hardening law is rather common in solid mechanics, it does not apply to large deformations where the stress tends to saturate or even drops with strain. For example, after several ECAP passes the microhardness (and thus the strength) tends to saturate [136, 173, 174] or exhibits a maximum and then decreases slightly with increasing strain [175, 176]. This apparent breakdown of the Ludwik-Hollomon power law may be corrected by using an alternative constitutive law first proposed by Voce [177] as an empirical relation between stress σ and plastic strain ε_{pl} (cf. also [178-180]):

$$\frac{\sigma(\varepsilon_{pl})-\sigma_s}{\sigma_y-\sigma_s}=exp\left(-\frac{\varepsilon_{pl}}{\varepsilon_c}\right) \tag{10}$$

where σ_y is the yield stress and ε_c is the quantity that characterises the rate of variation of stress with strain towards its saturation level σ_s. The corresponding strain hardening rate $h=\partial\sigma/\partial\varepsilon$ is expressed as:

$$h=h_0\left(1-\frac{\sigma}{\sigma_s}\right) \tag{11}$$

providing a linear stress dependence of the strain hardening rate. Here $h_0=\sigma_s/\varepsilon_c$ is the strain hardening rate extrapolated to zero stress. It is commonly associated with Stage II hardening. Mecking and Lücke [181], Kocks [182] and Mecking [183] derived such a linear relation for the tensile stress-strain curves of FCC metals by considering the dislocation density evolution. Possible extensions of this approach to large strains are discussed in the review paper by Kocks and Mecking [184]; see also [58] for an in-depth discussion of the constitutive strain hardening behaviour at large strains. Unlike the Ludwik-Hollomon equation, Eq. (10) does account for stress saturation with increasing strain. For this reason, it

has been widely used in mechanistic descriptions of large strain deformation. Chinh et al. [185, 186] employed the Voce equation to describe the strain hardening behaviour in ECAP-processed aluminium over a broad range of testing temperatures, including both the region of plasticity controlled by thermally activated dislocation glide at low temperatures and the diffusion-controlled plasticity regime at high temperatures. In an attempt to fit the experimental data, they proposed a different type of the constitutive law in the form of

$$\sigma = \sigma_0 + \sigma_1 \exp\left(-\frac{\varepsilon_{pl}^n}{\varepsilon_c}\right) \tag{12}$$

where σ_0 , σ_1 , ε_c and the exponent *n* are constants which may be used to fit the experimental data. Equation (12) fulfils the various requirements on the σ vs. ε_{pl} relation, as it reduces to the Voce-type equation when *n*=1 and its Taylor expansion at small strains gives an equation of the form $\sigma = \sigma_0 + K\varepsilon_{pl}^n$, which is identical with the Ludwik equation, Eq. (8). The relation expressed by Eq. (8) is purely phenomenological. Its deficiency is a lack of an explicit or implicit relation with the microstructure and dislocation structure evolution. Being convenient as a mathematical description of the strain hardening behaviour of materials, it is often used in FEM codes. However, it is neither capable of describing different stages of strain hardening nor can it be easily justified for both small and large strain ranges.

In 1997, Prangnell et al. performed the first 2D plain strain FEM simulation of the ECAP process [187] emphasising the significance of friction for the kinematics of plastic flow in the dies with different channel geometries. Friction is undoubtedly of great importance in general metal forming and that is why it is routinely included in modern FEM codes [188]. Figure 5 illustrates the flow patterns predicted by 2D FEM for different frictional conditions and die configurations. Nearly ideal simple shear was predicted in well-lubricated conditions with low friction, whilst non-uniform shearing and a dead-metal

zone caused by high friction levels in a simple (static) die was found. These computational results are in fair agreement with experiments performed by Segal and co-workers [150, 151, 189]. The role of friction in SPD processing was highlighted in many publications [139, 190-199]. The significance of friction for ECAP processing was also confirmed by 3D FEM simulations [200].

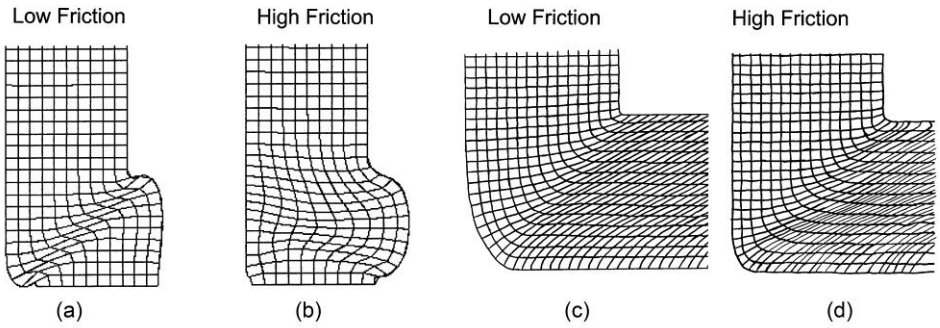

Figure 5. Illustration of the flow patterns predicted by 2D FEM for different frictional conditions and die configurations: (a),(c) well-controlled shearing facilitated by extremely low friction or a sliding exit channel floor; and (b),(d) inefficient, nonuniform shearing and a dead-metal zone caused by high friction levels in a simple (static) die. (Here a and b were adapted from [190] and c and d from [196] (reproduced with permission))

As seen in Figure 3, the channel geometry can be varied by using different values of the channel angle [201, 202], or the outer corner angle [139, 192, 193, 198, 203-205], or both [137, 194, 206, 207]. The shape of the entry channel can also be made different from that of the exit channel (thus deviating from pure ECAP) [208, 209]. The vast majority of FEM simulations were carried out with a view to assess the influence of the die geometry, process conditions, and the intrinsic properties of the billet material on strain distribution in the ECAP-processed billets. For instance, in a suit of publications Nagasekhar and co-authors investigated the influence of tool angles, strain hardening behaviour of the material (adopting the Ludwik-Hollomon model) and friction between the billet and die (adopting the Coulomb friction law) in 2D plane strain simulations with elastic-plastic material properties of aluminium alloy AA1100 [204] and 3D simulations for copper [210] for conventional ECAP as well as ECAP with specific channel shapes, such as V-shape [211], T-shape [212] and X-shape die configurations [213]. The effect

of the type of the friction model - Coulomb vs. shear friction - in numerical analysis of the ECAP process was considered by Balasundar and Raghu [214]. They demonstrated that the shear friction is preferable in FEM codes because the predictions of this model are closer to experimentally observed deformation pattern and strain distribution across the processed billet.

With friction taken into account, it was shown in particular that an optimum in strain homogeneity in the sample with a lesser propensity for dead zone formation can be achieved, without any detrimental side effects, for the channel angle $\Phi = 90°$ and the outer corner angle $\Psi = 10°$, cf. also [215-217]. A typical simulated flow pattern and the equivalent stress distribution in the deformation zone of the billet passing through the die with different values of the channel angle are shown in Figure 6. As predicted by Segal [131, 151, 189] considering mechanics of a rigid-plastic body in the ECAP process, deformation is confined to a thin layer at the plane where the two channels meet. Within that layer deformation by simple shear occurs. For strain hardening materials, under the same zero friction condition, the deformation zone spreads out through an arc around the crossing plane of the channels due to the formation of a dead zone [218, 219]. When both strain hardening and friction are included, the shape of the deformation zone changes considerably. With $\Psi = 0°$ (cf. Figure 3a), the deformation zone is very wide and is no longer in the form of an arc. This strain pattern happens to be closer to the computational predictions (clearly observable with deformed mesh in Figure 5a). FEM simulations commonly show that with an increase in the outer corner angle, the arc of the deformation zone spreads as shown in Figure 6b-d [204, 215, 216, 220]. Hence, by reducing the outer corner angle a narrowing of the deformation zone can be achieved.

To raise the process efficiency and reduce the number of processing steps, ECAP tool designs with either U- or S-shape channel configuration were considered. In view of drastically increased loads, modelling is essential in assessing the viability of the proposed tool design and its optimisation [195, 201-203, 208, 220, 221].

Another factor, which has long been identified as a major one in ECAP processing and the resultant material properties, is back pressure [129, 131, 150, 222-225]. Back pressure was shown to be crucial for enabling uniform simple shear deformation [129], but it is comparatively rarely considered in numerical simulations [137, 193, 196, 197, 203, 226].

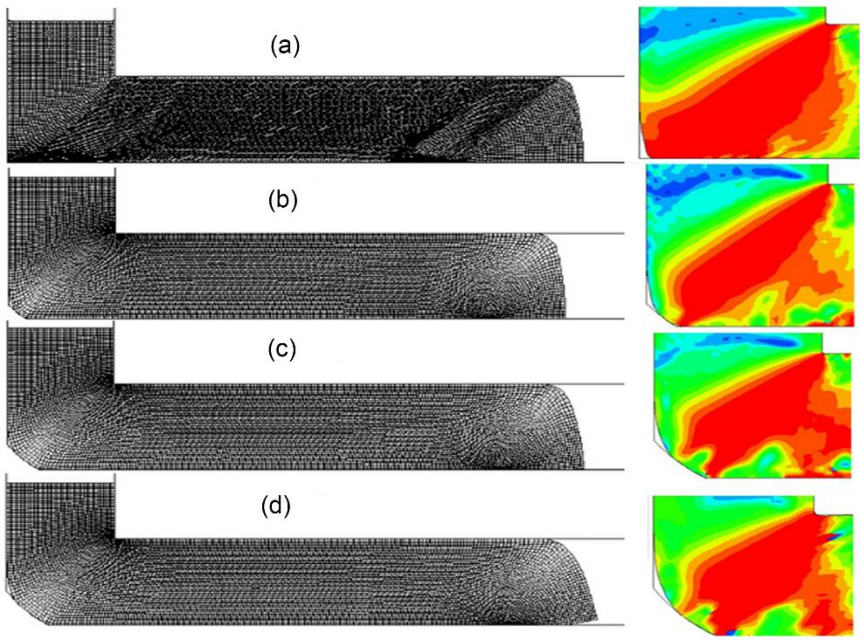

Figure 6. Results of FEM simulation showing the effect of the shape of the outer corner on the flow pattern and the equivalent von Mises stress distribution in the deformation zone. Simulation performed with **Φ=90°** and (a) **Ψ=0°,** (b) **Ψ =10°, (c) Ψ =20°, (d) Ψ =**28°. **(Adopted from [204], reproduced with permission.)**

Summarising the outcomes of numerous FEM simulations of ECAP, it can be concluded that the strain distribution in the deformed billet is strongly affected by the channel shape, tool angle, friction, and back pressure. The strain is most uniform if the deformation zone is as narrow as possible. This is best achieved with a sharp die corner and appropriate back-pressure, as was recognised in the original work by Segal et al. [129]. Using a slip line model, these authors explicitly formulated the hydrostatic pressure condition for "ideal" *simple shear* deformation with complete filling of the outer die corner, which according to them is achieved if the friction between the workpiece and the die walls is negligibly small and the operating punch pressure in the inner channel p_1 is related to the back pressure p_0

through $p_1 = p_0 + 2k\cot\Phi$, where k is the material's shear yield stress. Extending Segal's approach, Lee proposed an upper bound analytical solution taking into account friction during ECAP [227]. If a 'razor-blade thin' deformation zone is formed, the simple shear conditions assumed by Segal et al. [129] in deriving Eq. (1) prevail and the magnitude of simple shear the billet undergoes agrees well with the predicted values. In all other cases the shear strain is significantly lower than expected from Eq. (1). This is due to a partial bending of the billet, which results in the strain distribution being non-homogeneous (by up to 40% across the billet's width for a 120° die). Equation (1), therefore, corresponds to an upper bound that can only be achieved under ideal conditions. It follows from the above analysis that dies designed with a smoothed internal corner will certainly promote undesirable bending of the billet and reduce its homogeneity, as well as the overall level of shear.

2.3. Effects of heat generation

The tool temperature and the heat generation effects during SPD were considered in several simulations [135, 190, 193, 195, 197, 219, 228, 229]. DeLo and Semiatin in their early FEM analysis of ECAP evaluated the effect of friction in a systematic way. More importantly, beside considering the plastic flow behaviour of the workpiece, they accounted for the effects of preheat temperature, heat generation due to mechanical work and interfacial heat transfer between the workpiece and the die [190]. Since many engineering alloys experience flow softening under hot-working conditions and, consequently, are prone to flow localisation, the motivation to perform realistic simulations accounting for these effects is very clear and important. Consideration of heat transfer and of friction between the workpiece and the side walls of the tooling required a 3D approach to full analysis of hot ECAP. Strain rate sensitivity of the processed material was included into FEM codes for both two-dimensional and three-dimensional non-isothermal models. The heat generation resulting from deformation was computed and flow stress data were adjusted in the simulation routines accordingly. The temperature

increment ΔT in the deformation zone due to plastic deformation was calculated in a simplified way using the adiabatic approximation (see below):

$$\Delta T = \frac{\beta_T \left(\bar{\dot{\varepsilon}}\right)}{\rho_d c_v} \int \bar{\sigma} d\bar{\varepsilon} \tag{13}$$

where T is the absolute temperature, σ is the flow stress, (henceforth a superposed dot denotes time derivative and a bar refers to the average value). The material constants ρ_d and c_v are the mass density and specific heat, respectively; β_T represents the fraction of mechanical work that is converted into heat. The result of a correction for deformation heating in FE simulation is an increased amount of flow softening compared to that observed in 'uncorrected' compression data [190].

Despite the demonstrated efficacy of 3D simulations in modelling heat flow, such simulations were less successful than the 2D FEM simulations, Figure 7, in predicting overall deformation and equivalent strain contours [190], see also [135]. These difficulties of 3D FEM simulations were attributed to problems with mesh density and element behaviour highlighting the challenges in realistic FEM simulations. The simple shear deformation concentrated in a narrow band during ECAP requires a very fine mesh in the deformation zone and frequent re-meshing which can be more easily implemented in 2D FEM codes. Consequently, a much greater number of elements, memory and computation time are required for an equivalent 3D simulation. This is a technical issue, though, which does not undermine the recognition that 3D simulations are more appropriate in principle [146, 195, 198, 228, 230-232].

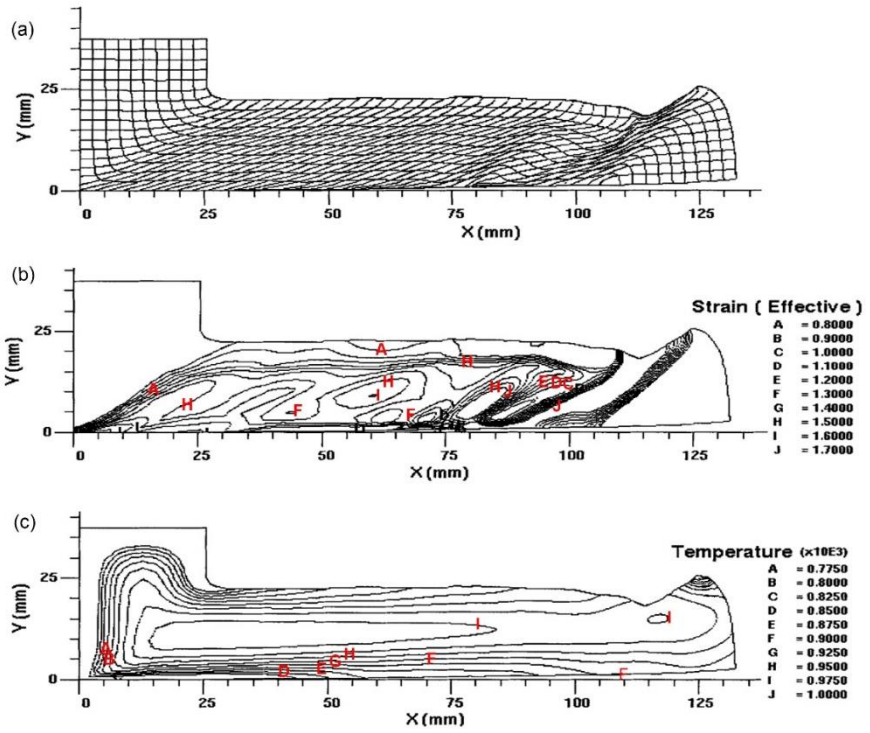

Figure 7. FEM-predicted grid distortions, temperature contours, and effective strain contours from a 2D nonisothermal ECAP simulation of Ti-6Al-4V with flow softening at 985 °C (from [190] reproduced with permission)

2.4. Strain localisation during ECAP

In the absence of heat transfer between the workpiece and tooling, which was tacitly assumed in deriving Eq. (13), the tendency to flow localisation was estimated from the flow localisation parameter α_S defined as [191]:

$$\alpha_S \equiv \frac{1}{\dot{\varepsilon}}\frac{\delta\dot{\varepsilon}}{\delta\varepsilon} = -\left\{\left(\frac{1}{\sigma}\frac{\partial\sigma}{\partial\varepsilon}\right)\Big|_{\bar{\varepsilon},T} + \left(\frac{\partial\sigma}{\partial T}\right)\Big|_{\bar{\varepsilon},\dot{\bar{\varepsilon}}}\left(\frac{1}{\sigma}\frac{dT}{d\varepsilon}\right)\right\}\left(\frac{1}{m}\right) \tag{14}$$

It was demonstrated that materials with a high degree of softening and a low strain rate sensitivity *m*, which is defined in the same sense as that in Eq. (9) as $m = \left(\partial \ln\sigma / \partial \ln\dot{\varepsilon}\right)\Big|_{\varepsilon,T}$, tend to undergo severe shear localisation. Flow localisation sets in only if α_s is positive. Semiatin et al. noted that the

development of appreciable strain localisation occurs for α_S of 3 at typical cold-working temperatures [233] or 5 at hot-working temperatures [234].

Lapovok et al. [235] studied strain localisation during ECAP in terms of a simplified power-law constitutive model by considering gradient plasticity. This was done by introducing a second-order gradient term associated with the incompatibility stresses between neighbouring grains, giving rise to the following expression for the shear stress

$$\tau\left(\gamma,\dot{\gamma}\right)=\tilde{\mu}\left(\dot{\gamma}\right)\dot{\gamma}^{m}\left(\gamma_0+\gamma\right)^{-\tilde{p}(\dot{\gamma})}-\tilde{c}\frac{\partial^2\gamma}{\partial y^2} \tag{15}$$

Here, in accordance with a gradient plasticity model due to Estrin and Mühlhaus [236], the coefficient $\tilde{c}$ was assumed to be proportional to the Young's modulus *E* and the square of the grain size *d:* $\tilde{c}=\tilde{a}Ed^2$ (where $\tilde{a}$ is a constant). The deformation dynamics was modelled using the classical continuity equation of solid mechanics:

$$\rho_d\frac{\partial u}{\partial t}=\frac{\partial\tau}{\partial\gamma} \tag{16}$$

with a shear stress gradient entering on the right-hand side and ρ_d denoting the density of the material. Linear stability analysis of the fundamental solution of Eqs.(15) and (16) with $\dot{\gamma}=\partial u/\partial y$ and $\gamma=\int_0^t\left|\dot{\gamma}\right|dt$ was performed by introducing small perturbations, in the exponential form $\delta\phi=\delta\phi_0 e^{\eta(t-t_0)}e^{i2\pi y/\lambda_w}$, of the fluctuating variables $\phi=\left(u,\gamma,\tau\right)$ at a time t_o. The wavelengths λ_w for which the growth rate η of the perturbations turns out to be positive were determined in dependence on the material properties (including grain size and strain rate sensitivity) and processing conditions (strain, strain rate, strain gradient, etc.). These wavelengths define the spatial periodicity of an emerging strain localisation pattern. The model was verified for magnesium alloy AZ31 deformed by ECAP at 250°C with different ram speeds and different back pressure values. The predicted deformation band

patterns agreed favourably with the observed ones, including such detail as the shift of the spectrum of the preferred wavelengths upon the variation of back-pressure.

Although most published FEM calculations assumed the Ludwik-Hollomon or Voce type strain hardening behaviour of a material, some simulations were also conducted under the assumption of ideal plasticity [198, 206, 208] or viscoplasticity [237]. In some hybrid models, ideal plasticity was considered as a limiting case for strain hardening [197, 221] or as a model to be compared with strain hardening ones [191, 192, 194]. Two different strain hardening curves for reversed loading (taking place for 180° billet rotation between two consecutive passes of ECAP) were used by Figueiredo et al. [238]. Three different kinds of hypothetical material stress-strain behaviour, typical of those encountered in cold and hot working, were investigated by Semiatin et al. [191]: (i) Ludwik-Hollomon type strain hardening, (ii) rigid-perfectly plastic response, and (iii) strain softening response, cf. Figure 8 where the deformation curves are shown for these three situations.

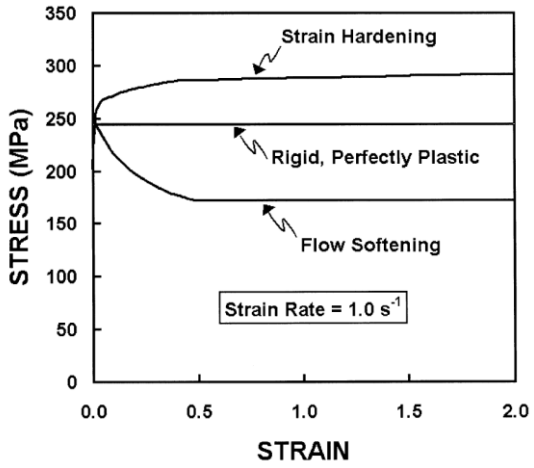

Figure 8. Deformation curves used in isothermal FEM simulations with different strain hardening models [191] (reproduced with permission).

Using similar assumptions, Kim [239] simulated plastic flow in a strain hardening material (with 1100Al taken as an exemplary case) and a nearly perfect elastic-plastic material (6061Al-T6). It was found, Figure 9a and b, that a larger corner gap is formed in the material with a higher strain hardening rate

because the softer outside part of the workpiece in the deforming region flows faster in a strain hardening material than in a non-hardening one. The results of these simulations are in good agreement with experimental data presented by Segal [189], Figure 9c and d. Besides, Kim demonstrated that the corner gap formation reduces the strain in the outside region of the workpiece, increases the strain in the inside region, and diminishes the average strain. A computational result already mentioned above and well-supported experimentally is that the strain distribution in a workpiece with a larger die corner gap becomes more non-homogeneous.

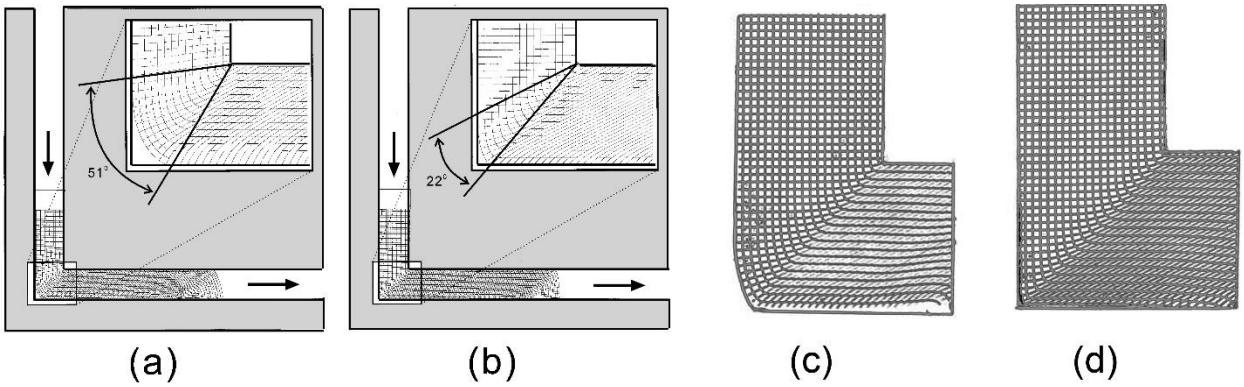

Figure 9. FEM-predicted grid distortions for (a) a strain hardening material (1100Al) and (b) a nearly perfectly plastic material (6061Al-T6) (adapted from [239], reprinted with permission). (c) and (d) represent experimental data for a Φ = 90° and Ψ =0° die showing a distortion of the coordinate grid for a strain hardening material and non- strain hardening material, respectively (adopted from Segal [189], reproduced with permission).

SPD processability of hard-to-deform materials was addressed in an experimental study accompanied with FEM modelling by Semiatin et al. [240, 241]. They investigated the deformation behaviour of commercial purity (CP) titanium (grade 2) and AISI 4340 steel during ECAP at temperatures between 25 °C and 325 °C and nominal strain rates between 0.002 and 2.0 s^{-1}. CP titanium underwent segmented failure under all conditions except at low strain rates and high temperatures, while 4340 steel deformed uniformly except at the highest temperature and greatest strain rate, at which condition it also exhibited segmented failure. CP Ti was found particularly susceptible to shear localisation during

ECAP; uniform flow occurred only at high temperatures and low strain rates. By contrast, 4340 steel exhibited uniform deformation under all conditions, apart from the high temperature and high strain rate case mentioned. Observed shear banding and shear failure were interpreted in terms of the tendency for strain concentration as quantified by the flow localisation parameter α_s introduced in Eq. (14). Viscoplastic modelling and FE simulations were applied to elucidate failure modes under non-uniform plastic flow during non-isothermal ECAP and the model predictions were found to be in good agreement with the experimental findings. Based on the understanding of the effect of material properties on the tendency for flow localisation supported by both FEM calculations and experiments, Semiatin et al. proposed countermeasures to inhibit non-uniformity of plastic flow during ECAP [240, 241]. Localised shear banding was also found by very recent FEM simulations of ECAP of AA6060 using a phenomenological constitutive model that included both isotropic and kinematic hardening [242]. The preponderant role of the latter in strain localisation under ECAP was highlighted by the authors.

Extreme grain refinement of metals usually involves multiple ECAP passes [2, 3, 126, 243]. Such processing can follow various strain paths, for which the strain hardening behaviour of the material being deformed may be different [2, 4, 129, 136, 150, 152, 244, 245]. Although accounting for plastic anisotropy is essential for accurate simulations of large plastic deformations during metal forming processes, the strain path effects are relatively rarely considered in FEM modelling [246-249]. Rather, a universal equivalent stress vs. equivalent strain curve of the material is employed for all processing steps. An example is multiple pass deformatin by route A ECAP considered by Rosochowski [203]. This approach was modified by Figueiredo et al. [238] who presented a methodology of FEM analysis for two-pass ECAP processing of copper following route C, which involves a strain reversal. The consideration of strain path effects changed the final strain distribution in the material and led to a lower ram force in the second pass compared with the results based on a universal stress–strain curve for all passes. Mahallawy et al. [237] applied a 3D rigid-viscoplastic finite element analysis to Al–Cu

alloys for ECAP following routes A and Bc. Experimental and FEM results were found to be in agreement, both showing that route A leads to greater strain homogeneity across the workpiece than route Bc. Strain localisation and tensile stresses lead to fracture, which was simulated in the works cited above [190, 191, 250]. Strain rate sensitive material models were considered by several groups [191, 217, 228, 230]. In particular, Kim et al. [220] showed that the strain rate decreases with the channel angle and the die corner angle. The magnitude of the corner angle was found to exert a much stronger effect on the strain pattern than that of the channel angle, owing to an expansion of the deformation zone and reduced deformation time caused by an increase in the corner angle.

Finite element analysis that included the Gurson model of damage was carried out by Lee et al. [251] to rationalize the densification behaviour and the elimination of residual porosity in the aluminium alloy 6061 matrix containing SiC particles by ECAP. Damage models were also included in the simulations of the ECAP processing by Lapovok [252]. The evolution of damage (porosity) in cast Al6061 alloy was successfully predicted in terms of a stress index, which represents the ratio of hydrostatic pressure to equivalent shear stress.

Simulations using models that account for microstructure in the context of FEM analysis are scarce. In reference [253], strain distribution results were used to obtain the textures developed during ECAP. A dislocation-based strain hardening model due to Tóth et al. [254, 255] was implemented in a finite element code which enabled the dislocation cell size evolution in copper to be predicted [256]. In a companion paper, texture evolution was calculated using the same modelling frame [257]. The model was also successfully used in simulations of the response to ECAP processing of Al [256] and IF steel [258]. Most recently, this model was also used for simulations of ECAP deformation of Cu and Al alongside two other dislocation-density based models [259], and the benefits of the model by Estrin et al. [255] were highlighted. Although stress and reaction forces are routinely available from FEM

simulations, only a few workers used these results to evaluate material behaviour, tool pressure, and the process force under severe plastic deformation [192, 203, 210, 217, 228, 260]. The consequent and successful use of the dislocation density based models in FE simulations of severe plastic deformation by the research group of Hyoung Seop Kim (see, for instance, [261, 262]) should be mentioned, but this is an exception rather than the rule.

As mentioned above, most of ECAP simulations used a two-dimensional model assuming plane strain, which had obvious benefits in terms of the cost of re-meshing and computational time in general. However, for billets with a circular or rectangular cross-section in situations when friction and heat effects are significant, three-dimensional simulation is more appropriate, as shown in several publications [146, 195, 198, 228, 230-232].

As the microstructure evolves and gets refined with increasing strain, conventional FEM codes face the mentioned necessity of re-meshing and the associated difficulties with precision and efficiency, especially in handling large deformations. To minimise this mesh dependency problem, the finite volume method (FVM) was proposed and used successfully, for example, in multi-pass ECAP simulations [198, 228, 230, 263]. Another problem which grows ever more challenging in the conventional computational methods such as finite element or finite volume analysis is the problem of simulation of nucleation and propagation of discontinuities such as cracks during SPD processing. In most cases, these techniques cannot handle such behaviour because of their strong reliance on the mesh. Consequently, their inherent structure is not well suited to dealing with discontinuities which do not coincide with the original mesh lines. Re-meshing in each step of the simulation to keep the mesh lines coincident with the discontinuities throughout the simulation inevitably introduces many computational problems.

A group of numerical techniques which aim at addressing the re-meshing problem in many FEM simulations is represented by the so-called mesh-free or meshless methods. A variety of these

techniques has emerged and developed to a highly matured state in the past two or three decades [264]. Originating from particle hydrodynamics and gas dynamics, they rely on the nodes (particles or points), not on lines (or meshes). The application of these methods to simulation of SPD processes is still scarce, but a few successful examples of application of a rigid-plastic/viscoplastic element free Galerkin method to simulate the plastic flow during ECAP are encouraging [265, 266]. The most popular mesh-free methods are smoothed particle hydrodynamics (SPH) [267, 268] and the material point method (MPM) [269]. Such models do not suffer from the problem of large mesh deformation and the necessity of re-meshing common to FE models in a Lagrangian framework, or the difficulty of tracing the material's history in the Eulerian formulation. Studies of ECAP processing by both SPH [270] and MPM [271] showed the efficacy of these methods and the consistency of the results obtained by the meshless techniques and the FE analysis.

From the above discussion it is evident that the shape of the deformation zone, strain homogeneity and ultimately the microstructure evolution in the deformed samples are affected by several factors. These include the intrinsic material properties, particularly strain hardening behaviour, the die design, friction, and processing parameters, such as back pressure, ram speed, and temperature. Being reasonable as a first approximation, the 2D FEM simulations assuming plain strain conditions have obvious limitations when (i) very large plastic deformations are involved, (ii) the shape of the billet is other that rectangular, (iii) friction effects are of concern, and (iv) heat effects cannot be neglected. Thus, for realistic simulations 3D FEM is the computational tool of choice [228, 272].

Because of the significance of ECAP among the SPD processing technologies, its simulations have been considered in this section at length. FEM simulations of SPD processes other than ECAP are less numerous, while being similar to those of ECAP in essence. Some of them will be considered in Section 5.

2.5. Strain rate and temperature effects during ECAP

Microstructural evolution during SPD involves a plethora of mutually interacting mechanisms, including dislocation glide, recovery by dislocation annihilation, and possibly recrystallisation and grain growth. These are chiefly thermally activated processes and, as such, they are strongly influenced by two extrinsic variables – strain rate and temperature, which are often interrelated through thermomechanical coupling. In what follows we examine the significance of these two variables in modelling of SPD processing in some detail.

Estimates for strain rate during ECAP

Berbon *et al.* [171] showed that the microstructure of pure Al and an Al-1% Mg alloy processed by ECAP is dependent on the pressing speed. There have been several attempts to estimate the strain rate using different modelling approaches. Semiatin et al. [191] evaluated the strain rate in the ECAP process by FEM modelling, though only roughly because of the coarse mesh size they used. Assuming the die geometry shown in Figure 3b, Kim [135, 220] provided simplified estimates of the average strain rate. The results were then compared with the accurate 3D FEM analysis performed in isothermal conditions corresponding to low ram velocities.

The average deformation time during ECAP can be defined in a first order approximation as the dwell time of the material within the localised deformation zone in the geometry shown in Figure 3b as:

$$\Delta t = \frac{d_{die}}{u}\frac{\Psi}{\sqrt{2}} \tag{17}$$

Medeiros et al. [273] provided a more detailed derivation of the dwell time. The resultant values for Δt they obtained are quite similar to those estimated by Kim [135], however. By combining Eq. (2) for the strain and Eq. (17) for the deformation time, a strain rate equation for ECAP is obtained:

$$\dot{\varepsilon} = \frac{1}{\sqrt{3}}\left[2cot\left(\frac{\Phi}{2}+\frac{\Psi}{2}\right)+\Psi cosec\left(\frac{\Phi}{2}+\frac{\Psi}{2}\right)\right]\frac{\sqrt{2}}{\Psi}\frac{u}{d_{die}} \tag{18}$$

The analytical calculations according to Eq. (18) were found to be in good agreement with the results of FEM modelling, as shown in Figure 10.

The analytical mechanistic approaches to deformation histories during ECAP processing developed by Tóth et al. [156] and Beyerlein and Tomé [159] are quite appealing in that they allow for explicit calculation of velocity gradients and associated strain rate tensor components. Using the flow line representation given by Eq.(4), Tóth et al. derived the following transparent expressions for the strain rate $\dot{\varepsilon}_{ij}$ components accounting for the curvature of the flow lines and the size of the die:

$$\begin{aligned}
\dot{\varepsilon}_{xx} &= -u\left(1-n_{fl}\right)\left(d_{die}-x\right)^{n_{fl}-1}\left(d_{die}-y\right)^{n_{fl}-1}\left(d_{die}-x_0\right)^{1-2n_{fl}}, \\
\dot{\varepsilon}_{yy} &= u\left(1-n_{fl}\right)\left(d_{die}-x\right)^{n_{fl}-1}\left(d_{die}-y\right)^{n_{fl}-1}\left(d_{die}-x_0\right)^{1-2n_{fl}}, \\
\dot{\varepsilon}_{xy} &= \frac{1}{2}u\left(1-n_{fl}\right)\left(d_{die}-x_0\right)^{1-2n_{fl}}\left[\left(d_{die}-x\right)^{n_{fl}}\left(d_{die}-y\right)^{n_{fl}-2}-\left(d_{die}-y\right)^{n_{fl}}\left(d_{die}-x\right)^{n_{fl}-2}\right],
\end{aligned} \tag{19}$$

(with u denoting the ram speed).

For the equivalent (von Mises) strain rate it follows

$$\begin{aligned}
&\dot{\varepsilon}_{eq} = \sqrt{\frac{2}{3}\dot{\varepsilon}_{ij}\dot{\varepsilon}_{ij}} = \\
&\frac{1}{\sqrt{3}}u\left(n_{fl}-1\right)\left(d_{die}-x\right)^{n_{fl}-2}\left(d_{die}-y\right)^{n_{fl}-2}\left(d_{die}-x_0\right)^{1-2n_{fl}}\left[\left(d_{die}-x\right)^2+\left(d_{die}-y\right)^2\right]
\end{aligned} \tag{20}$$

The strain rate profile along a flow line predicted by Eqs.(19) is shown in Figure 11 as a function of the angular position of the flow line, defined in Figure 4. The model predicts a significant increase of the strain rate along the symmetry plane of the die and the distribution of the strain rates appears more pointed for larger n_{fl} . Considering that the n_{fl} values increase nearly monotonically from top to bottom, the model correctly captures the inhomogeneity of the strain rate distribution in the ECAP billet. Furthermore, at variance with Segal's original model, Eqs.(19) shows that the shear strain $\dot{\varepsilon}_{xy}$ is non zero.

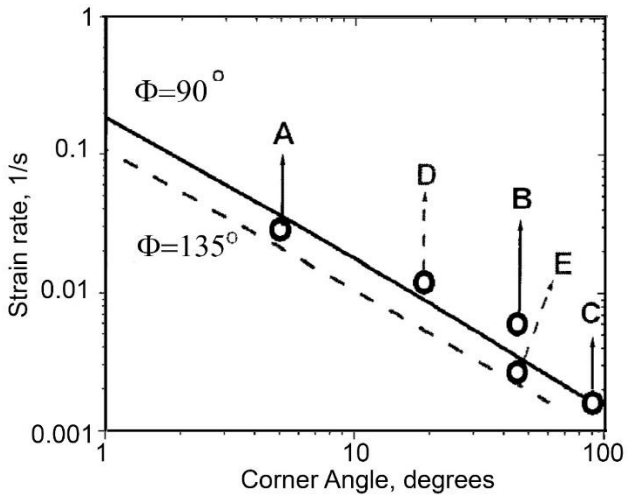

Figure 10. Average strain rate as a function of the corner angle Ψ. Straight lines represent the results obtained from Eq. (12) for two values of the channel angle Φ. The circles correspond to the data for the following combinations of the angles: (A) Φ= 90°, Ψ =7°; (B) Φ=90°, Ψ = 45°; (C) Φ=90°, Ψ =90°; (D) Φ=135°, Ψ =40° and (E) Φ= 135°, Ψ =45°. The ram speed to die diameter ratio (u / d_{die}) was set at 0.0033 s^{-1}. (After [135], reprinted with permission)

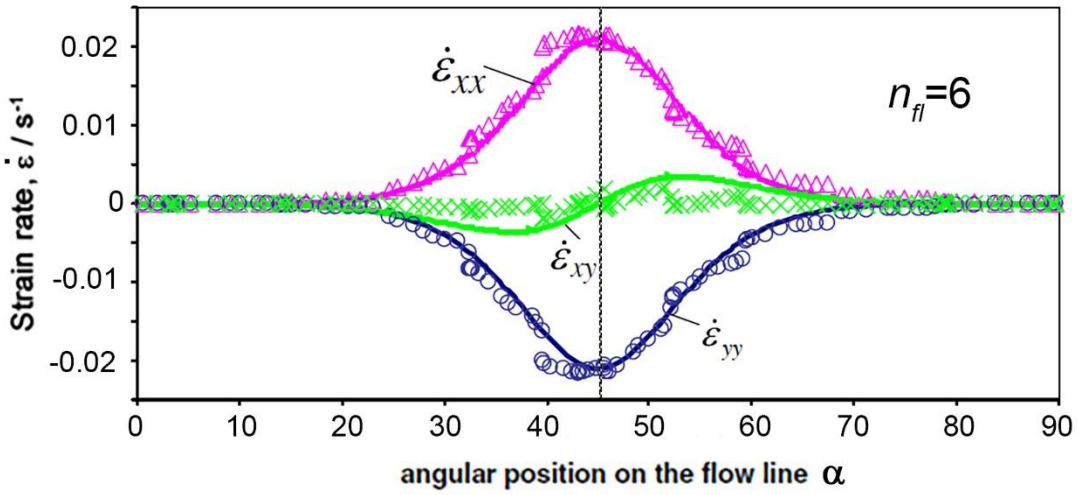

Figure 11. Strain rate profile (solid lines) along a flow line for ECAP deformation for n_{fl}=6. An excellent agreement with the results of FEM simulations (symbols) is seen. (From[96], see also [156] for results with other n_{fl} values; reprinted with permission).

Estimates for temperature effects during SPD

While the strain rate can easily be calculated and modelled numerically from simple geometry and kinematics considerations, the picture is more complicated with regard to the thermal effects, which require careful approximations to be made.

Since the mechanical properties of engineering materials are temperature dependent, estimates of the deformation-induced temperature rise are important for determining a material's response and microstructure formation. Two thermal conditions, which determine the temperature field in a billet, are naturally distinguished in attempts to interpret and model experimental results. In one extreme case, the heat generated within the deformation zone as a result of energy dissipation there is efficiently removed from the deformation zone either to an external 'thermal bath' or directly to the bulk of a massive billet. The temperature rise in this case, which is referred to as the *isothermal* one, is negligible and the deformation temperature is adequately represented by the initial temperature. In the other extreme, when *adiabatic conditions* prevail, say at very high strain rates, the temperature can rise appreciably. As an example, in a structural HY-100 steel deformed dynamically at a strain rate of 1.4 $\times 10^3$ s^{-1} the maximum temperatures measured by Marchand and Duffy [274] during localised shear band formation was as high as 460±50 °C. The real thermal conditions during most metal forming operations, including SPD processing, usually lie between these two extremes. The average strain rates within the deϕormation zone during SPD processing do not exceed 0.2-1 s^{-1} (and usually are much lower), as can be estimated ϕor typical deformation conditions using Eq. (18). For this strain rate range, the adiabatic conditions are hardly fulfilled and the deformation, even in shear bands that are sometimes observed during SPD, cannot be commonly regarded as adiabatic.

The most widely used, although not always adequately argued, approach towards modelling deformation-induced thermal effects and energy storage during microstructure evolution is based on a simplest energy balance analysis that follows from the first law of classical thermodynamics. The energy

balance approach has been comprehensively reviewed by Bever et al. [275] and more recently by Stainier [276]. It states that the elementary mechanical work dA done by the external forces is split into an increment of heat, dQ, and an increment of the internal energy of the system, dU:

$$dA = dQ + dU \tag{21}$$

Here the kinetic energy of the plastically deforming body has been ignored. It should also be born in mind that the mechanical work is generally path-dependent and thus the elementary increments of work and heat are represented by incomplete differentials. For simplicity, we retain the symbol *d* to denote the differential in all terms in Eq. (21). A portion dW_{el} of the total mechanical work dA expended on a deforming solid is elastic and recoverable, while the remainder - the plastic work dW_{pl} - is irrecoverable. The latter is mostly, but not entirely, converted into heat dQ. The part of the plastic work that is not converted into heat represents the stored energy of mechanical work dU. This energy is stored in the crystal lattice defects created in the course of plastic deformation. Disregarding the elastic part, Eq. (21) can thus be re-written as

$$dW_{pl} = dQ + dU \tag{22}$$

Taylor, together with Farren and Quinney, [277, 278] were the first to perform a series of experiments on the latent energy remaining stored in copper after cold working. Without specifying microstructural mechanisms for energy storage and strain hardening, which were unknown at that time, they concluded that "*the fact that the absorption of latent energy and the increase in strength with increasing strain both cease when the same amount of cold work has been applied suggests that the strength of pure metals may depend only on the amount of cold work, which is latent in them*." Bever et al. [275] and Benzerga et al. [279] emphasised that the partitioning of the plastic work into heat generation and energy storage is of interest in a wide range of contexts. The defect structure in a cold worked ductile metal, particularly in a severely deformed one, is generally metastable so that, with time, it evolves so as

to reduce its stored energy. In this sense, the stored energy of cold work plays a significant role in driving "static" recovery and recrystallisation in polycrystalline metals [280, 281]. Particularly, it has been shown that pure FCC metals such as copper or aluminium are prone to relatively quick recrystallisation after SPD [282, 283]. For example, high purity (5N) Cu subjected to eight passes of route Bc ECAP recovered completely to the conventional coarse grain state after one year storage at ambient temperature. Knowledge of the fraction of the mechanical work converted to heat is essential for prediction of thermomechanical coupling phenomena such as thermal softening that promotes plastic instabilities [284, 285], including necking and shear banding. Thermomechanical coupling plays a critical role in selection of the deformation mode prevalent in rapid SPD processes, such as machining and projectile penetration where the adiabatic approximation is well justified [286]. The popular constitutive relations for high strain rate deformation proposed by Johnson and Cook [287] from purely mechanistic considerations and by Zerilli and Armstrong [288], who included the grain size dependence of stress and dislocation-based effects of strain hardening, strain-rate hardening, and thermal softening, provide the necessary thermomechanical coupling. Furthermore, since the stored energy is associated with the internal stress state of the material, it has a direct connection with the occurrence of the Bauschinger effect. Indeed, the large energy stored in the material during SPD results in a pronounced Bauschinger effect observed under cyclic loading in many ECAP-manufactured ultrafine grained materials, including Cu, Ti, Ni, Fe-Ni, and Al-Mg-Sc alloys, etc. [289, 290]. Because of the importance of the stored energy of cold work for many physical phenomena in deformed materials, there is a large literature aimed at its experimental determination, see, e.g., [275, 291-294]. The stored energy of cold work in metals is associated with the production and evolution of a variety of crystal lattice defects including, primarily, lattice dislocations and grain or sub-grain boundaries, as well as twins and stacking faults. The rate of accumulation of stored energy varies with strain and strain rate, and its magnitude can usually be

related to stress. Thus, the evolution of the stored energy in a material is intimately connected with the evolution of its defect structure.

As stated above, a number of assumptions are often made for the analysis of the energy balance of a deforming solid to be tractable analytically. These simplifying assumptions usually include an additive decomposition of a strain increment into an elastic and a plastic part, a relation between stress and elastic strain adopted from isotropic linear thermoelasticity, and the use of the linear Fourier heat conduction law. Under these assumptions, the first law of thermodynamics is reduced, for the case of uniaxial loading, to the following form [292] (see also [295] for details of the derivation of this equation and the underlying assumptions):

$$\rho_d c_v \frac{\partial T}{\partial t} = \beta_T \sigma \dot{\varepsilon}_{pl} - \alpha_T E T \dot{\varepsilon}_{el} + \kappa \frac{\partial^2 T}{\partial x^2} \tag{23}$$

with the total heat flux rate on the left-hand side and the elastic strain ε_{el} and the plastic strain ε_{pl} being functions of the coordinate *x* and time *t*. The material constants κ, α_T, and E are the thermal conductivity, thermal expansion coefficient, and Young's modulus, respectively. Equation (23) implies that the heat removal from the deformation zone is controlled by heat conduction in the material, rather than heat exchange with the environment through the specimen surface, which is assumed to be flat. In the opposite case when the latter process is the slower of the two, the last term in Eq. (23) should be replaced with $(2h/R)(T - T_0)$, where T_0 is the ambient temperature, h is the heat exchange coefficient, and R is the radius of the specimen (assumed to be cylindrical) [296]. In this case, deformation-induced temperature increment in steady state reads

$$T - T_o = \frac{\beta_T \sigma \dot{\varepsilon}_{pl} R}{2h} \tag{24}$$

There is a consensus that most of the energy of plastic deformation, W_{pl}, yet not all of it, is converted to heat. The conversion coefficient, i.e. the fraction of the plastic energy rate $\beta_T = \dot{Q} / \dot{W}_{pl}$, is material and process specific, but it can typically be set at about 0.9 [278]. The limitations on the applicability of this equation, e.g. those associated with the assumed constancy of the material parameters c_v, κ and β_T, were discussed by Tsagrakis and Aifantis [297] in connection with a gradient thermo-viscoplasticity model for adiabatic shear banding.

The deformation-induced heat release can cause microstructural changes and affect the microstructure evolution, e.g. through the temperature-dependent parameters governing the dislocation recovery rate (see section 3.2).

The increment in plastic work per unit volume during deformation can be expressed as

$$dW_{pl} = \sigma \dot{\varepsilon} dt \tag{25}$$

and the integral plastic work per unit volume is obtained as $W_{pl} = \int \sigma \dot{\varepsilon} dt = \int \sigma d\varepsilon$. In the case of SPD processes, this energy per pass is quite large. Referring to ECAP of a material with a yield stress σ_y of, say, 300 MPa and a strain per ECAP pass of $\varepsilon \approx 1$, Korn et al. [298] provided and estimate $W_{pl} \approx 3 \times 10^6$ J·m^{-3}, or 0.3 J·g^{-1}, which is a considerable figure (although the latent heat of fusion for copper is still three orders of magnitude higher). A mathematically more rigorous solution for the power dissipated during ECAP process in different regions of the die was obtained by Paydar et al. [138] based on the upper-bound theory. To attain ultimate grain size reduction, SPD processing is usually performed at as low homologous temperature as possible, say, at ambient temperature, which is roughly $0.3T_m$, (where T_m is the melting temperature) for such metallic materials as Al, Cu, Ni, or Fe. Due to generation of a significant density of dislocations in a deforming body at this temperature, SPD triggers a sequence of structural transformations that convert a random distribution of dislocations to bundles, dislocation cells with low misorientation angles across their boundaries, and eventually - and most importantly - to

highly refined and highly misoriented grain structures [299-307]. This chain of processes leads inevitably to a progressive increase in flow stress and an ensuing rise in the rate of energy dissipation for SPD processing at low homologous temperatures [169]. With regard to the question of how seriously the grain size distribution is affected by the heat developed during ECAP, Korn et al. [298] highlighted three most significant factors: 1) the maximum temperature attained locally in the shear deformation zone during ECAP, 2) the time an element of material spent at the site of this maximum temperature, and 3) the rate of decay of temperature during cooling of the ECAP-processed billet.

Only few direct measurements and indirect estimations of temperature changes during SPD processing were reported. These were summarised recently by Zhilyaev et al. [308]. For example, Yamaguchi et al. [169] used thermocouples embedded in billets and measured temperature increments of 25–30 °C during an ECAP pass in initially annealed pure aluminium. Zhilyaev et al. [309] gave an estimate of 140 °C for the temperature rise during HPT of an as-cast Na-added Al-7 wt% Si alloy from indirect evidence, based on the observed changes in precipitate distributions. Shear plane temperatures as high as the melting temperature T_m were reported for plane strain machining under certain process conditions [310].

Frictional losses in the ECAP process are a further source of heat compounding the deformation-induced heat release. Kim [311] considered the friction-related heat generation as an additive term on the left-hand side of Eq. (23) and used a simple Newtonian viscous friction model as an approximation under well lubricated conditions. In this case, the rate of heat flux generated by friction between the die walls and the workpiece is proportional to the normal stress f_s and the relative velocity u between the bodies in contact. The respective differential is given by

$$dq_f = f_s du = m_f \left(\sigma / \sqrt{3}\right) du \tag{26}$$

where m_f is the coefficient of friction. Ignoring the contribution from the thermoelastic effect and all temperature gradients within the main deformation zone (i.e. dropping the second and the third terms on the right-hand side of Eq.(23)) reduces the energy balance to an elementary relation between average quantities:

$$\rho_d c_v V \Delta T = \beta_T \sigma \varepsilon_{pl} V - 0.5 m_f \left(\sigma / \sqrt{3}\right) u S_A \Delta t - S_A h_T \Delta T \Delta t \tag{27}$$

Here *V* is the volume of the main deformation zone and S_A its surface area. The dwell time Δt is given by Eq. (17). In writing the first term on the right-hand side it was tacitly assumed that during ECAP the stress saturates quickly to a level represented by σ. The factor 0.5 in the second term stems from the assumed equipartitioning of the friction heat between the workpiece and the die. The third term accounts for the heat transfer from the workpiece (considered to be heated adiabatically) to the die. The coefficient h_T, which is proportional to the thermal conductivity κ, describes the efficiency of this heat transfer. Accordingly, the following simple relation provides an estimate for the temperature increment ΔT in the shear deformation zone:

$$\Delta T = \frac{\beta_T \sigma \varepsilon_{pl} + 0.5 m_f \left(\sigma / \sqrt{3}\right) u \left(S_A / V\right) \Delta t}{\rho c_v + \left(S_A / V\right) h_T \Delta t} \tag{28}$$

From the geometrical considerations the volume and the surface area of the primary deformation zone are $V = \left(\pi^2 / 4\right) d_{die}^3 \left(\Phi / 2\pi\right)$ and $S_A = \left(\pi^2 d_{die}^2\right)\left(\Phi / 2\pi\right)$, respectively, with d_{die} denoting the diameter of the die. Using this simple analytical formula, with S_A and V estimated for $\Psi = \pi / 4$ and $\Phi = \pi / 2$, employing Eq. (2) for the plastic strain ε_{pl}, and taking β_T=0.9, m_f=0.2 (a typical value for cold forming of metals with conventional lubricants), and h_T = 2×10^3 W·m^{-2}·K^{-1}, Kim [311] obtained a fair agreement between the calculated values of ΔT and the experimental results of Yamaguchi et al. [169] for Al and Al-Mg alloys deformed by ECAP with different ram speeds *u*, Figure 12.

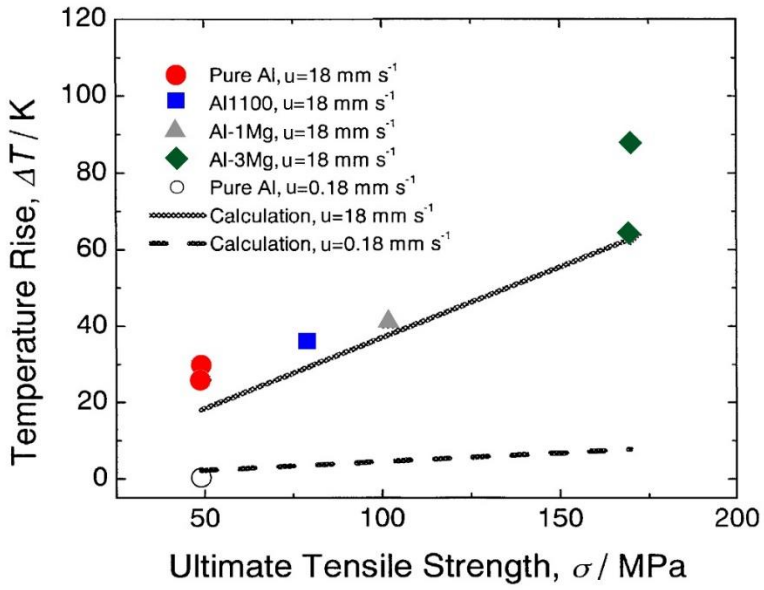

Figure 12. Comparison of the calculated and experimental temperature increments during ECAP of Al-based materials (*u*=18 mm/s or 0.18 mm/s) (after [311], reproduced with permission).

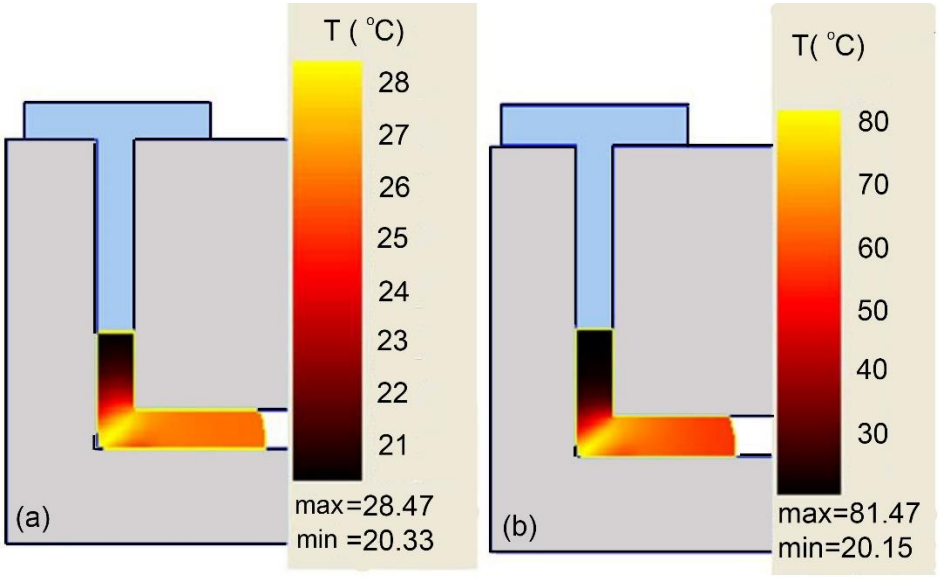

Figure 13. FEM simulation of the temperature distribution in a Cu billet during ECAP, computed with $h_T = 2 \times 10^3$ Wm^{-2} K^{-1}. The figures show the effect of the ram speed *u* : a) *u* = 1mm·s^{-1}, b) *u* = 10 mm·s^{-1} (after [298], reproduced with permission).

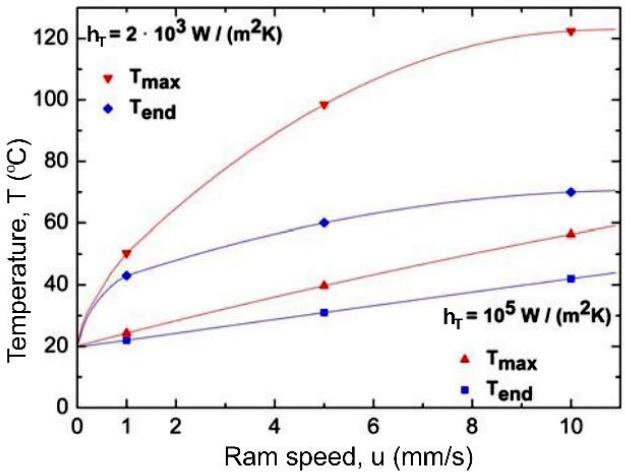

Figure 14. Summary of the results of FEM simulations of the maximum temperature T_{max} in the shear deformation zone and temperature T_{end} at the deformed end of a Cu billet, plotted as a function of the ram speed *u* for two different values of the heat transfer coefficient (h_T =2×10^3 W·m^{-2} ·K^{-1} and h_T =10^5 W·m^{-2} ·K^{-1}) (adopted from [298], reproduced with permission).

It follows from a comparison of the first and the second terms in the numerator of Eq. (28) that the main contribution to ΔT arises from the work of deformation, whereas the heat of friction is almost negligible. This result highlights the significance of adiabatic heating in the ECAP deformation process unequivocally.

Korn et al. [298] applied the same procedure to estimate the temperature increment ΔT in the case of a copper billet. Assuming a yield stress of 350 MPa (representative for UFG copper [176, 290]) and a typical value of $\varepsilon \approx 1$, and with the same other variables as those used by Kim, the temperature rise ΔT was estimated at approximately 64 °C, 89 °C and 94 °C for ECAP speeds of 1mm/s, 5mm/s and 10mm/s, respectively. These values correspond to T_{max} of 84°C, 109°C and 114°C. They are in fair agreement with the values of T_{max} obtained by FEM simulation, cf. Figure 13 and Figure 14.

Temperature increments under HPT are typically less pronounced. Thus, Edalati et al. [229] performed FEM modelling of the temperature profiles for aluminium, copper, iron and molybdenum subjected to HPT at realistic anvil rotation speeds. In their simulations, slippage and the associated friction heat was accounted for. A temperature rise was observed at the early stages of straining which

then saturated to steady levels of a few tens of degrees at large strains. The temperature increment was found to be higher for harder materials, in reasonable agreement with Eq. (13). For all materials, the temperature increase became more significant with increasing processing time, rotation speed, applied pressure and the distance from the disc centre. Despite the giant plastic work done during processing by HPT, the magnitude of the temperature increments for the selected model metals relative to their melting temperatures was not significant, however. It should be noted that these advanced simulations render essentially the same conclusions as those drawn by Bridgman in his landmark paper [160].

The simplistic thermodynamic analysis complemented with FEM simulations has shown that depending on the material and process conditions SPD may involve an appreciable temperature increase. This is particularly true for ECAP processing. It can thus be concluded that microstructure evolution during SPD at low homologous temperatures can be influenced not only by the initial processing temperature but also by deformation-induced heating effects.

Microstructure evolution during SPD in non-isothermal conditions

Kuhlmann-Wilsdorf [312, 313] has systematically advanced the principles of classic equilibrium thermodynamics to the so-called *low-energy dislocation structure* (LEDS) theory of low temperature dislocation-based crystal plasticity. This theory is essentially based on Taylor's theory of work hardening which assumes that the external stress is related to the dislocation structure in a unique way. The deformation-induced microstructure is supposed to correspond to a minimum-energy configuration and to be in equilibrium at a given applied stress during deformation.

Although the equilibrium thermodynamics approach propagated by Kuhlmann-Wilsdorf has been criticised as one disregarding the dissipative, far-from-equilibrium nature of the deformation processes [314], the minimum-energy principle seems to work well in many cases. It was tacitly employed by Zhilyaev et al. [308] who proposed a simple model for grain size evolution under SPD-

induced adiabatic heating, incorporating the temperature- and rate dependent processes. The following basic assumptions were made explicitly or implicitly. (1) The evolution of the mean grain size $\bar{d}$ is controlled by two competitive processes - grain refinement with increasing strain (or time) and elastic energy storage in grain boundaries, leading to grain coarsening that would reduce their free energy:

$$\dot{\bar{d}} = \dot{\bar{d}}^{-} + \dot{\bar{d}}^{+} \tag{29}$$

Here the time derivatives $\dot{\bar{d}}^{-}$ and $\dot{\bar{d}}^{+}$ denote the rate of grain refinement and grain coarsening, respectively. (2) Adiabatic conditions prevail so that the thermoelastic heating term in Eq.(23) is negligible compared with the heating due to plastic work. (3) Based on the analysis by Kim [311] and Korn et al. [298], the friction effects can be neglected as well, provided the appropriate lubrication conditions are fulfilled. Assuming further that most of the part of the plastic work that gets stored in the defect structure goes into the free energy of graiboundaries (i.e. neglecting such energy storage channels as generation of vacancies and dislocations) Zhilyaev et al. [308] found the following kinetic equation for the rate of decrease of the grain size:

$$\frac{d\bar{d}^{-}}{d\varepsilon} = -\frac{c_{GB}\sigma\bar{d}^{2}}{3\gamma_{GB}} \tag{30}$$

Here c_{GB} is the fraction of the plastic work stored in the grain boundaries and γ_{GB} is the grain boundary energy per unit area. The driving force for grain growth at a given temperature was considered to be controlled by diffusion and the kinetic equation for grain growth with respect to time or strain can be written as

$$\frac{d\bar{d}^{+}}{dt} = \frac{2\gamma_{GB}}{\bar{d}}\frac{\Omega}{w}\frac{D}{k_B T}, \quad \Rightarrow \quad \frac{d\bar{d}^{+}}{d\varepsilon} = \frac{2\gamma_{GB}}{\dot{\varepsilon}\bar{d}}\frac{\Omega}{w}\frac{D}{k_B T} \tag{31}$$

where Ω is the atomic volume, w is the width of the grain boundary and k_B the Boltzmann constant. The diffusion coefficient D is given by $D = D_V + \frac{w}{3\bar{d}}D_{GB}$, where D_V is the bulk diffusivity and D_{GB} is

the grain boundary diffusivity. We note that the first term in D gives rise to a linear and the second one to a parabolic growth law. The overall kinetics of the evolution of the average grain size $\bar{d}$ with strain is obtained by combining Eqs. (30) and (31):

$$\frac{d\bar{d}}{d\varepsilon} = \frac{2\gamma_{GB}}{\dot{\varepsilon}\bar{d}}\frac{\Omega}{w}\frac{D}{k_B T} - \frac{c_{GB}\sigma\bar{d}^2}{3\gamma_{GB}} \tag{32}$$

The temperature variation within the sample under the assumed adiabatic conditions is then expressed as

$$\frac{dT}{d\varepsilon} = \frac{(1-c_{GB})\sigma}{\rho c_v} - \xi\frac{dT}{d\varepsilon}, \quad \Rightarrow \quad \frac{dT}{d\varepsilon} = \frac{(1-c_{GB})\sigma}{(1+\xi)\rho c_v} \tag{33}$$

where ξ is a purely phenomenological coefficient describing heat transfer to the exterior of the workpiece (note that it is not identical to h_T in Eq. (28)). Equation (33) is a compromise between the general heat conduction equation, Eq. (23), and its simplified version, Eq. (28).

It should be mentioned that Eq. (32) predicts an inverse power-law relation between the flow stress and the average grain size in steady state, when $\frac{d\bar{d}}{d\varepsilon} = 0$, which Pougis et al. [315] refer to as the Derby equation. The exponent of 1/3 following from Eq. (32) is different from the one obtained by Pougis et al., which was found to be close to 1/2, thus replicating a Hall-Petch type of grain size dependence.

In their model, Zhilyaev et al. do not restrict themselves to steady state conditions, however. Rather, they assume that quite generally, the dependence of the flow stress on the average grain size is expressed in terms of the Hall-Petch relation [8]:

$$\sigma = \sigma_0 + K_{HP}\bar{d}^{-1/2} \tag{34}$$

Here σ_0 is a 'friction' stress that encompasses the contributions of strengthening effects other than the grain size one. The Hall-Petch parameter K_{HP} is generally a strain rate and temperature-dependent quantity, which has been interpreted in terms of dislocation processes as a microstructure-sensitive

material parameter. Three major groups of models are to me mentioned in this context: (i) the historically first group of pile-up models [20], work hardening models [316-318] and grain boundary source models [21, 319, 320], which are a natural corollary of the dislocation-based kinetic approach to strain hardening considered below. The Hall-Petch relation was also recovered in a study on the grain boundary Frank-Read (FR) mechanism [22] where it was noticed that thermally activated operation of FR sources, which was earlier invoked to explain the grain size dependence of the strain rate sensitivity of the flow stress, is to be ruled out. Gryaznov [321] proposed a generalised form of the Hall-Petch relation to extend its applicability to nanostructured materials by accounting for dislocation slip, dislocation storage and the influence of disclination-type defects. Armstrong and Rodrigues [322] have explained the dependence of K_{HP} on temperature and strain rate (as observed, e.g., in the work cited above [100]) by combining the dislocation mechanics-based thermal activation analysis and the dislocation pile-up model, which results in the following expression for the Hall-Petch parameter

$$K_{HP} = M\left(\frac{M_S \pi G b \tau_C}{2\alpha_d}\right)^{1/2} \tag{35}$$

Here M and M_S are the Taylor and Sachs orientation factors, respectively, $\alpha_d \approx 0.8$ is a numerical constant and τ_C is the shear stress associated with local obstacles to dislocations. The strain rate and temperature dependence of this quantity for *FCC* metals with relatively high stacking fault energy, e.g. for Cu and Ni, is associated with the cross-slip shear stress, and it is this dependence that shows in K_{HP}. Since a large body of indirect data provides evidence that in the temperature range (0.1-0.5)T_m the value of K_{HP} is only weakly dependent on temperature in *FCC* metal and alloys, this dependence can be ignored in modelling as a first approximation [323].

Equations (32)-(34) form a closed set of equations for the evolution of the average grain size and temperature during deformation (ECAP in the case considered by Zhilyaev et al.), provided the stress

can be considered as a slow variable compared to $\bar{d}$ and *T*. Using this model, various regimes of grain size evolution were considered with reference to the magnitude of the parameter ξ. Of particular interest is the case $\xi \to 0$ when adiabatic conditions prevail and an initial strain interval of grain refinement may be followed by grain coarsening at larger strains. This is illustrated schematically in Figure 15, which shows the average grain size as a function of the cumulative strain. The results of numerical simulations for pure Cu and Al are shown in Figure 16 where the experimental data points and the calculated curves for the strain dependence of the average grain size are plotted. They indicate that the original grain size is reduced by a factor of >10^2 at a strain of 5–6 before it increases slightly upon further straining. The results of the simulations are seen to be in fair agreement with the bulk of experimental data for the two materials.

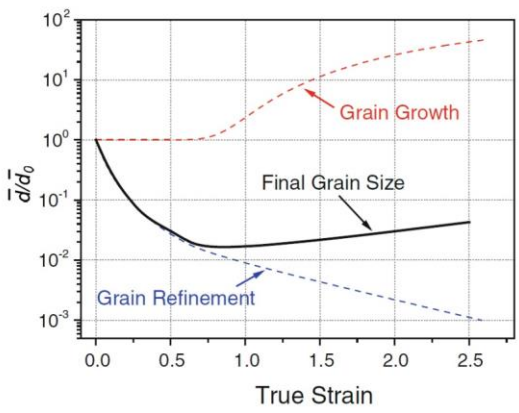

Figure 15. Schematic of the variation of the average grain size (normalised with respect to its initial value $\bar{d}_o$) with strain combining grain refinement and grain growth during SPD (from [308], reproduced with permission). The solid line corresponds to the resultant grain size.

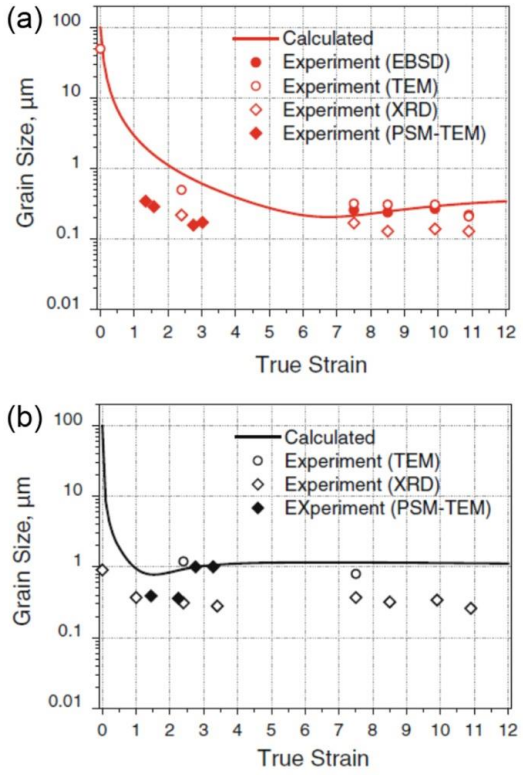

Figure 16. Average grain size as a function of cumulative true strain for copper (a) and aluminium (b). The solid lines show the results of numerical simulations (from [308], reproduced with permission)

Overall, the model developed in [308] shows qualitatively (and even semi-quantitatively) that SPD under isothermal conditions should result in a continuous refinement of the grain size. This reflects the strengthening effect of grain refinement and a corresponding increase in flow stress as SPD straining proceeds. Saturation of grain size refinement reflects a balance between grain refinement due to straining and grain growth due to the sample temperature rise associated with deformation-induced adiabatic heating.

Despite some doubts one may have about the validity of the physical argumentation underlying Eq. (33) (regarding both the thermodynamics and the kinetics of the processes involved), the advantage of this approach is that it allows evaluating the role of the model parameters, particularly the heat exchange coefficient ξ , in the evolution of the grain size during SPD. Uncertainties and limitations used in this modelling approach stem from the simplifications adopted to make the analysis tractable.

Although this can be accepted as a first approximation, a more elaborate approach accounting for non-equilibrium character of virtually all processes underlying the microstructure formation has yet to be proposed. Furthermore, disregarding the role of dislocations in the energy dissipation and storage is another oversimplification, and this needs to be rectified within a dislocation based approach. In addition, such processes as grain fragmentation under SPD processing are to be included in an explicit way, as will be discussed below, in Section 3.2.

3. Microstructure-based phenomenological modelling of severe plastic deformation

Microstructure-related constitutive models of strength and plasticity of metals and alloys are preferable to purely phenomenological models. Due to their physical foundations, the former are usually more economical than most phenomenological models in terms of their architecture and the number of adjustable parameters involved. Besides, these parameters have a clear physical interpretation. This provides the microstructure-based models with a greater predictive capability, particularly with the ability to predict how these parameters depend on the alloy composition of the material and its processing history. A reliable foundation for microstructure-related constitutive models has been laid by the dislocation theory. Industries as diverse as automotive, aerospace, and electronics have been benefiting from the use of integrated computational models which employ dislocation theory based approaches [324]. Because of the complexity of the mechanisms underlying dislocation plasticity, some unresolved problems with dislocation theory based constitutive modelling still remain, however. The words of Cottrell about modelling of strain hardening, who described it some 65 years ago [325] as "the first problem to be attempted by dislocation theory and the last to be solved" are still relevant.

Due to the progress in constitutive modelling achieved by materials scientists over the last two decades, the outlook on its ability to tackle the SPD processing both analytically and computationally is optimistic. In this section, we shall be focusing on the microstructure-related modelling 'toolbox' available for description and prediction of the behaviour of metallic materials under SPD. Process optimisation in this area relies more and more on computational modelling. Microstructure-based models capturing the physics of the deformation processes, and yet robust enough to be used efficiently in finite element codes, are in demand. Here we present modelling approaches that satisfy this demand. In our earlier review [326], we provided some insights into the specifics of modelling of SPD processes. In the present section we shall discuss a broader range of modelling techniques based on the microstructure-based approaches to constitutive modelling. It will also be demonstrated how irreversible thermodynamics of plasticity leads to the classical constitutive equations that go back to the work of Kocks [182] (see also [23, 184, 327]). More complexity will then be introduced in the constitutive equations where it is needed for an adequate description of the detail of severe plastic deformation. Examples of calculations of the material behaviour during various SPD processes will then be given. Throughout this section, problems that need to be resolved by future model development will be identified and discussed.

An important ingredient of any microstructure model is a reliable description of the dislocation density evolution. In the next section, we give an overview of an approach to such a description using irreversible thermodynamics to provide a new interpretation of existing semi-phenomenological models.

3.1. Evolution of dislocation ensembles: an irreversible thermodynamics approach

The foregoing analyses of the grain size evolution were footed on the first law of classical equilibrium thermodynamics. In reality, however, a plastically deforming solid is an open system exchanging energy with its surroundings. Therefore, regarding plastic deformation as a highly dissipative process [328] suggests that the irreversible thermodynamics principles formulated by Onsager,

Prigogine and Bridgman [329-332] should be applied as the governing concept. As distinct from equilibrium thermodynamics, the second law of thermodynamics of irreversible processes is formulated in terms of the entropy production. A concept of fundamental importance in thermodynamics of irreversible processes is the notion of a non-equilibrium stationary state, which plays a role analogous to that of the equilibrium state in classical equilibrium thermodynamics. According to the second law, all internal processes must terminate when collectively they can no longer produce entropy. A stationary state has then been reached and it represents a minimum in the rate of entropy production, which is zero.

Being a highly dissipative process, plastic deformation involves many scales and manifests itself in a variety of patterns. Characterising and predicting patterning in the dislocation population that accompanies plastic deformation of crystalline solids is a particularly challenging problem addressed in numerous publications [60, 333-335]. The patterns may be different with regard to their inner length scale or, by contrast, exhibit a scale-free behaviour [328].

For a system undergoing multiple irreversible processes, the entropy $d_i S$ generated per unit volume during a time interval *dt* is the sum of the individual contributions of all irreversible processes involved. This is expressed mathematically as

$$d_i S = \sum_{K=1}^{N} d_i S^K > 0 \tag{36}$$

where *N* is the number of irreversible processes taking place in the system and $d_i S^K$ is the entropy generated due to the K^{th} process. $d_i S^K$ is determined by the dissipated energy per unit volume W_{dis}^K associated with the K^{th} process [280]:

$$d_i S^K = \frac{dW_{dis}^K}{T} \tag{37}$$

In Onsager's theory [329, 330] the rate of entropy production in a thermodynamic system out of equilibrium, but where local equilibrium exists, is expressed as the sum of the products of generalized forces X_K and their corresponding thermodynamic fluxes J_k for the individual irreversible processes involved:

$$\frac{d_i S}{dt} = \sum_{k=1}^{N} X_k J_k > 0 \tag{38}$$

Onsager proposed a linear relation between thermodynamic fluxes and the generalised forces in the form $J_k = \sum L_{ki} X_i, \quad (L_{ki} = L_{ik})$ where L_{ki} is the matrix of kinetic coefficients, which are independent of J_k and X_i. Finding these coefficients is a formidable task. To derive a relation between mutual interactions of simultaneous processes in a system, an extremum principle of irreversible thermodynamics is usually invoked, e.g. Onsager's principle of *maximum* rate of entropy production or Prigogine's principle of *minimum* rate of entropy production.

Assuming a local equilibrium in the system, Ziegler [336, 337] proposed a maximum entropy production principle to find $X_k(J_k)$ in the explicit form: *if irreversible force* X_i *is prescribed*, *then the actual flux* J_i, *which satisfies the condition* (36), *maximises the entropy production*. A similar principle, originally proposed by von Mises in the solid mechanics context, appeared in the mathematical theory of plasticity developed by Drucker [338], Hill [339] and others in the 1950s. Referred to as the von Mises principle of maximum plastic dissipation [340], it states that the total power of plastic deformation per unit volume is maximised subject to the yield condition expressed in terms of the stress and strain hardening characteristics for a given strain rate.

Ghoniem et al. [341] adapted the general irreversible thermodynamics formalism to the discrete dislocation dynamics (DDD) modelling framework. Benzerga et al. [279] combined the irreversible

thermodynamics with the discrete dislocation dynamics approach, which enabled them to calculate the stored energy of cold work for planar single crystals under quasi-static tensile loading.

A central theme of a series of recent communications by Langer [10, 342, 343] was the need for physics-based, nonequilibrium analyses in developing predictive dislocation-based theories of strain hardening of polycrystalline materials. He and his co-authors developed a statistical thermodynamic dislocation theory, which has then been used for the analysis of the mechanical response of pure copper and the effect of grain size on the strain hardening curves. It was proposed that the description of the dynamic behaviour of polycrystalline aggregates can be furnished with two main intrinsic variables - the total dislocation density and the characteristic temperature χ defined for any dislocation configuration in the statistical thermodynamic sense as $\chi = dU_C / dS_C$ with U_C and S_C being the energy calculated for a given ensemble of dislocations and the corresponding configurational entropy, respectively. A good predictive capability of the elegant theory put forward by Langer will certainly provide a strong impetus to further modelling work.

The irreversible thermodynamics framework was also used in our treatment of plastic deformation [344]. The deforming crystal was considered as an open system evolving towards a steady state. The differential of the total entropy flux was presented as $dS = d_i S + d_e S$, where $d_i S$ is the entropy production term associated with the changes in the inner microstructure (and is always positive) and $d_e S$ is the term corresponding to heat exchange with the exterior. Huang et al. [345, 346] applied Prigogine's principles of irreversible thermodynamics [331] to dislocation-based modelling of strain hardening. This approach was modified in our work using a composite-like microstructural model, in which the dislocation cell interiors and dislocation cell walls are treated as separated 'phases' of the material. In both models, the elementary entropy production $d_i S$ during a shear strain increment $d\gamma$ is

related to the energy dissipated due to three primary dislocation reactions - generation, motion, and annihilation entering the right-hand side of Eq. (38) additively, yielding

$$d_i S = \frac{1}{T}\left(\frac{1}{2}Gb^2 d\rho^+ + \tau b < \lambda > d\rho^+ + \frac{1}{2}Gb^2 d\rho^-\right) \tag{39}$$

Here $d\rho^+$ and $d\rho^-$ are the increments of the total dislocation density associated with dislocation production and recovery (annihilation), respectively. (Note that $d\rho^-$ is a negative quantity.) Further quantities entering Eq.(39) are the magnitude of the dislocation Burgers vector, *b*, the shear modulus, *G*, the resolved shear stress, τ, acting in the dislocation glide plane, and the dislocation mean free path, $< \lambda >$. The latter variable scales with the average dislocation spacing as $< \lambda > \sim 1/\sqrt{\rho}$ with $\rho = \int d\rho = \int d\rho^+ + \int d\rho^-$ being the total dislocation density [38]. The dislocation density is the principal internal variable that determines the resolved shear stress τ, which scales with $\sqrt{\rho}$ according to the Taylor relation:

$$\tau = \alpha Gb\sqrt{\rho} \tag{40}$$

Here α is a numerical factor depending on the dislocation arrangement and the mode of deformation (typically ~ 0.1-0.4) [184, 314]. The value of α tends to reduce as deformation proceeds and the dislocation pattern becomes heterogeneous with increasing lattice misorientations arising from an increasing density of GNDs as has been reviewed recently by Mughrabi [347]. A 'friction stress', which stems from interactions of a gliding dislocation with the Peierls relief and crystal lattice defects other than dislocations, can be assumed to be negligible, at least for pure FCC metals after a sufficiently large strain, for which reason it has not been included in the last expression. Equation (40) is ubiquitous: virtually all conceivable dislocation-dislocation interaction mechanisms lead to this relation (with α being dependent on the specific mechanism). It is also supported by a huge body of experimental data and discrete dislocation dynamics computer simulations [119]. Combining Eqs. (39) and (40) one obtains the entropy production term:

$$d_i S = \frac{(1+2\alpha)Gb^2}{2T} d\rho + \frac{(2+2\alpha)Gb^2}{2T} d\rho^- \tag{41}$$

The entropy flux $d_e S$ is produced by the dissipation of most of the plastic work $\tau d\gamma$ as heat [331] and is given by

$$d_e S = -\frac{\tau d\gamma}{T} \tag{42}$$

In terms of the evolution of a dislocation population, strain hardening is seen as a result of the competing processes of generation and annihilation of dislocations. The average distance a dislocation travels before it gets annihilated ('the mean free path') is a key characteristic that governs strain hardening. It may be related to the average dislocation spacing or some geometry features of microstructure extraneous to the dislocation population. Dislocation patterning is known to start developing early on, already after a small strain following the onset of plastic flow, and it obviously affects the evolution of the mean free path. Details of these processes are not well understood [348], but activation of multiple slip systems is seen as a major factor leading to patterning, cf. [119]. Multiple slip systems are activated already in Stage II of strain hardening giving rise to tangled dislocation networks, which further evolve to stable dislocation cell configurations. These patterns, which emerge as a result of irreversible self-organisation, comprise dislocation-rich 'cell walls' separating cell interiors that have a lower dislocation density. This kind of structure offers itself to a description in terms of the mentioned 'composite' model [349, 350] that was employed in our work [344].

According to the model [344], dislocation structure is composed of the cell-wall 'phase' with the volume fraction f_w and the cell interior 'phase' with the volume fraction f_c. Here the subscripts *c* and *w* stand for cell interiors and cell walls, respectively. Obviously, $f_w + f_c = 1$ holds. Applying a rule of mixtures and the Taylor relation, Eq. (40), for each of the two phases, the shear stress τ is expressed as a weighted sum of the contributions of the two 'phases'

$$\tau = f_w \tau_w + f_c \tau_c = f_w \alpha G b \sqrt{\rho_w} + f_c \alpha G b \sqrt{\rho_c} \tag{43}$$

and ρ_w and ρ_c are the dislocation densities in the two phases.

An empirical fact based on a vast body of experimental evidence, mainly from transmission electron microscopy (TEM) work, is that the average dislocation cell size d_c scales inversely with the square root of the total dislocation density $\rho = f_w \rho_w + f_c \rho_c$. This relation can be expressed [351] as $\rho = a / d_c^2$, where a is a proportionality coefficient. A similar scaling relation holds for the dislocation density in the cell walls, $\rho_w = a_w / d_c^2$, where a_w is another proportionality constant. Combining the last three equations, one obtains $\rho_c = \frac{a - a_w}{f_c} \rho_w = \beta \rho_w$ - a proportionality relation between ρ_c and ρ_w, which replicates that reported by Mughrabi [349]. Replacing ρ_w with ρ in Eq. (43), which is legitimate due to the condition $\rho_w >> \rho_c$, now leads to the following expression for the shear stress:

$$\tau = \alpha G b \left(\frac{f_w}{d_c} + \sqrt{\beta} f_c \sqrt{\rho_w} \right) \tag{44}$$

Accordingly, Eq. (42) can be rewritten as:

$$d_e S = -\left(\sqrt{\beta} f_c \sqrt{\rho} + \frac{f_w}{d_c} \right) \frac{\alpha G b d\gamma}{T} \tag{45}$$

By combining Eqs. (41) and (45) one obtains

$$\frac{dS}{d\gamma} = \frac{(1+2\alpha) G b^2}{2T} \frac{d\rho}{d\gamma} + \frac{(2+2\alpha) G b^2}{2T} \frac{d\rho^-}{d\gamma} - \left(\sqrt{\beta} f_c \sqrt{\rho} + \frac{f_w}{d_c} \right) \frac{\alpha G b}{T} \tag{46}$$

As an elementary annihilation event involves two dislocations, the annihilation rate obeys an equation for second-order annihilation kinetics:

$$\frac{d\rho^-}{dt} = \rho^2 b^2 \nu_0 e^{-\frac{\Delta G}{k_B T}} \tag{47}$$

The pre-exponential factor ν_0 in this equation is of the order of the Debye frequency ν_D. The activation energy ΔG is associated with that for dislocation climb, which is considered to be the governing annihilation mechanism. Hence, ΔG can be identified with the activation energy for self-diffusion. A simplifying assumption hidden in Eq. (47) is that annihilation occurs primarily in the cell walls. The density ρ_w of participating dislocations was replaced with ρ. Relating the shear rate to the average dislocation glide velocity $\langle v \rangle$ through the Orowan relation $\dot{\gamma} = \rho b \langle v \rangle$, one obtains

$$\frac{d\rho^{-}}{d\gamma} = \frac{\rho b \nu_0}{\langle v \rangle} e^{-\frac{\Delta G}{k_B T}} \tag{48}$$

An equation for the rate of variation of the overall entropy is finally obtained by substituting of Eq. (48) in Eq. (46):

$$\frac{dS}{d\gamma} = \frac{(1+2\alpha) G b^2}{2T} \frac{d\rho}{d\gamma} + \frac{(2+2\alpha) G b^2}{2T} \frac{\rho b \nu_0}{\langle v \rangle} e^{-\frac{\Delta G}{k_B T}} - \left(\sqrt{\beta} f_c \sqrt{\rho} + \frac{f_w}{d_c} \right) \frac{\alpha G b}{T} \tag{49}$$

As seen from Eq. (49), this rate is determined by the instantaneous value of the dislocation density and its shear strain derivative.

The thermodynamic system under consideration evolves to its steady-state. Even though this steady-state is a non-equilibrium one, it is defined by the condition $\frac{dS}{d\gamma} = 0$, thus yielding:

$$\frac{d\rho}{d\gamma} = \frac{2\alpha f_w}{1+2\alpha} \cdot \frac{1}{b d_c} + \frac{2\alpha \sqrt{\beta} f_c}{1+2\alpha} \cdot \frac{\sqrt{\rho}}{b} - \frac{2+2\alpha}{1+2\alpha} \cdot \frac{b \nu_0}{\langle v \rangle} e^{-\frac{\Delta G}{k_b T}} \rho \tag{50}$$

Equation (50) has a familiar form: it recovers the evolution equation for the dislocation density obtained by Kocks, Mecking and Estrin (KME) [23, 184, 327, 352] in a semi-phenomenological way:

$$\frac{d\rho}{d\gamma} = \frac{k_0}{b \langle \lambda \rangle} + \frac{k_1 \sqrt{\rho}}{b} - k_2 \rho \tag{51}$$

with the notation

$$k_0 = \frac{2\alpha f_w}{1+2\alpha}, \quad k_1 = \frac{2\alpha\sqrt{\beta}\, f_c}{1+2\alpha}, \quad k_2 = \frac{2+2\alpha}{1+2\alpha} \cdot \frac{b\nu_0}{\langle v \rangle} e^{-\frac{\Delta G}{k_B T}} \tag{52}$$

The coefficients k_0, k_1 and k_2 of the KME model can now be re-interpreted in terms of the parameters of the two-phase model via Eq.(52). The dislocation density evolution model in this simplified single internal variable form was presented in a number of publications [184, 352]. It has generated a substantial literature, in which the model was further developed, cf. [353-355].

In the one-internal-variable approach presented, the variation of the single internal variable, the average dislocation density, with strain can be found by integrating Eq. (51). The stress–strain curve in the Stage III strain hardening range can then be obtained using Eq. (40). The parameters k_1 and k_2 entering these equations can easily be found from strain hardening data [23]. Further aspects of the dislocation-density based, one-internal-variable models are discussed in Section 3.2. An adequate description of deformation stages beyond Stage III requires the use of a two-internal variable approach [255] where the evolution of ρ_w and ρ_c is considered in greater detail, cf. Section 3.3.

Concluding this section, it can be stated that the irreversible thermodynamics approach to dislocation-based plasticity of metals leads to a simple description of the dislocation density evolution and strain hardening. It recovers the well-known evolution equation of the one-internal-variable KME model [23, 182, 184, 327, 356, 357], but redefines the coefficients in that equation.

3.2. One-internal-variable models

A seminal model, which has set the scene for microstructure-based plasticity modelling and remains influential to the present day, is the Kocks-Mecking model [23, 182, 184, 327] that has been mentioned above repeatedly. The model hinges on the idea that the shear stress τ is determined by a dislocation contribution proportional to the square root of the total dislocation density ρ. This

dependence is given by Eq. (40), whose origin in the thermally activated dislocation glide is not obvious from the commonly used power-law strain rate dependence of the factor α :

$$\alpha = \alpha_o \left(\frac{\dot{\gamma}}{\dot{\gamma}_0} \right)^{1/m} \tag{53}$$

(Note that the strain rate sensitivity index m is the inverse of the exponent $m*$ in the Ludwig-Hollomon equation (9). The constant α_0 represents the athermal resistance to dislocation glide, i.e. the strength of dislocation-dislocation interactions at absolute zero temperature. The thermally activated character of the dislocation glide [288, 352, 358] is accounted for by the temperature dependent parameters m and $\dot{\gamma}_0$.

It is easily recognised [356] that the relation between $\dot{\gamma}$ and τ that follows from Eqs. (40) and (53)), $\tau = \alpha_o G b \sqrt{\rho} \alpha \left(\dot{\gamma} / \dot{\gamma}_0 \right)^{1/m}$, is equivalent to a physically motivated Arrhenius equation [358], if the exponent *m* is linked to the activation volume V_a for the underlying thermally-activated process:

$$m = V_a \tau / k_B T \tag{54}$$

This interpretation means that at sufficiently low temperatures *m* is inversely proportional to the absolute temperature *T* and is much greater than unity, while $\dot{\gamma}_0$ is temperature independent. This low temperature case (roughly below half the melting temperature) corresponds to the dislocation glide controlled regime. At sufficiently high temperatures, where dislocation controlled plasticity prevails *m* can be taken to be a constant; an Arrhenius-type temperature dependence then resides in $\dot{\gamma}_0$ [23, 182, 184, 327, 356].

In addition to the kinetic equation, $\tau = \alpha_o G b \sqrt{\rho} \alpha \left(\dot{\gamma} / \dot{\gamma}_0 \right)^{1/m}$, a further equation describing the evolution of the dislocation density is required. Equation (51) provides a general structure of such an evolution equation. The main microstructure-related quantity in this equation, the dislocation mean free path $\langle \lambda \rangle$, can be associated with the average spacing between the dislocations. Alternatively, once a dislocation cell structure has been formed, $\langle \lambda \rangle$ can be associated with the dislocation cell size. Both characteristic lengths are inverse in $\sqrt{\rho}$, so that the evolution equation for ρ can be written as

$$\frac{d\rho}{d\gamma} = \frac{k_1}{b} \sqrt{\rho} - k_2 \rho \tag{55}$$

The proportionality coefficient k_1 is, of course, different for these two cases, but the mathematical form of the evolution equation is the same. As a matter of fact, the transition from a random dislocation distribution to a self-organised cell structure can be describes through a suitable ansatz for a strain dependence of k_1.

Here a historical note is due. While this type of model is commonly associated with the names of Kocks and Mecking, some other authors also deserve credit for introducing the dislocation density evolution approaches. In particular, a tribute should be paid to Janusz Klepaczko who has been developing similar concepts independently [359]. A cognate model was put forward by Malygin [360]. Yngve Bergström has also been promoting the use of an evolution equation akin to Eq. (51) in its simplest form:

$$d\rho / d\varepsilon = M \left(\frac{1}{b \langle \lambda \rangle} - k_2 \rho \right) \tag{56}$$

considering the case of a constant dislocation mean free path $\langle \lambda \rangle$ [361]. Gottstein and Argon [362] have

extended Eq. (56) by considering the effect of subgrain boundary motion on the dislocation density evolution.

The dislocation mean free path $\langle\lambda\rangle$ in this equation can be governed by obstacles of various kinds at which gliding dislocations get immobilised. This is the term through which a lot of physical metallurgy can be captured. Thus, $\langle\lambda\rangle$ can be determined by the average spacing between non-shearable particles, the average distance between twins, the lamellae spacing in a lamellar structure, or the grain size, to name just the most common types of obstacles to dislocation glide. The latter case is of particular interest in the context of deformation of ultrafine grained materials produced by severe plastic deformation. However, identifying $\langle\lambda\rangle$ with the average grain size in modelling SPD processing is only sensible if the grain size is already saturated and does not vary in the process of deformation or if its variation with strain is known or can be modelled [363]. Holmedal [364] has recently redefined the mean free slip length enabling a straightforward geometrical interpretation that can be directly compared to the grain size. He suggested that the distribution of obstacles in the slip plane can be characterised by a fractal dimension so that the athermal storage rate of dislocations in Eq. (56) is proportional to $\langle\lambda\rangle^{D_F-2}$, which is particularly relevant for fine grained materials (a similar in sense assumption was made earlier by Hähner et al. [365] who argued that dislocation cell structures can be regarded as self-similar fractals characterised by power-law distributions of cell sizes, thus modifying the dislocation storage term in the KME equation. This idea was further promoted by Vinogradov et al. [344] who demonstrated the significance of the fractal dimension as an informative index to follow the spatial evolution of dislocation structures. With increasing grain size the dependence on the fractal dimension becomes weaker and it can be neglected for coarse grained pure metals where the classical interpretation of $\langle\lambda\rangle$ applies.

Examples of successful application of the KME model that employs an evolution equation for the dislocation density in the form of Eq. (51) can be found in [23, 182, 184, 327, 356]. Dalla Torre et al. [176] have tested the Kocks-Mecking and Estrin-Mecking model approach in an attempt to fit experimental tensile stress-strain curves of commercially pure copper deformed by ECAP to various strains (up to the cumulative equivalent strain of 16). As demonstrated, both models are applicable almost equally well, and both show an excellent agreement of model predictions with experimental data in Figure 17.

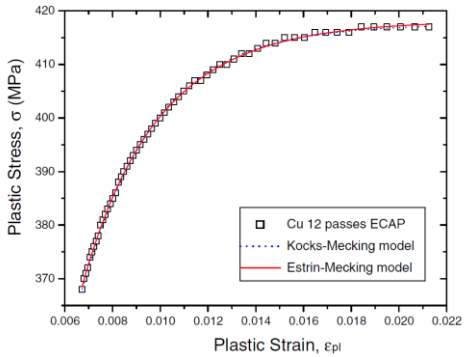

Figure 17. Results of least square fitting of the experimental true stress *vs.* true strain curve for Cu deformed by 12 ECAP passes (route Bc) at room temperature to the curves predicted by the Kocks-Mecking and Estrin-Mecking models (after [176], reproduced with permission)

An important aspect of the mechanical behaviour of UFG materials is their tensile ductility. The one-internal-variable model turns out to work well in predicting this property. If elongation to failure is controlled by the onset of necking, the corresponding necking strain can be calculated with the aid of linear stability analysis of Eq. (51), which governs the evolution of the dislocation density [366]. In a recent paper [367] we looked at the condition for tensile instability following from the KME model and found that for strain-rate insensitive materials ($1/m \to 0$) it reduces to the well-known Considère criterion (see [172] for a general review of plastic instabilities and their modelling). For non-zero $1/m$, the instability condition is akin to (yet not identical with) Hart's criterion. For the case when Eq. (56) holds, the tensile instability condition, in its simplified form, can be written as

$$\frac{\theta}{\sigma}+\frac{1}{m\varepsilon^{BEM}}\left(1-\frac{\sigma_0}{\sigma}\right)=1 \tag{57}$$

The new acronym 'BEM' introduced here refers to the model by Bergström [361] and Estrin & Mecking [23], corresponding to $k_1=0$, which is most appropriate for the case of small grain size d. (For this case, the dislocation mean free path $\langle\lambda\rangle$ is identified with d.) The quantity ε^{BEM} denotes the strain at the onset of necking and σ_0, as above, is a 'friction' stress at the onset of plastic flow (i.e. at the elastic-plastic transition). In the Kocks and Mecking (KM) formulation, $k_0=0$ in Eq. (51), the instability criterion reads as

$$\frac{\theta}{\sigma}\left(1-\frac{1}{m}\right)+\frac{1}{m\varepsilon^{KM}}\left(1-\frac{\sigma_0}{\sigma}\right)=1 \tag{58}$$

The main point made in Ref. [367] is that both conditions, Eqs. (57) and (58), are primarilty determined by the dynamic recovery coefficient k_2. Analysis of the stress-strain curves performed by Dalla Torre et al. [176] using a non-linear curve fitting has demonstrated that the magnitude of k_2 for copper specimens after ECAP is an order of magnitude larger than for the initial (non-deformed) coarse grained material. The role of the dynamic recovery coefficient k_2 was evaluated in Ref. [367] for UFG copper processed by ECAP to different numbers of passes, up to *N* = 12 [176, 368]. The experimental data and the model predictions were consistent. Both showed an increase in ductility of UFG copper with increasing number of ECAP passes. The effect was attributed to the observed decrease of k_2 with the progress of straining leading to a UFG microstructue with a large proportion of high-angle grain boundaries. In the analysis given in Ref. [367], all model parameters enter the expressions for the onset of necking. Remarkably, only one of them, k_2, appears in the pre-logarithmic factor, while the other ones (σ_0, k_0, and k_1) enter logarithmically. This becomes obvious from the explicit relations for the

necking strain, ε_{N0} , predicted by Yasnikov et al. Ref. [367] for the case when the Kocks-Mecking model applies:

$$\varepsilon_{N0}^{KM} = \frac{2}{k_2 M} \ln \left(\frac{1 + \frac{k_2 M}{2}}{1 + \frac{\sigma_0}{\alpha G b M \frac{k_1 / b \langle \lambda \rangle}{k_2}}} \right) \tag{59}$$

An equation for the BEM model similar to Eq. (59) in spirit, but more cumbersome mathematically, can be found in the original paper [367].

Thus, quite generally, among all model parameters, k_2 is the primary parameter that controls the necking strain. This is reflected in the graph for the necking strain ε_{N0} as a function of k_2 shown in Figure 18. The graph compiles the experimental data on copper available in literature [176, 369] and in the authors' own database. All data points are seen to fall on the same master curve, which is represented by a hyperbola, with good accuracy. An excellent agreement between the observed trends and the model predictions is evident. Similar results confirming the veracity of model predictions were reported for UFG copper and 316L austenitic steel [370, 371].

In line with the early work [372, 373] and more recent detailed investigations [344, 374-376], these results underscore the importance of the dynamic recovery parameter k_2 in the evolution of the dislocation density towards a steady state and the onset of necking that aborts this development. The experimental value of the phenomenological coefficient k_2 can readily be obtained from uniaxial tensile test data, e.g. by using a recipe proposed in [23] (cf. also [366, 367, 370, 377]). Assuming a specific microscopic dynamic recovery mechanism, the analytical form of the coefficient $k_2 = k_2(\dot{\gamma}, T)$ can also be obtained from theory. For example, Huang et al. [378], who modelled plastic deformation of metals

in terms of the Friedel-Escaig compact cross-slip mechanism [379], arrived at the following expression for the rate of dynamic recovery in FCC metals:

$$k_2 = \frac{Gb^4}{8\pi\,\chi_{SFE} V_a}\frac{\nu_D}{\dot{\gamma}}\exp\left[-A\ln\left(\frac{Gb^4}{16\pi\,\chi_{SFE} V_a}\frac{\nu_D}{\dot{\gamma}}\right)+\frac{\tau V_a}{Gb^3}\right] \tag{60}$$

Here χ_{SFE} denotes the temperature dependent stacking fault energy and *A* is a numerical constant (of the order of unity) for a given temperature.

With regard to the main object of this review, *viz.* ultrafine grained materials, it is instructive to note that very high values of k_2, on the order of several hundred, were reported for UFG materials produced by SPD, for which the KM approach to modelling of strain hardening of Cu [176], Ti [380], Al-Mg alloy AA5056 [381, 382], and 316L austenitic stainless steel [370] was applied. The predicted trends can easily be verified using the experimental data for these materials.

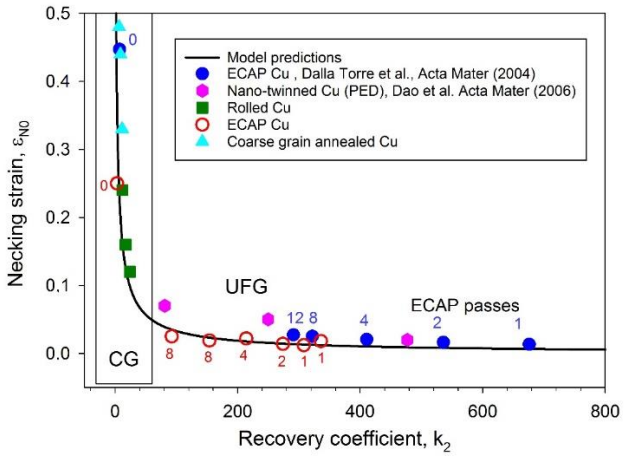

Figure 18. The calculated strain to the onset of necking (solid line) and the experimental data points as a function of the dynamic recovery coefficient k_2 for coarse grain (CG) and ultrafine grained (UFG) copper processed by ECAP. The calculated curve corresponds to a hyperbolic relation between ε_{N0} and $k_2 M$, cf. Eq. (59). The low tensile ductility of UFG copper after processing is seen to improve with the number of ECAP passes (cf. similar diagrams in [367] and [383]).

Because of the thermally activated nature of dynamic recovery, the coefficient k_2 is temperature and strain rate dependent. This dependence is represented in the form

$$k_2 = k_2\left(\dot{\gamma}, T\right) = k_2^*\left(T\right)\left(\frac{\dot{\gamma}}{\dot{\gamma}_0}\right)^{-\frac{1}{n^*}} \tag{61}$$

The parameter n^* in the exponent is, like *m*, much greater than unity [384]. To validate Eq. (61), we tested well annealed coarse grained copper and iron polycrystals with approximately the same grain size of 200 μm. In the strain rate range from 5×10^{-4} to 5×10^{-2} s^{-1}, k_2 did obey the $k_2 \sim \dot{\gamma}^{-1/n^*}$ relation. The value of *n** was found to be about 100, which is close to the exponent *m* entering the strain rate dependence of the flow stress through Eqs. (40) and (53) [184]. Similar results were also obtained for Cu tested over a wider range of strain rates from 10^{-4} to 1 s^{-1}, Figure 19 [184] (cf. Fig. 3 therein). The validity of Eq. (61) can thus be regarded as confirmed.

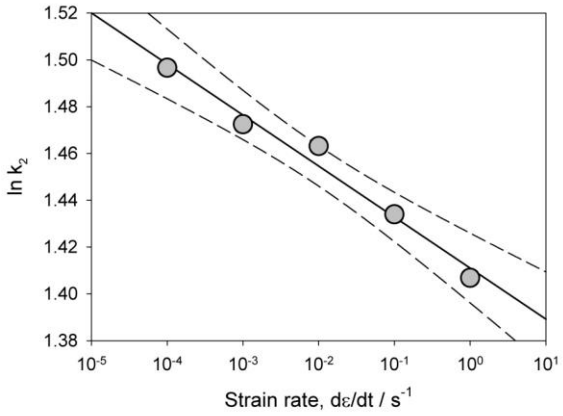

Figure 19. The dependence of the dynamic recovery coefficient k_2 on the strain rate for polycrystalline copper showing agreement with Eq. (61) (from [366], reprinted with permission, experimental data adopted from [184])

The differences in the deformation behaviour of FCC and BCC materials stem primarily from different crystallography of dislocation glide and cross-slip, as well as from the significance of the

double-kink mechanism of dislocation motion in the Peierls relief in BCC metals and alloys that will be discussed below. As a result, dislocations in BCC metals show greater propensity to annihilate (cf. the thermostatistical analysis of recovery processes in FCC and BCC metals performed in [376] and [375], respectively). This implies that the coefficient k_2 for BCC metals should be higher, which is, indeed, observed experimentally. Indeed, as shown in Figure 20 where data for polycrystalline Cu and Fe are compared, an excellent agreement with Eq. (59) is found: the smaller k_2, the greater is the uniform elongation up to the onset of necking, as given by ε_{N0}. The expected strain rate dependence of k_2 (Eq.(59), see also [367] and Figure 19), is also confirmed by Figure 20.

Obviously, Eq. (55) does not apply when the dislocation mean free path is controlled by extraneous obstacles, rather than dislocation-dislocation interactions. The length scale determining $\langle\lambda\rangle$ can be associated with such microstructural features as twin spacing, particle spacing in dispersion-hardened materials, lamellae spacing in lamellar materials, etc. In this case, the evolution equation, Eq. (55), assumes the form $d\rho / d\gamma = 1/b\langle\lambda\rangle - k_2\rho$ [380, 382, 384], which is mathematically equivalent to Eq. (56). For the ultrafine-grained materials, which are of main interest here, $\langle\lambda\rangle$ can be identified with the average grain size d or dislocation cell size d_c.

In this case, as well, the onset of necking is governed by the dynamic recovery coefficient k_2. The conclusions about the preponderance of k_2 as the control parameter in the instability condition still apply. Hence, high k_2 values are responsible for extremely small uniform elongation commonly observed for UFG metals [4, 384].

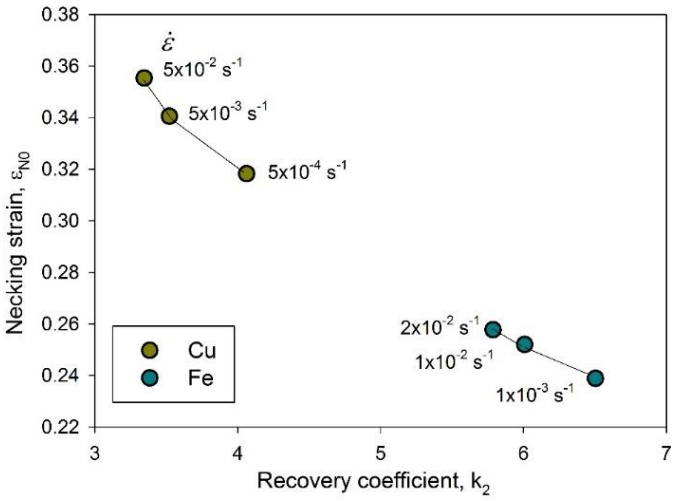

Figure 20. Experimentally found relation between the strain to the onset of necking, ε_{N0}, and the dynamic recovery parameter k_2 for pure polycrystalline copper and iron tested at different strain rates indicated on the graph. An excellent agreement with predictions by [366] is noted: the smaller the magnitude of k_2, the greater is the uniform elongation as represented by ε_{N0} (from [366], reprinted with permission)

The significance of the work by Yasnikov et al. [366, 367] is seen in the recognition that the Considère condition for necking can be derived from the evolution laws for the dislocation density – the governing internal variable of a microstructure-based constitutive model. The explicit form of the necking strain predicted on the basis of the Kocks-Mecking dislocation model highlighted the leading role of *dynamic recovery rate* in the onset of necking. By applying this approach to the case of strain rate sensitive materials, a modified instability condition, Eq. (58), with an added stabilising term proportional to $1/m$, was derived.

It is remarkable that essentially the same one-internal-variable approach that was considered for monotonic deformation turns out to be applicable to describing the material behaviour under cyclic loading. As a matter of fact, despite the complexity of the microstructures created by SPD, the cyclic behaviour of metals with a resulting UFG microstructure permits a simpler description than in the case of conventional coarse-grained poly- or monocrystalline materials. The reason is the absence of

dislocation patterning within the UFG structures. Indeed, the characteristic dimensions of the major structural elements - grains or dislocation cells - are smaller than the characteristic length scale of would-be dislocation structures that would form by self-organisation during cyclic loading. Vinogradov et al. [380, 382] suggested that in light of this argument it is sensible to describe the shape of a stable hysteresis loop and the cyclic stress–strain curve of UFG materials in terms of the one-internal variable approach. Assuming, as above, that the dislocation mean free path $\langle\lambda\rangle$ is controlled by the grain (or dislocation cell) size, integration of Eq. (51) with $k_1 = 0$ and the initial condition $\rho(0) = \rho_0$ yields:

$$\rho(\varepsilon) = \frac{k_0}{k_2 bd}\left(1 - e^{-Mk_2\varepsilon}\right) + \rho_0 e^{-Mk_2\varepsilon} \tag{62}$$

Combined with Eq. (31), this relation provides a simple analytical expression for the flow stress as a function of strain:

$$\sigma(\varepsilon) = M\alpha Gb\sqrt{\frac{k_0}{k_2 bd}\left(1 - e^{-Mk_2\varepsilon}\right) + \rho_0 e^{-Mk_2\varepsilon}} \tag{63}$$

where M is the Taylor factor, which connects the shear-related quantities with the axial ones: $d\gamma = Md\varepsilon$ and $d\tau = d\sigma / M$. To approximate the cyclic hysteresis loop, Vinogradov et al. [380, 382] applied a slightly different variant of the KME model. It reduces to the model originally proposed by Essmann and Mughrabi [372] for dislocation annihilation:

$$\tau = \alpha Gb\sqrt{\frac{1 - \exp\left(-2y\gamma / b\right)}{d\, y}} \tag{64}$$

Here y is the 'annihilation length' for the dislocation density evolution during stable cyclic deformation. It represents a capture radius of a dislocation residing in a grain boundary within which trapping of a passing dislocation would occur. The model involves the assumption that mobile dislocations generated at a grain boundary pass through the grain and disappear at the opposite grain

boundary. This assumption is supported by molecular dynamics simulations [385-388] which demonstrated the efficacy of grain boundaries as sources and sinks for dislocations. A similar picture is provided by an elaborate analytical dislocation bow-out model for dislocation nucleation at grain boundaries in ultra-fine grain materials [320]. It considers the following stages of the process: (i) a dislocation is emitted from a grain boundary source, (ii) it bows out between the pinning points located at the boundary, (iii) yielding occurs when the dislocation takes a semi-circular shape and (iv) the dislocation breaks away from the source and travels across the grain thus producing an increment in plastic strain. TEM evidence also suggests that during cyclic loading no dislocation accumulation occurs within the fine grains. Indeed, TEM observations did not reveal substantial differences between the initial and the post-fatigue structures in pure FCC metals (provided no fatigue-induced dynamic grain coarsening occurs [389, 390]). A good agreement of the model predictions and the experimental results for UFG Al-Mg alloy AA5056 [380, 382] and titanium [380, 382] produced by ECAP was found, cf. Figure 21 and Figure 22. This is surprising in view of the simplifications made. A major simplification was that back stresses associated with plastic incompatibility between the two 'phases' were not considered. A characteristic ascending part of the stable hysteresis loop of the ECAP-processed poly- and monocrystalline copper, cf. Figure 21a, is similar to that reported in Refs. [380, 382] for AA5056. An excellent agreement between the experimental hysteresis loops and the experimental data fitted by the functions given by Eq. (63) or Eq. (64) is remarkable.

An ideal object for trialling various dislocation-based strain hardening models is a single crystals whose crystallographic orientation with respect to the processing tool is well controlled in experiment. With this in mind, copper single crystals with a {110} initial crystallographic orientation were pressed through a 90^{o} ECAP die [26, 28]) and then subjected to uniaxial push-pull cyclic loading. Figure 21 and Figure 22 show the results of these tests. It is seen that during a single ECAP pass no high-angle grain boundaries were formed, Figure 22b. The observed microstructure characterised by a well-developed

cell structure [391, 392] is consistent with fragmented structures formed at large strains that were found by early experimental observations [393, 394]. A very large strengthening effect, which was found comparable in magnitude with that for copper polycrystals of the same purity deformed by ECAP under the same conditions, was obviously achieved entirely due to dislocation storage in a network of cell walls with low angles of misorientation. Not surprisingly is that such dislocation ensembles tend to recover during cyclic plastic deformation giving rise to a well-known cyclic softening. The KME model correctly captures this phenomenon as well by appropriate setting of initial conditions for the dislocation density [380, 382]. Furthermore, the cyclic stress-strain curve characterising the cyclic hardening or softening response for conventional polycrystals and fine-grained specimens manufactured by SPD can also be approximated by an equation of the same type, cf. Figure 21b. Klemm, Mughrabi and Höppel [395, 396] applied essentially the same model for cyclic deformation of UFG nickel processed by various SPD techniques. Both groups of researchers arrived at the same, in effect, conclusions. They also obtained similar values for the dislocation mean free path entering Eq. (64) explicitly as *d* and the annihilation distance, *y,* which is contained in k_2 implicitly. A further example of a successful interpretation of the stable cyclic hysteresis loops in terms of the KME approach was reported for UFG titanium fabricated under different SPD processing schedules [4, 397]. A reasonably good agreement between the model fit and the experimental data was observed, similar to a good accord between modelling and experiment found in Refs.[380, 382, 395, 396]. An interesting detail is that in the low strain limit, Eq. (63) reduces to

$$\sigma \approx M\alpha Gb\sqrt{\frac{\left(k_0 - k_2\rho_0\right)M\varepsilon}{b\,d} + \rho_0} \tag{65}$$

which represents the Hall–Petch type strengthening: a $\sigma \propto d^{-1/2}$ dependence of the flow stress at a fixed strain is recovered, in agreement with the experimentally observed stress-strain behaviour for both monotonic and cyclic modes of deformation and in harmony with a group of strain hardening

models of the Hall-Petch relation [316-318]. The fatigue limit of many metals with UFG structure: produced by SPD also follows the same trend [380].

An approach more rigorous methodologically would require accounting for the composite-like structure comprised of dislocation-rich walls and dislocation-depleted cell interior. This would encourage invoking two-internal variable models distinguishing between at least two kinds of dislocations involved: 'cell' and 'wall' (or 'mobile' and 'immobile') dislocations differed by their density and mobility, as outlined above. A proper account of back stresses is also a necessary ingredient of any model aiming at describing cyclic plastic deformation as has been illustrated in a model by Estrin et al. [398] for ordinary polycrystals).

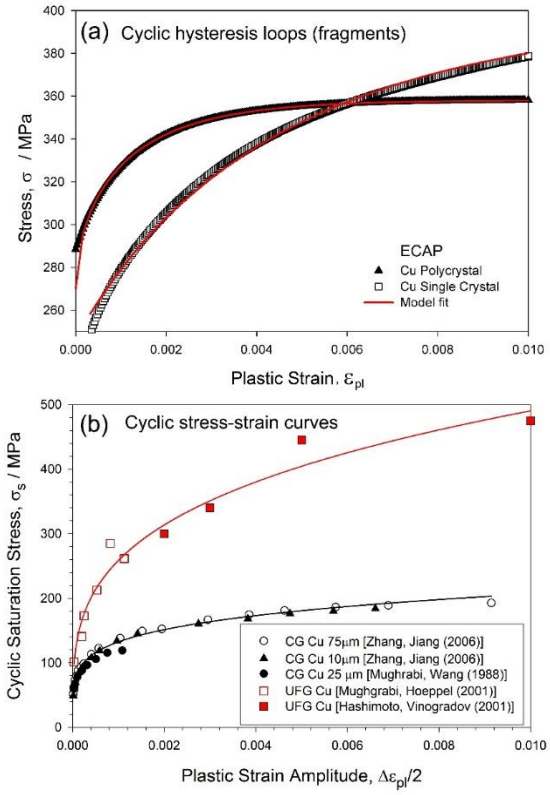

Figure 21. Ascending parts of the stable hysteresis loop of pure 99.96% copper poly- and single-crystals subjected to one ECAP pass through a 90° die at ambient temperature. Curve fits by Eq. (63) are shown by solid lines. The references to the data used are given in [380, 382].

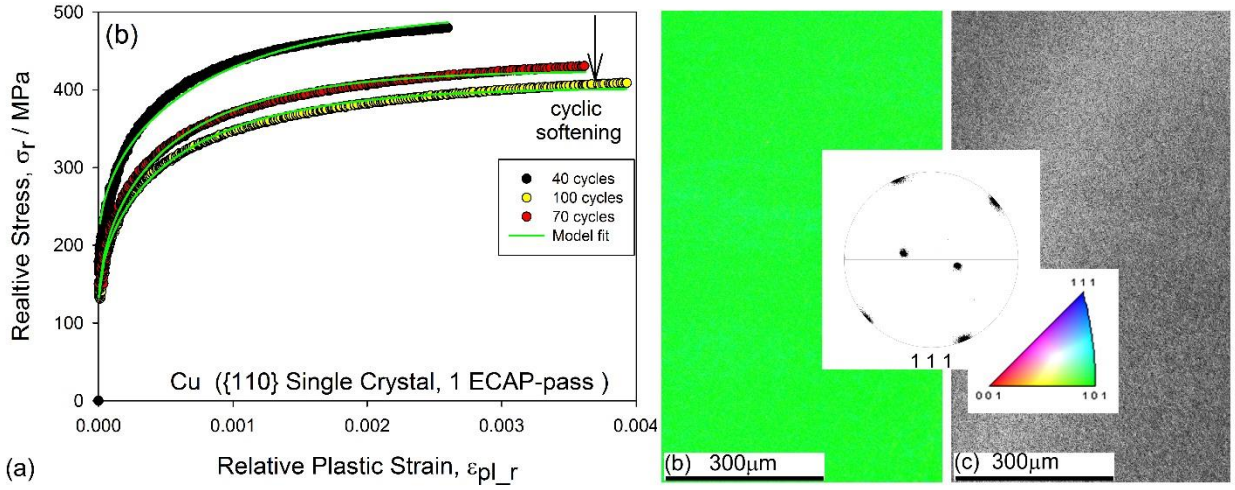

Figure 22. Fragments of the cyclic hysteresis loops obtained for a {110} oriented copper single crystal after one ECAP pass. Cyclic softening is illustrated by the reduction in the stress amplitude with increasing number of cycles; curve fits by Eq.(63) are shown by solid lines (a); the EBSD map (b) and the secondary electron image (c) of the same single crystal after the first ECAP pass do not exhibit any high angle grain boundaries; the inset shows a (111) pole figure [26, 28] reproduced with permission.

As mentioned above, the quality of the model predictions based on the assumed dislocation density evolution expressed by Eq. (51) is surprisingly good, given that this evolution equation does not reflect any specificity of UFG materials. Bouaziz et al. [399] modified this model to provide it with the specificity the original one-internal-variable model was lacking. The premise they used was that there exists a critical grain size d_{crit} below which no further grain refinement would occur regardless of how severe the deformation is (this assumption is well supported by abundant experimental data [400-402], cf. Figure 23. They defined this critical quantity as the grain size for which the time for a dislocation to traverse a grain is equal to the time it takes the dislocation arriving at the opposite grain boundary to be accommodated there. The accommodation was assumed to be furnished by diffusion-controlled relaxation processes. The corresponding expression for the critical grain size reads

$$d_{crit} = \left(\frac{D_{GB}\, b}{\dot{\gamma}} \right)^{1/3} \tag{66}$$

where D_{GB} is the grain boundary diffusivity. For $d << d_{crit}$, the diffusional relaxation is predominant and grain boundaries lose their ability to impede dislocation motion. Obviously, in this case the Hall-Petch relation loses its validity, as well. In this regime, strain hardening vanishes, too. The critical grain size is governed by strain rate and, through the grain boundary diffusivity, temperature. More specifically, d_{crit} can be reduced by increasing the strain rate or dropping the temperature.

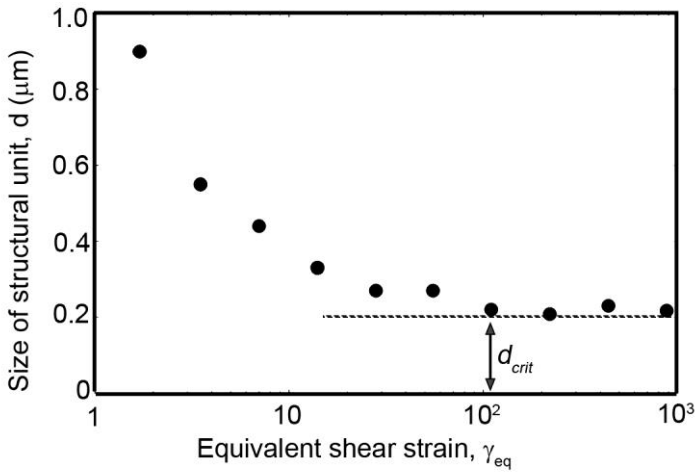

Figure 23. Size of a structural element in Cu deformed by HPT to giant strains at room temperature as a function of equivalent strain (adapted from [402], reprinted with permission)

To 'smoothen' the transition from strain hardening to no-strain-hardening behaviour when the average grain size passes through the $d = d_{crit}$ 'watershed', Bouaziz et al. [399] suggested modifying Eq. (51) in the following way:

$$\frac{d\rho}{d\gamma} = \frac{k_o}{bd} P + \frac{k_1\sqrt{\rho}}{b} - k_2\rho \qquad (67)$$

The factor

$$P = \exp\left[-\left(\frac{d_{crit}}{d}\right)^3\right] \tag{68}$$

switches off the effect of dislocation storage at grain boundaries for $d << d_{crit}$ by eliminating the first term on the right-hand side of Eq. (67). This modification of the KME model, whilst retaining all its features, including an increase of strain hardening with grain refinement as long as $d > d_{crit}$ holds, predicts a precipitous decline in the dislocation storage (and hence a loss of strain hardening) once the grain size drops below d_{crit} .

Constitutive modelling of materials with a high Peierls stress

The constitutive models outlined above tacitly assume that the Peierls stress, which is always present in a crystalline material [38], is sufficiently small, which is the case for FCC metals and alloys. However, the inherent flexibility of the constitutive modelling allows for easy adaptation to other systems where the Peierls barrier for dislocation motion can no longer be neglected, e.g. in body centred cubic (BCC) metals. An example was provided in [403], where the strain hardening of ferritic steels was modelled. To a first approximation, the Peierls stress σ_p entered Eq. (40) for the flow stress as the additive contribution along with the dislocation-related stress:

$$\sigma = \sigma_P + M\alpha_0 Gb\sqrt{\rho}\left(\frac{\dot{\varepsilon}}{\dot{\varepsilon}_0}\right)^{1/m} \tag{69}$$

The Peierls stress represents an activation barrier for dislocation motion in the crystal lattice, and as such it is temperature and strain rate dependent. This has to be accounted for in the model, along with the possible influence of the dislocation density. Considering the thermally-activated kink mechanism for the dislocation motion in a BCC lattice, an appropriate relation is obtained for the average dislocation velocity entering the Orowan equation for the plastic strain rate as [38]:

$$\dot{\varepsilon} = \frac{\rho_m b}{M} v_D \frac{2bh_k^2 a_k}{k_B T} \frac{\sigma_P}{M} \exp\left(-\frac{F_k^{'}(\sigma_P / M) + W_m}{k_B T} \right) \left(\frac{\tilde{L}}{\tilde{L} + X} \right) \tag{70}$$

Here $F_k^{'}(\sigma_P / M)$ denotes the Peierls stress dependent energy required to create a kink on a dislocation, W_m stands for the activation energy for kink migration along the dislocation line, and a_k and h_k are kink geometry parameters (both are of the order of the Burgers vector *b*). The parameter X defines the average distance between individual kinks on the dislocation line, which, in thermal equilibrium, is given by the equation

$$X = 2a_k \exp\left[F_k^{'}(\sigma_P / M) / k_B T \right] \tag{71}$$

The quantity $\tilde{L}$ stands for the distance between the pinning points on the dislocation line. In the case when the pinning points are associated with dislocation forest junctions, $\tilde{L}$ scales with the inverse square root of the dislocation density, as noticed above. Accordingly, for small dislocation density, when $\tilde{L} >> X$ holds, the last factor in Eq. (70) reduces to unity and the single kink formation energy enters the exponential in Eq. (70) . In the opposite limit case, $\tilde{L} << X$, the last factor in Eq. (70) is given by $\tilde{L} / X$, so that the *double* kink formation energy turns out to be rate controlling. Using a particular form of the stress dependence of the kink formation energy [404]

$$F_k^{'}(\tau) = F_k \left[1 - \left(\frac{\tau}{\tau_p} \right)^{0.8} \right]^{1.3} \tag{72}$$

where τ_p is the Peierls shear stress at absolute zero temperature, this model has been successfully applied to describing the mechanical behaviour of a TRIP steel with co-existing ferritic and austenitic phases [405].

Although the above model for high Peierls stress materials represents the strain hardening behaviour of conventional coarse-grained BCC materials quite well, the additive form of Eq. (62) is a simplification. A more elaborated theory, which does not rely on a simple 'de-coupling' of the contributions of the localised obstacles and the Peierls relief to the overall stress, was presented in [406, 407]. Still, the above simplified additive model can be applied to account for differences in the deformation behaviour of ultrafine-grained FCC and BCC materials. Specifically, striking differences in the strain rate sensitivity of their flow stress [408] can be rationalized in this way. Indeed, for UFG materials $\tilde{L}$ may be identified with the grain size d suggesting pinning of dislocations at grain boundaries.

Assuming $d \ll X$, Eqs. (70)-(72) yield

$$\dot{\varepsilon} = \frac{\rho_m b}{M} \nu_D \frac{b h_k^2 \tilde{L}}{k_B T} \frac{\sigma}{M} exp\left(- \frac{2F_k \left[1 - \left(\sigma / \sigma_p \right)^{0.8} \right]^{1.3} + W_m}{k_B T} \right) \tag{73}$$

It is noted that through X, a second single kink formation energy enters the exponential. Hence, the total activation energy is controlled by the *double kink energy,* as distinct from the case of $X << min\left\{ d, \rho^{-1/2} \right\}$, which applies for conventional, coarse-grained materials, for which the expression for the strain rate reads

$$\dot{\varepsilon} = \frac{\rho_m b}{M} \nu_D \frac{2 b h_k^2 \tilde{L}}{k_B T} \frac{\sigma}{M} exp\left(- \frac{F_k \left[1 - \left(\sigma / \sigma_p \right)^{0.8} \right]^{1.3} + W_m}{k_B T} \right) \tag{74}$$

By inverting these equations one obtains the following expression for the UFG case

$$\sigma = \sigma_p \left\{ 1 - \left\{ \frac{W_m}{F_k} + \frac{k_B T}{2F_k} \ln\left(\frac{\dot{\varepsilon}}{\dot{\varepsilon}_o} \right) \right\}^{1/1.3} \right\}^{1/0.8} \tag{75}$$

For the coarse grain case, the relation between the flow stress and the logarithm of the strain rate reads

$$\sigma = \sigma_p \left\{ 1 - \left\{ \frac{W_m}{F_k} + \frac{k_B T}{F_k} \ln\left(\frac{\dot{\varepsilon}}{2\dot{\varepsilon}_o} \right) \right\}^{1/1.3} \right\}^{1/0.8} \tag{76}$$

Here the notation

$$\dot{\varepsilon}_0^* = \frac{\rho_m b v_D}{M} \frac{b h_k^2 a_k}{k_B T} \frac{\sigma}{M} \tag{77}$$

has been introduced.

A comparison of Eqs. (75) and (76) shows that the strain rate sensitivity of the flow stress, $S = \partial\sigma / \partial \ln \dot{\varepsilon}$, for a body-centred cubic UFG metal is just about one half of that for its coarse-grained counterpart (a weak logarithmic dependence of $\dot{\varepsilon}_0^*$ on stress can, of course, be neglected). The above considerations provide an alternative to the screw dislocation starvation argument of Cheng et al. [408], or, for that matter, may work in concert with it.

Constitutive modelling of hexagonal materials

The mechanical response of materials with HCP lattice represent a significant challenge to constitutive modelling. Indeed, the scarcity of independent slip systems active in HCP metals at low homologous temperatures leads to plastic incompatibilities between the adjacent grains, which need to be considered in the model. This can be addressed by introducing the incompatibility-induced back stress σ_B and including it on the right-hand side of Eq. (69) as an additive term, as suggested in [409, 410]:

$$\sigma = \sigma_P + M \alpha_0 G b \sqrt{\rho} \left(\frac{\dot{\varepsilon}}{\dot{\varepsilon}_0} \right)^{1/m} + \sigma_B \tag{78}$$

The kinetic equation describing the evolution of the back stress is written as

$$\frac{d\sigma_B}{d\varepsilon} = \left(\tilde{K} - \left(\tilde{Q} + \frac{\tilde{R}}{\dot{\varepsilon}} \right) \sigma_B \right) \tag{79}$$

where the phenomenological parameters introduced have the following meanings: $\tilde{K}$, which scales with the elastic modulus, represents the rate of linear increase of the incompatibility stress with strain, $\tilde{Q}$ is a temperature dependent parameter which characterises the rate of dynamic relaxation of the incompatibility stress, and $\tilde{R}$ controls the rate of time-driven, diffusion-controlled static relaxation. The KME model extended in this way, with a slight modification, was shown to predict the deformation behaviour of an HCP alloy Zircaloy-4, including its response to monotonic loading and strain rate jumps [409], in an excellent way, cf. Figure 24.

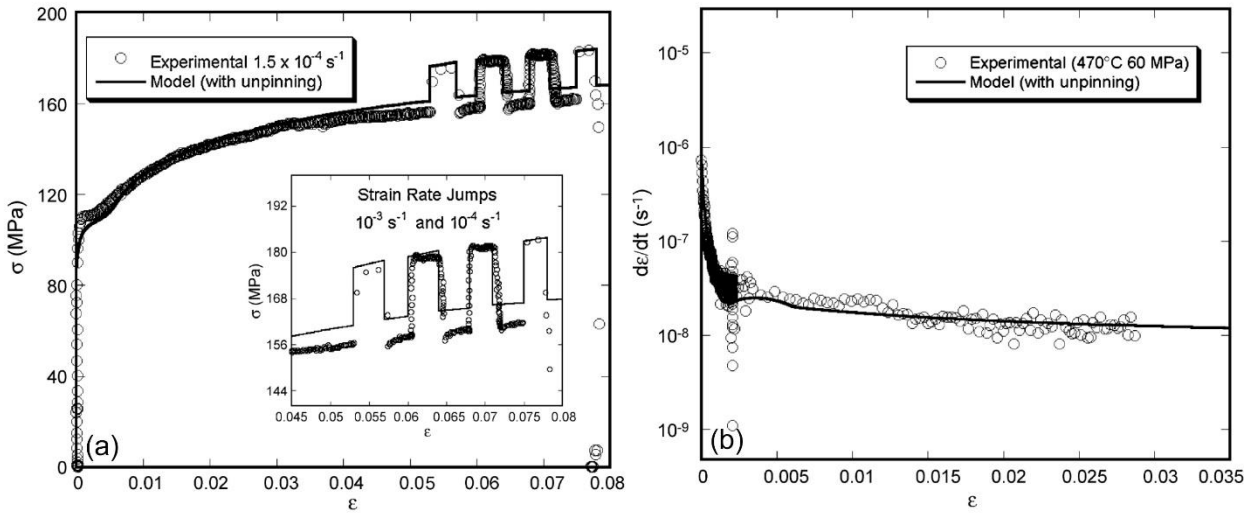

Figure 24. Mechanical behaviour of recrystallised Zircaloy-4 at 470°C: stress-strain curve at constant strain rate and strain rate jump testing (a) and creep rate curve at 40 MPa (b). Experimental data and model results are represented by open circles and solid lines, respectively [409].

Inclusion of deformation twinning in the constitutive modelling

In order to account for twinning in a constitutive description of the hardening behaviour of cubic or hexagonal metals, the dislocation-based model was extended further by Bouaziz et al. [411-413].

They considered the freshly formed twin boundaries bounding the deformation twins as effective obstacles to dislocation motion, thus causing a 'dynamic Hall-Petch effect' due to grain fragmentation by twin lamellae. The model predictions were found to be in good agreement with tensile test results for ferritic and austenitic steels. However, Gil Sevillano et al. [414, 415] questioned this model because it only took into account the effect of internal back stresses caused by dislocations in the structure. They proposed an alternative model that was built on the assumption that strength of the thin twin lamellae represents a significant contribution to the overall strength of the twinned aggregate. The strength of a twin lamella was considered to be very large compared to that of the matrix owing to its small (nanometre scale) thickness. The twin lamellae thus experience a forward internal stress while the matrix is under a back stress - in line with the two-phase 'composite' model due to Mughrabi [350]. However, this model still awaits experimental verification in terms of the internal stress distribution between the twins and the matrix. With regard to HCP metals, a contribution to plastic strain due to twinning was included [410] in the way suggested by Bouaziz et al. [416] for low stacking-fault alloys (TWIP steels). Following that work, evolution of the twin volume fraction F was considered as a sigmoidal function of strain:

$$F = F_o + \left(F_\infty - F_o\right)\left[1 - \exp\left(-\frac{\varepsilon - \varepsilon_{onset}}{\tilde{\varepsilon}^*}\right)\right] \tag{80}$$

The parameter $\tilde{\varepsilon}^*$ controls the rate of growth of F from an initial value F_0 at the strain ε_{onset}, at which twinning sets in, to a saturation one, F_∞, reached asymptotically as strain increases. The total strain is represented as a sum of two components: the strain due to dislocation glide, ε_g, and that produced by twinning ε_t. In the differential form this reads as

$$d\varepsilon = (1-F)d\varepsilon_g + \varepsilon_t dF \tag{81}$$

Since twin boundaries can serve as sources of dislocations, the evolution equation for the total dislocation density, Eq. (51), was modified by including an additive twin-induced contribution on the right-hand side:

$$\frac{d\rho}{d\varepsilon_g} = M\left[k_1\sqrt{\rho} + \frac{1}{bd_m} + \frac{F}{2eb(1-F)}H\left(\varepsilon-\varepsilon_{onset}\right) - k_2\rho\right] \tag{82}$$

Here e is the twin thickness and d_m is the mean grain size.

For an experimental verification, the above version of the one-internal-variable model was tuned for α-titanium [410]. Figure 25 represents an example of good agreement between the experimental data and calculated deformation curves (including strain rate jump episodes) is shown in It should be mentioned that a provision for accounting for small grain-size effects is included in the model through the second term on the right-hand side of Eq. (80). Application of the model to UFG titanium and other fine-grained HCP metals are thus possible.

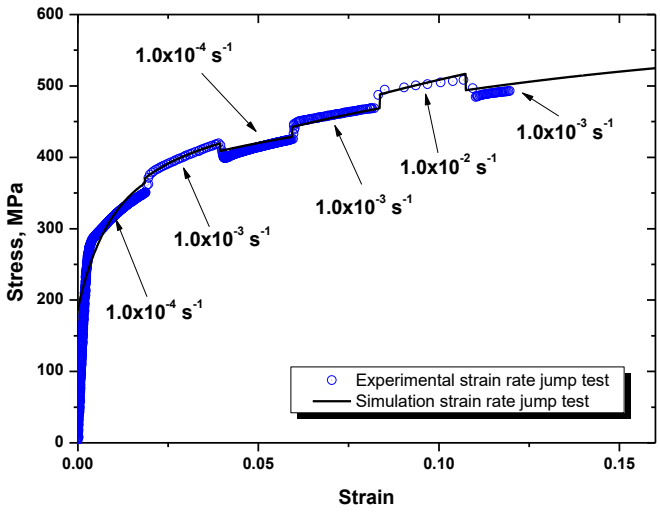

Figure 25. A comparison between the calculated and the experimental stress-strain curves for α-Ti deformed in tension at room temperature [410].

Inclusion of twinning as an important ingredient of constitutive modelling may appear to be less relevant in the context of UFG materials, as the role of twinning is reduced upon grain refinement [417, 418]. However, experimental evidence suggests that twinning does occur in UFG metals with sufficiently low stacking-fault energy [419-423] and, even more surprisingly, in high stacking-fault energy materials such as aluminium [424] and nickel [425], which do not exhibit twinning under normal testing conditions. Thus, twinning should be considered as a possible deformation mode in an extended constitutive model for UFG metals. As suggested above, this can be done through an appropriate evolution equation for the dislocation density, such as Eq. (82), and an additional equation describing the evolution of the twin volume fraction. The common approach suggested in earlier models and expressed by Eq. (80) is to consider the variation of F with strain. In our current thinking, however, this evolution is better represented in terms of the variation of F with stress, rather than strain. The stress-driven variation of the twin volume fraction was a basis for our recent model [426]. The main assumptions of the model can be summarised as follows. (i) As often observed in experiment [420], a twin nucleated in a fine grain shoots through the entire grain. Accordingly, its length is dictated by the grain size *d*. (ii) The average thickness of the nucleated twin, e, is considered to be grain size independent. (iii) The generated twin is assumed to be in equilibrium for which case Friedel's formula for the shear stress for twinning [40] can be applied:

$$\tau \cong \frac{G}{2} s \frac{e}{d} \tag{83}$$

Here *s* is the amount of shear strain produced by the twin. (iv) Twinning is not considered to be a significant contributor to plastic strain. It is activated gradually as the stress rises owing to strain hardening due to dislocation glide controlled plasticity. Smaller and smaller grains get engaged in twinning with growing stress according to Eq. (83). This gives rise to a continual increase of the twin volume fraction. (v) The grain size distribution in the material is described by a function $f(d)$, which in

[426] was taken to be log-normal. This form of the distribution function, while not being binding, is supported by experimental evidence abundant in literature, see, e.g. [427].

Under these assumptions, the growth rate of the twin volume fraction is governed by the rate with which the grain population is 'scanned' for those grains which are ripe for twinning at a given stress level. In terms of the derivative with respect to strain, this relation reads

$$\frac{dF}{d\varepsilon} = \tilde{\chi}\frac{ed^2}{d_m^3} g(\sigma)\frac{d\sigma}{d\varepsilon} \tag{84}$$

Here $\tilde{\chi}$ is a parameter that contains as a factor the fraction of grains capable of undergoing twinning, which is texture-dependent. Further quantities in Eq. (84) are as follows: $g(\sigma) = f(d(\sigma))\frac{M^2 Gse}{2\sigma^2}$ and $d = d(\sigma)$ is a function of the current flow stress $\sigma = M\tau$ with τ given by Eq. (83).

The model outlined was shown to work very well for the case of a conventional, coarse grained material. It was validated by tensile tests, scanning electron microscopy, and acoustic emission measurements on Mg alloy ZK60 [426]. Figure 26 demonstrates a very good agreement between modelling results and experimental data on the evolution of the twin volume fraction assessed by the advanced acoustic emission technique employed. Model verification for UFG materials is yet to be provided.

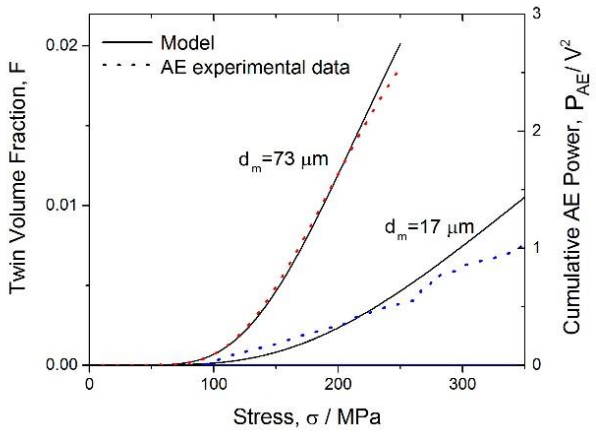

Figure 26. Twinning model verification for Mg alloy ZK60 for two values of the average grain size, d_m=73 μm and 17 μm (after [426], reproduced with permission).

3.3. Two-internal-variable models

As demonstrated in the foregoing sections, it can be considered as established that one-internal-variable models based on the Kocks-Mecking approach provide a reliable description of mechanical response of metals and alloys, especially for low to moderate strains. However, they do not account for the occurrence of late stages of strain hardening beyond Stage III [58, 428]. Stages IV and V extend well into a range of very large strains pertinent to SPD processing. This calls for more sophisticated models that would adequately describe a material's behaviour at very large strains. Two-internal-variable models have a better chance to satisfy this expectation, as they possess greater flexibility in describing microstructure evolution during SPD processing and the mechanical properties of the processed materials [429]. As discussed in Section 3.1, a dislocation cell structure emerged during plastic deformation can be seen as a pre-cursor of the final grain structure to be formed at large strains, particularly under SPD. Splitting the dislocation population into cell interior and cell wall dislocations [254, 255, 350, 430-433] already mentioned above appears to make more sense in the case of cell-forming materials than subdividing it into mobile and immobile dislocations, as was done in Refs. [185, 429, 434]. Our first-hand experience with constitutive models involving two dislocation densities [254,

255] gives us confidence that they are well suited for modelling in the SPD realm. These models are presented below, along with other models based on similar concepts.

The underlying assumption is that a dislocation cell structure already exists. The overall share stress is then given by a linear combination of two components (cell walls and cell interiors), each of them being related to the respective dislocation density (ρ_w in the walls and ρ_c in the interior). The key characteristic of the dislocation structure, *viz.* the average dislocation cell size, d_c , is assumed to be inversely proportional to the square root of the total dislocation density *ρ:*

$$d_c = K_o / \sqrt{\rho} \tag{85}$$

where K_o is a constant. This is a safe assumption, which follows from dimensional considerations repeatedly proven by TEM observations [351]. Similarly to Eq. (43), ρ , is given by a weighted sum of the dislocation densities in the two 'phases' of the material:

$$\rho = f_w \rho_w + (1 - f_w)\rho_c \tag{86}$$

There is an obvious relation between the volume fraction of the cell walls, f_w , and the geometrical parameters of the cell structure, i.e. the cell size and the wall thickness, *w*. Regardless of the cell morphology, f_w can quite generally be expressed as

$$f_w \cong 3w / d_c \tag{87}$$

where d_c represents the characteristic size of the cells. For instance, for spherical grains it can be interpreted as the average sphere diameter, while for cuboidal grains it can be interpreted as the average cube size. As seen from Eqs. (85) and (86), the cell size will typically decrease during the deformation process, owing to an increase in the dislocation density. His would mean that f_w is an increasing function of strain. Experiment shows an entirely different behaviour, however. In the case of

copper deformed to large strain in torsion, f_w was found to continuously drop from an initial value f_{wo} to a lower saturation value $f_{w\infty}$. The variation of f_w with the plastic shear strain γ is well represented by a heuristic equation [254, 255]:

$$f_w = f_{w\infty} + \left(f_{wo} - f_{w\infty} \right) \exp\left(-\gamma / \tilde{\gamma} \right) \tag{88}$$

The rate of decrease of the cell volume fraction described by this equation is determined by a model parameter $\tilde{\gamma}$. Considering Eq. (87), the observed decrease of f_w represented by Eq. (88) can only mean that the wall thickness must decrease with strain fast enough to compensate for the decrease in the cell size. This 'slimming' of cell walls may be associated with progressive annihilation of dislocations, which a random or 'redundant' in the cell walls in the sense that they do not contribute to misorientation between the cells separated by the walls. We note that the above heuristic relation can be replaced by another one, based on the idea that w should scale with $1/\sqrt{\rho_w}$. With the ansatz $w \cong 1/\sqrt{\rho_w}$ one obtains by combining Eqs. (85) and (86): $f_w \cong (3/K_o)\sqrt{\rho/\rho_w}$. The ratio of the dislocation densities in this formula is not a constant, but rather contains f_w. Accordingly, it can be regarded as an implicit equation that needs to be solved in order to calculate the variation of the volume fraction of cell walls with strain. Within a reasonable range of values of the model parameters, a decline of f_w with strain is predicted.

A practical assumption in applying the two-internal-variable model under consideration is to assume that Taylor-type (iso-strain) condition holds for the cell interiors and the cell walls, i.e. that the plastic strain in these two 'phases' is the same. A set of coupled differential equations that describe the evolution of the dislocation densities in the two 'phases' reads

$$\frac{d\rho_w}{d\gamma} = \frac{6\beta^*(1-f_w)^{2/3}}{bdf_w} + \frac{\sqrt{3}\beta^*(1-f_w)\sqrt{\rho_w}}{bf_w} - k_2^*\left(\frac{\dot{\gamma}}{\dot{\gamma}_0}\right)^{-1/n^*}\rho_w \quad (89)$$

$$\frac{d\rho_c}{d\gamma} = \alpha^*\frac{1}{\sqrt{3}}\frac{\sqrt{\rho_w}}{b} - \beta^*\frac{6}{bd(1-f_w)^{1/3}} - k_2^*\left(\frac{\dot{\gamma}}{\dot{\gamma}_0}\right)^{-1/n^*}\rho_c \quad (90)$$

In earlier publications [254, 255], a physical interpretation of the various terms in Eqs. (89) and (90) was offered. For instance, the loss of cell interior dislocations to the walls is accounted for by the first term on the right-hand side of Eq. (89). The concomitant gain in the wall dislocation density is captured by the second term in Eq. (90). Dynamic recovery by dislocation cross-slip in the low-temperature regime typical for SPD processing finds its representation in the last term in both equations. Both exponents entering the model, *m** and n^*, can be taken to be inversely proportional to the absolute temperature *T*. Further model parameters, α^*, β^*, and k_2^*, are considered constant. If dynamic recovery in cell walls is controlled by dislocation climb, as assumed by Zehetbauer and co-authors [428, 431, 435], $\dot{\gamma}_o$ in Eq. (89) is no longer a constant. Rather, it is given by an Arrhenius equation. The activation energy in this equation is that for self-diffusion; the exponent *n** is a constant. In modelling of SPD, whose signature feature is a high hydrostatic pressure, the model needs to be modified to include the pressure dependence of dynamic recovery by climb [436]. This was done in [222] where an exponential pressure dependence of the dynamic recovery term was included in the last term in Eq. (89). With this modification, the model was used to elucidate the effect of back pressure on the ECAP processing of an Al alloy [222].

A further modification of the set of the evolution equations (89) and (90) for the dislocation densities in cell forming metals was proposed by Hosseini and Kazeminezhad [437]. Keeping the basic assumptions the same as in the general two-internal variable model considered above, their model makes a distinction between edge and screw dislocations and divides the whole population of

dislocations into three categories: mobile and immobile dislocations in the cell interior and immobile dislocations in cell walls. The authors assumed that the recovery in the cell interior occurs by cross-slip of screw dislocations while the recovery kinetics in cell walls is governed by climb of edge dislocations. The set of the evolution equations for the cell interior and cell wall dislocation densities according to Ref. [438] reads as follows:

$$\begin{aligned}\frac{d\rho_c}{dt} &= \frac{\alpha^*}{\sqrt{3}}\frac{\sqrt{\rho_w}}{b}\dot{\gamma}_w - \frac{6\beta^*}{bd(1-f_w)^{1/3}}\dot{\gamma}_c - \frac{\chi^* \nu_D \sqrt{\rho_c}}{l'}\left[\exp\left(\frac{\frac{\tau_c^0}{G}Q_{cross-slip}}{k_B T}\right)\right] \\ \frac{d\rho_w}{dt} &= \frac{6\beta^*(1-f_w)^{2/3}}{bd\,f_w}\dot{\gamma}_c + \frac{\sqrt{3}\beta^*(1-f_w)\sqrt{\rho_w}}{bf_w}\dot{\gamma}_c - \frac{\delta^* G b^3 D_L \rho_w^2}{k_B T}\end{aligned} \tag{91}$$

where D_L is the lattice diffusivity, $Q_{cross-slip}$ is the activation energy for the cross-slip of screw dislocations, l' is the size of a potential site for cross-slip and δ^* and χ^* are numerical constants. Although this attempt to provide more microscopic details of the recovery process is appealing, the way in which recovery was treated in that model is questionable. Indeed, the recovery effects enter both equations (91) as *static* recovery terms, since a factor representing the strain rate is missing in these terms. This is radically different from the original equations (89) and (90) where the recovery was introduced as a *dynamic*, strain-rate driven process, which is consistent with the underlying philosophy of the KME approach. Despite this deficiency with handling the recovery processes, in their subsequent work [438] the same authors demonstrated that their approach is capable of accounting for strain softening at large strains - a phenomenon which will be discussed in more detail in Section 5.2.

The applicability of the model outlined above hinges on the validity of Eq. (85) that establishes a relation between the dislocation cell size and the total dislocation density. As mentioned above, this scaling relation follows from dimensional considerations and is universally accepted. It is also supported

by stochastic modelling of dislocation populations [63]. However, the validity of Eq. (85) for non-steady state deformation still awaits a rigorous proof, cf. [4].

The dislocation-based constitutive modelling based on equations (89) and (90) or their modifications were used to account for experimental data over a wide range of strain, including giant strain values attained during SPD. While having many commonalities, the models proposed in literature are different in detail of the microscopic mechanisms of dislocation processes considered, cf. early work by Argon and Haasen [439] and more recent publications by Nes and Marthinsen [354, 355].

For example, to model dislocation density evolution in deformed pure Al, Chinh et al. [185] have recently employed a two-internal-variable approach proposed by Kubin and Estrin [284, 429, 434], which was originally developed to account for plastic instabilities associated with the Portevin–Le Chatelier effect in solid solutions. In this approach, which was not intended specifically for description of large deformations, the cellularity of the dislocation structure was not considered. The two dislocation densities comprising the total one, $\rho = \rho_m + \rho_f$, are the densities of mobile (ρ_m) and forest (ρ_f) dislocations. They obey the following differential equations [434]

$$\begin{aligned} \frac{d\rho_m}{d\gamma} &= C_1 - C_2\rho_m - C_3\rho_f^{1/2} \\ \frac{d\rho_f}{d\gamma} &= C_2\rho_m + C_3\rho_f^{1/2} - C_4\rho_f \end{aligned} \qquad (92)$$

The individual terms in Eqs. (83) have a transparent physical meaning, as they can be interpreted in terms of various dislocation reactions analogous to those underlying Eqs. (89)-(91). What distinguishes this set of equations from that given by Eqs. (89) and (90), is that the former is 'structureless'. While Eqs. (92), and (69) do provide an adequate description of the deformation behaviour of metals at small and moderate strains (which can be extended to large strains, as done in Figure 27 and Figure 28, they do not reflect any development of dislocation cell or grain structure, which is obviously their deficiency.

The two-internal-variable formulation can also be used for modelling high-speed severe deformation processes where heat release plays a substantial role. The model has a provision for considering the thermomechanical coupling through including a temperature dependence in the exponents *m** and *n** (or the reference strain rates $\dot{\varepsilon}_0$ and $\dot{\gamma}_0$), as was done recently in modelling impact deformation [440].

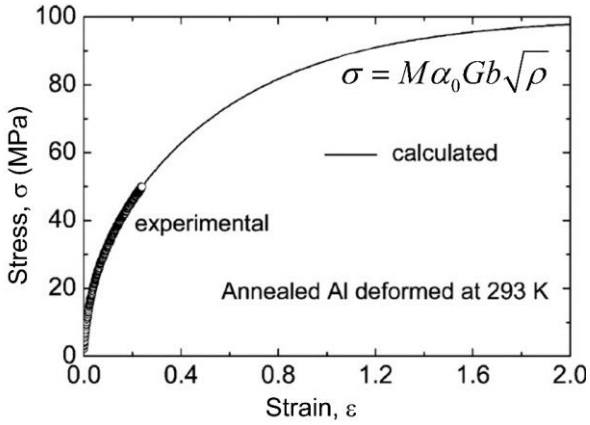

Figure 27. Experimental data for Al and the calculated stress-strain curve obtained by solving Eqs. (92) and (69) (from [185], reprinted with permission).

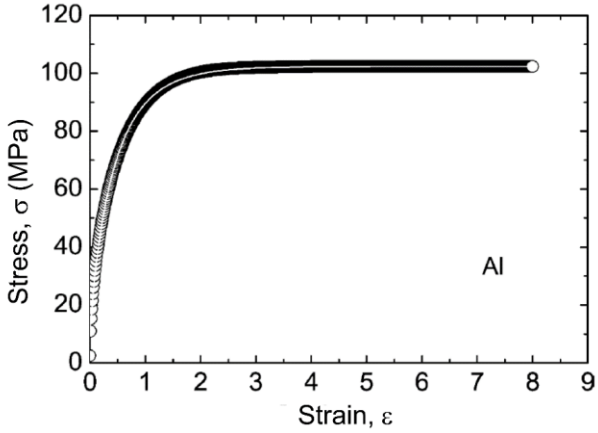

Figure 28. The σ vs ε curve for polycrystalline Al over a wide range of strain calculated by using the differentiated Voce equation, Eq. (10). (from [185], reprinted with permission).

The two-internal-variable formulation can also be used for modelling high-speed severe deformation processes where heat release plays a substantial role. The model has a provision for considering the thermomechanical coupling through including a temperature dependence in the exponents *m** and *n**

(or the reference strain rates $\dot{\varepsilon}_0$ and $\dot{\gamma}_0$), as was done recently in modelling impact deformation [440].

3.4. Constitutive modelling of multi-phase materials

The above considerations referred to single-phase materials. Constitutive modelling for multi-phase materials can b based on the same principles. One can distinguish between two principal cases, as can be illustrated for a two-phase material. In the first case, a second phase is represented by small dispersed particles and does not have any substantial load-bearing capability, so that stress sharing between the phases can be disregarded. The particles then play a 'passive' role, constituting obstacles to mobile dislocations of the majority phase ('matrix'). If, by way of example, the particles are non-shearable and are to be overcome by moving dislocations via the dislocation bowing-out (Orowan) mechanism, they contribute to the flow stress an additive term of the order of the Orowan stress, $\sigma_{Orowan} \cong MGb / L_p \cong MGb\sqrt{f_p} / R$ [441, 442]. Here L_p is the average particle spacing, *R* their radius, and f_p the volume fraction of the second phase. Similarly, shearable particles add a contribution of the order of $M\pi R\gamma_s / bLp$ (with γ_s denoting the surface energy) to the flow stress. There is another, more subtle, effect of second-phase particles that enters through the evolution of the dislocation density in the dislocation cells, e.g. Eq. (90), as a positive additive storage term inverse in L_p and also as a multiplicative factor in the dynamic recovery term (the last term in that equation) [443]. The latter factor accounts for a reduction of the dynamic recovery rate due to the need for a dislocation in contact with a particle to be detached from it by a mechanism proposed by Rösler and Arzt [444].

In the opposite case where a second phase does have a sizeable load-bearing capacity, the overall stress of a phase mixture encompassing the contributions from all phases has to be calculated. The simplest approach is to use a rule of mixtures, whereby the stress of the multi-phase material is given by a weighted sum of the constituent phases. The weight factors are taken as the volume fractions

of the respective phases, while the stress in a particular phase is calculated using a model for a single-phase material presented above in Sections 3.1-3.3. A more sophisticated treatment of the multi-phase nature of a material would involve an appropriate homogenisation technique, and the one originally proposed by Molinari et al. [445] is believed to be both versatile and reliable [446] [68].

As a convincing illustration of this approach, Ardeljan et al. [447] have developed a multiscale model for anisotropic deformation of multi-phase polycrystalline aggregates to large plastic strains. The proposed elasto-plastic strain rate- and temperature-sensitive model is footed on a dislocation-based hardening law in the spirit of Eqs. (89) and (90) combined with crystal plasticity-based finite element modelling, which bridges the single-crystal and polycrystal mechanical response. The model was successfully applied to study the texture evolution and the deformation mechanisms in a HCP-Zr/BCC-Nb layered composite under severe plastic deformation by accumulative roll bonding. Not only did the model predict the texture in both co-deforming materials to very large plastic strains, but it also provided an accurate simulation of the tensile behaviour of both constituent phases (HCP-Zr and BCC-Nb). Figure 29 represents a distribution of local stresses and strains obtained with the full account of the evolving dual-phase microstructure, including the variation of dislocation density and crystallographic grain reorientation in both constituents during deformation.

Thus, it can be concluded that the modelling approaches developed for single-phase materials can be extended to multi-phase ones.

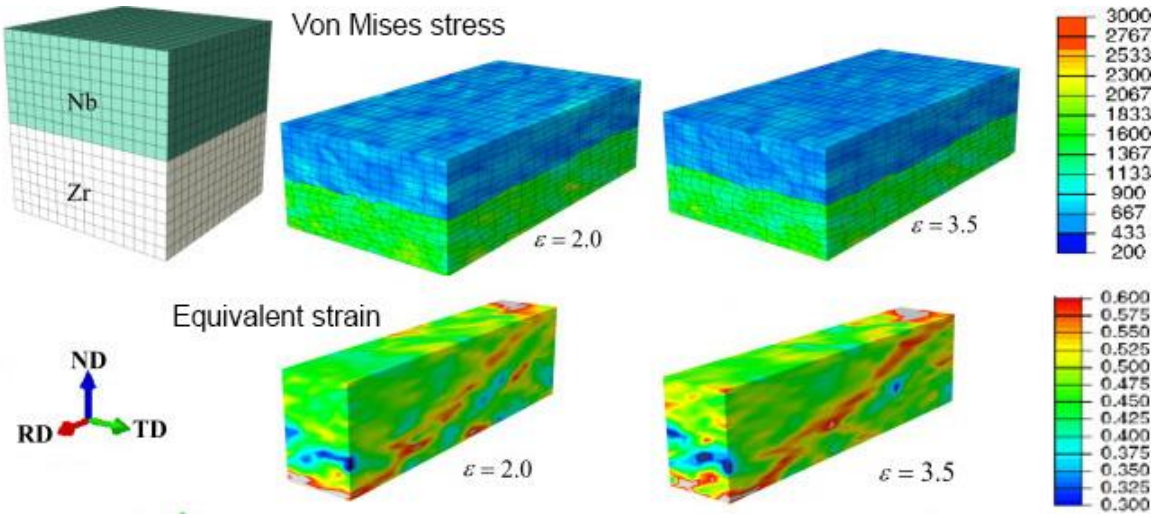

Figure 29. Initial FE mesh and deformed FE models of the Zr/Nb composite showing Von Mises stress and equivalent strain contours at strain levels indicated in the figures (adapted from [447]).

4. Possible scenarios for grain refinement

The scenario of grain refinement tacitly assumed in the foregoing section infers that the underlying process is the dislocation cell formation followed by cell size evolution according to Eq. (85). That is to say, the dislocation cell structure is assumed to be a pre-cursor of the new grain structure that develops with accumulation of misorientations across the cell boundaries. Evolution of misorientation between the dislocation cells in the process of straining was modelled by Estrin and Kim [448]. They considered the growth of the misorientation for low-angle boundaries with the influx of edge dislocations, assuming a local disbalance in the density of edge dislocations of opposite sign. A similar treatment, yet through a more involved dislocation density model, was proposed by Alexandrov et al. [449], who introduced the excess dislocation density in the boundaries. This simplistic consideration of the evolution of cell/grain misorientations was further improved by Pantleon [450] and Estrin et al. [451] on the basis of a probabilistic approach. The results of the latter studies account reasonably well for the misorientation angles associated with the so called incidental dislocation boundaries [452], but the models used do not apply to high-angle (geometrically necessary) grain boundaries [452] whose fraction

grows as a result of SPD processing. The Langevin approach leading to a Fokker-Planck equation for the distribution of misorientation angles [451, 452] appears to provide a promising frame for modelling the evolution of grain misorientations.

The above scenario is illustrated by Figure 30 [453] that shows the transformation of diffuse cell walls to small-angle grain boundaries, which, upon increase in misorientations, are converted to large-angle ones.

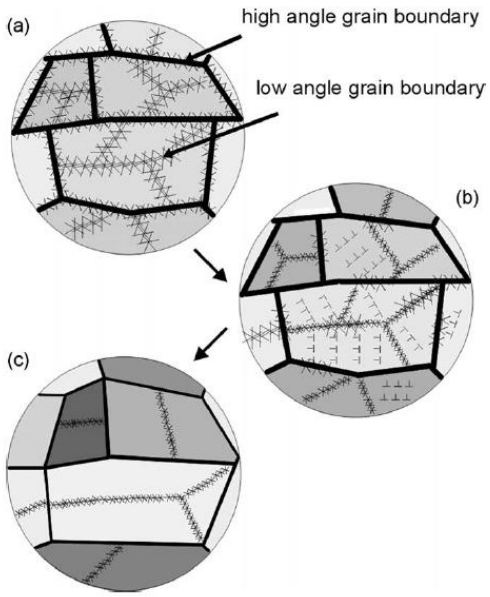

Figure 30. Schematic showing the microstructural evolution during ECAP processing: (a) diffuse low angle boundaries dominating after a few (say, two) passes, (b) transition state from low to high angle boundaries (e.g. after 8 passes), (c) stabilized microstructure (say, 16 passes). Note that the average grain size (including both high and low angle boundaries) stabilises after only a few passes (from [453], reprinted with permission).

In the grain refinement scenario in which the emerging grain structure inherits the length scale of the parent dislocation cell structure, there is an obvious limit to the attainable degree of grain refinement. Indeed, by combining the expression for the dislocation cell size, Eq. (85), with the Taylor

relation, Eq. (40), one arrives at a simple formula for the smallest attainable dislocation cell size d_c^{min} (i.e. the minimum grain size):

$$d_c^{min} \cong K_o M \alpha \frac{G}{\sigma_{theor}} \tag{93}$$

This relation shows that for typical values of K_o of the order of 10, $M \cong 3$, and $\alpha \cong 0.5$, the achievable grain size cannot be smaller than about 100b even for the stress level close to the theoretical strength σ_{theor}. That is to say, the grain refinement mechanism, in which grain subdivision occurs via the cell structure formation and its refinement during straining, cannot bring the average grain size below the 100 nm mark that defines a nano material. This is consistent with a huge body of experimental evidence on grain refinement by severe plastic deformation [4]. While the model predictions with regard to the mechanical behaviour and the emerging grain size based on the two-internal-variable model [254, 255] have been verified for various materials and SPD processes, there is still a pressing need to improve modelling with regard to grain fragmentation. A recently proposed approach [107] offers a a modelling frame suitable for a simple description of grain fragmentation in terms of lattice curvature evolution. It was suggested [107] that lattice curvature develops within a grain due to kinematic constraints imposed by the neighbouring grains. More specifically, the rotation of the crystallographic planes in the grain due to dislocation slip was considered to be retarded near the grain boundaries. The grain subdivision was associated with the emergence of geometrically necessary dislocations required to accommodate the resulting lattice curvature. Agglomeration of these geometrically necessary dislocations to new grain boundaries was proposed as the mechanism of fragmentation of a grain. It was suggested that the process of grain subdivision into new grains (owing to the occurrence of a zone near the grain boundaries where crystallographic plane rotations are inhibited by the grain boundaries and a middle part of the grain where they are not) leads to the emergence of a grain population with the grain size of $d/3$. This process of grain subdivision can go on and on leading to multiple generations of grains until the

dislocation glide mechanism causing the rotation of crystallographic planes ceases to operate. As mentioned above, this is the case when the grain boundaries no longer act as impenetrable obstacles to dislocations, as dislocations arriving at grain boundaries get accommodated there with the aid of grain boundary diffusion [399]. This occurs when the grain size drops below a critical level, d_{crit}, given by Eq. (66), whose estimated magnitude for room temperature deformation amounts to several hundred nanometres [4]. Toth et al. [454] also looked at the evolution of the misorientation distribution function during severe plastic deformation. The predicted shift of the distribution towards large misorientation angles, which was confirmed by experiments on ECAP processing of Cu, was attributed to the shape variation of the initial grains, effectively raising the volume fraction of the 'old' high angle boundaries. This concept, which is at variance with the commonly shared view that new grain boundaries emerging during SPD, acquire large misorientations in the process, calls for further investigations.

An approach to grain fragmentation associated with the rotation of slip planes was also taken by Kratochvíl et al. [455] who proposed a crystal plasticity based model to describe the material response to severe plastic deformation under HPT. Specifically, they assumed uniform deformation by double slip in plane-strain and considered the rotations of the slip systems caused by the imposed shear strain. They found local variations in the crystal lattice orientation and claimed these variations were responsible for microstructure fragmentation. Aoyagi and Shizawa [99] introduced geometrically necessary dislocations and geometrically necessary incompatibility tensorial terms corresponding to isolated dislocations and dislocation pairs into a strain gradient crystal plasticity model reproducing a grain subdivision process at large strains under pure share cold rolling deformation. In their model, new grain boundaries with large angles of misorientation were nucleated along the GNBs due to enhanced strain gradients associated with dislocation activity at the boundaries, which is in fair agreement with experimental observations. In contrast with the 'mainstream' notion of the grain subdivision process with gradual accumulation of misorientations, Seefeldt et al. [456] modelled the evolution of

misorientations across the cell boundaries as a 'nucleation and growth' process triggered by disclination nuclei randomly induced in the cell walls. In their model, these nuclei represented by dipoles of partial disclinations interact with statistically stored dislocations and spread along the walls by capturing incoming lattice dislocations, thus increasing the misorientation between the neighbouring cell blocks.

The above considerations of a grain refinement scenario based on gradual subdivision of the grains suggest that there are two limit grain sizes, *viz.* those given by Eqs. (66) and (85) (or (93)). Grain refinement will cease to occur once the greater of the two critical values of the grain size is reached. Both are in the range of several hundred nanometers, i.e. slightly above the true nano material range. The above scenario of a 'peaceful' transformation of dislocation cell structure to a grain structure was contrasted by a picture of a more 'violent' grain refinement down to nano scale by the so called dynamic plastic deformation (DPD) [457], which involves high strain rates and/or low deformation temperature (large values of the Zener–Hollomon parameter Z) [4]. The corresponding mechanism of grain refinement involves formation of nanotwin bundles [458], which transform to nanograins by fragmentation of twin/matrix lamellae due to interaction of twin boundaries with dislocations or shear banding. No model of these processes has been offered so far, and this is certainly an area to be considered in the future.

Saturation of grain fragmentation implied by the models discussed cannot be taken for granted, and there has been a long-standing discussion in literature on whether there is such a thing as 'saturation'. The question is related to that of whether saturation of the flow stress (i.e. asymptotic vanishing of strain hardening) occurs at large strains. The latter can be answered affirmatively. Indeed, the concepts based on dislocation density evolution do account for the occurrence of late strain hardening stages (including Stage IV and beyond) that eventually terminate in saturation of the flow stress [167, 255, 431, 459, 460], as do numerous experimental studies, see, e.g. [459-462]. It has been

claimed, however, that despite saturation in the intrinsic strain hardening capability of a material, some microstructural changes may still occur at very large strains [463], so the question of whether microstructural variation would eventually saturate still remains. More specifically, in the context of SPD processing, it is of interest to understand whether saturation of grain fragmentation does or does not occur. Pippan et al. [462, 464] strongly advocate the notion of saturation and provide convincing evidence for that. Moreover, it was shown in their work that the saturated grain structure was not very sensitive to strain path chosen (HPT vs. HPT + rolling), which speaks for certain 'universality' of microstructure development under very large strains. However, substantial differences in the saturated microstructure between monotonic and cyclic loading were established. A prominent role of grain boundary migration in the scale of the saturated grain size was also highlighted. The relative 'universality' of the grain structure development appears to be at odds with the analysis of Tomé et al. [465] who argued that strain hardening behaviour should be strain path dependent. A similar view is held by Beygelzimer et al. [167], whose point is that the intrinsic strain hardening derived from deformation tests for different strain paths should be different due to differences in texture and in the complexity of dislocation slip. At this stage, the issue is not fully resolved and more work is needed to establish whether saturation in grain fragmentation under SPD does take place and if so, whether it is strain path dependent or not.

5. Numerical simulations of SPD processes

5.1. FEM simulations of SPD processing

Literature on FEM simulations of SPD processing is quite substantial. Important contributions to this area by the research group of Prof. Hyoung Seop Kim of Postech, Korea – especially in relation to modelling of high-pressure torsion and equal channel angular pressing - should be noted. A

representative sample of this work can be found in [466]. Further publications in this field have been cropping up recently, cf. [467]. Most of them are based on phenomenological constitutive models, as represented by a recent publication on HPT modelling by FEM [92]. The authors used an elastic-perfectly plastic constitutive model to study the effects of contact friction conditions on the evolution of the distributions of the components of the stress tensor and the plastic strain in copper and highlighted strong heterogeneity of the plastic strain both along the radius and thickness of the sample within the first revolution of the anvils.

In Section 2.2 we considered simulations of the ECAP process in some details. FEM simulations were also applied to a range of other SPD techniques. Thus, ECAP with a rotary-die was considered by Yoon et al. [468]. Cyclic extrusion-compression (CEC) was analysed by Rosochowski et al. [469]. High pressure torsion (HPT) of disks was considered by Kim [470], Figueiredo et al. [261, 262, 471, 472] and Molotnikov et al. [384, 473]. As new SPD technologies and the areas of their possible application keep emerging, the significance of FEM methods for quick and efficient design of processing routes and tools increases. This has been successfully demonstrated in a recent study of a novel industrially scalable extrusion process for curved profiles [474] or a simple shear extrusion process [475-477]. In particular, FEM is indispensable in the modelling and simulation of deformation processing under extreme conditions such as low temperatures during cryo-SPD processing [478], or very high strain rate deformation in the high-speed machining [479] [480, 481].

Constrained groove pressing and constrained groove rolling were simulated by Lee and Park [482]. Following the FEM simulation-based strategy, new optimized processing schemes different from known SPD processes were proposed. For example, Luri et al. [145] offered a modified ECAP die configuration while Rosochowski et al. [483] developed an ECAP-like incremental process called *incremental ECAP* (I-ECAP) suitable for continuous processing. A large body of computational (chiefly

FEM-based) work on the SPD process known as twist extrusion and cognate processes has been discussed and evaluated in a recent review [484]. A successful exercise in analytical modelling of an axisymmetric forward spiral extrusion process [485] – yet another recent variety of SPD processing - employed an upper bound approach, developed earlier in the context of twist extrusion modelling [486].

Substantial efforts were also put in design and simulation of SPD processing of thin products [487, 488], notably thin-walled tubes [315, 489, 490]. A process dubbed tube channel pressing [491] was studied by Farshidi and Kazeminezhad [492] by employing FEM simulations. An assessment of a prospective Tube Twist Pressing process as a new SPD method for tubular materials by FEM simulations was presented by Babaei et al. [493]. All these techniques rely on a combination of large shear deformation and high hydrostatic pressure and in that sense they are akin to the 'mainstream' SPD processes, such as ECAP or HPT. A related technique for manufacturing thin-walled *cone-shaped* products [494] which utilises this kind of imposed conditions, was assessed on the basis of FEM simulations.

These examples of successes with simulation of 'classical' and emerging SPD processes demonstrate the power of solid mechanics in the analytical and computationally-assisted engineering of SPD and the potential of such approaches for future industry scale applications.

As repeatedly emphasised above, microstructure-based constitutive models have substantial advantages over the phenomenological, mechanistic ones, and it is encouraging that this view is becoming more and more accepted by the research community. As an example of the application of the two-internal-variable model [254, 255] we show the results for ECAP of Al [256], Figure 31. The calculated curves representing the evolution of the dislocation cell size and the equivalent stress as a function of the cumulative equivalent strain for the ECAP die (which for the channel angle of 90°

practically coincides with the number of ECAP passes) are in good agreement with the measured values. As discussed above, the emerging grain size was identified with the dislocation cell size.

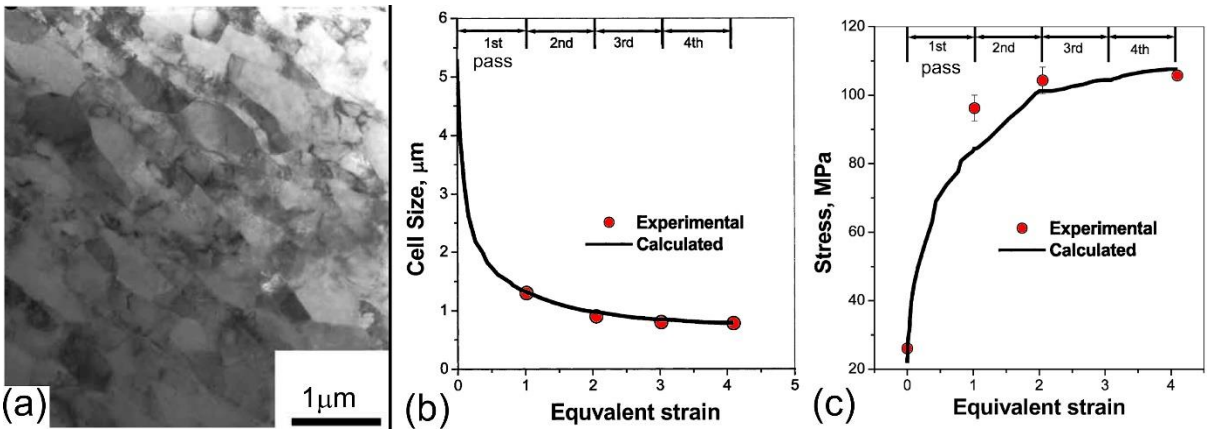

Figure 31. Refined grain structure of pure Al after four ECAP passes (a); the evolution of the dislocation cell size (b) and the variation of equivalent stress with equivalent strain for commercial purity Al (c) [256].

In several numerical simulation exercises addressing SPD processing, see, e.g. [495], it was established that the basic two-internal-variable model [254, 255] provides a potent and robust tool for predicting the material behaviour during processing as well as the properties of the processed material. For instance, in the above example of ECAP of Al, such aspects as nonuniformity of the microstructure produced was studied by finite element simulations [256].

The results shown in Figure 32 demonstrate how the cell size distribution (which, as mentioned above, is regarded to be tantamount to that of the grain size distribution) across the billet thickness progressively becomes more and more uniform with the number of ECAP passes. The average cell size (which is to become the average grain size when the cumulative strain is large enough for sufficient cell misorientations to develop) tends to saturate with strain at a level of about 800 nm. For other materials and with different SPD techniques, significantly smaller values of grain size are achievable [4]. Thus, for copper of commercial purity, the average cell/grain size was shown to drop to about 250 nm after eight

ECAP passes by Route Bc as illustrated in Figure 33a [496]. The concomitantly increasing gain in the yield strength with the number of passes seen in Figure 33b is quite impressive. Figure 33c illustrates a similar behaviour of Cu deformed by Route A ECAP as predicted by Tóth [96] who used the two-internal-variable cellular model based on Eqs. (89)-(90), which was combined with the flow line model [156] discussed above and the self-consistent viscoplastic model in the spirit of the Molinari and Tóth approach [497]. Compared to the results shown in Figure 33b, the modelled flow curve is considerably more detailed. It also accounts for stress drops due to the inter-pass breaks.

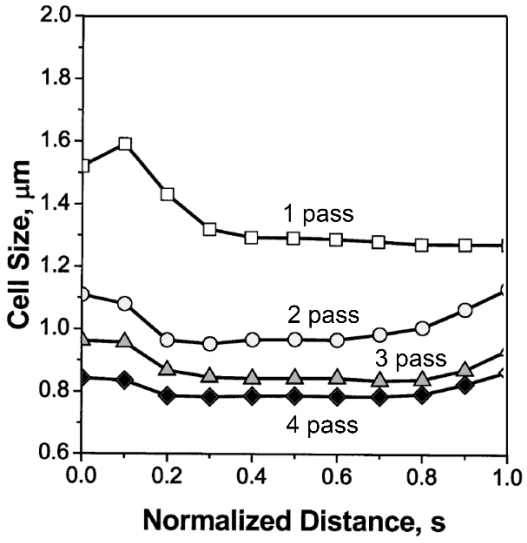

Figure 32. Evolution of the dislocation cell size across an Al billet with the number of ECAP passes. The quantity $\hat{s}$ denotes the distance from the bottom of the billet normalised with respect to the billet thickness [256].

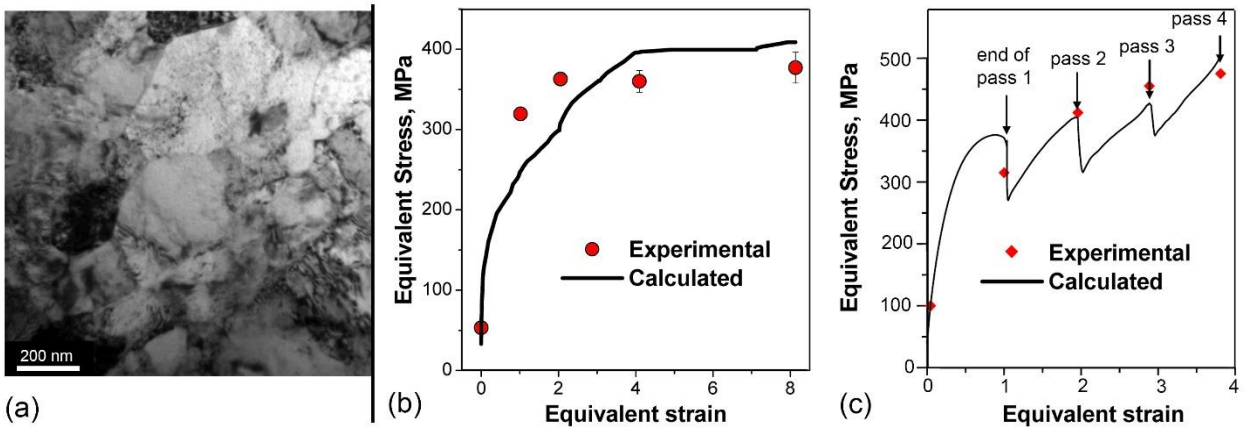

Figure 33. TEM image showing the microstructure of Cu after 8 ECAP passes (a) and evolution of the yield strength of copper as a result of ECAP processing to different numbers of passes via routes Bc (b) and A (c) (after [496] (a) and [96] (b), reproduced with permission).

An example of even more extreme grain refinement is shown in Figure 34, which displays the evolution of the calculated dislocation cell size in copper under high-pressure torsion [384] – a process discussed above and schematically illustrated in the same figure. For the vertical pressure of 8 GPa the cell/grain size attained a saturation value of about 120 nm, in close agreement with experimental data included in the diagram. The simulations [384] were based on the two-internal-variable model and additionally included a gradient plasticity term. The provision for gradient plasticity [473], which will be discussed in Section 7, helps explaining the development of nearly uniform, refined microstructure in an inherently non-uniform process such as HPT.

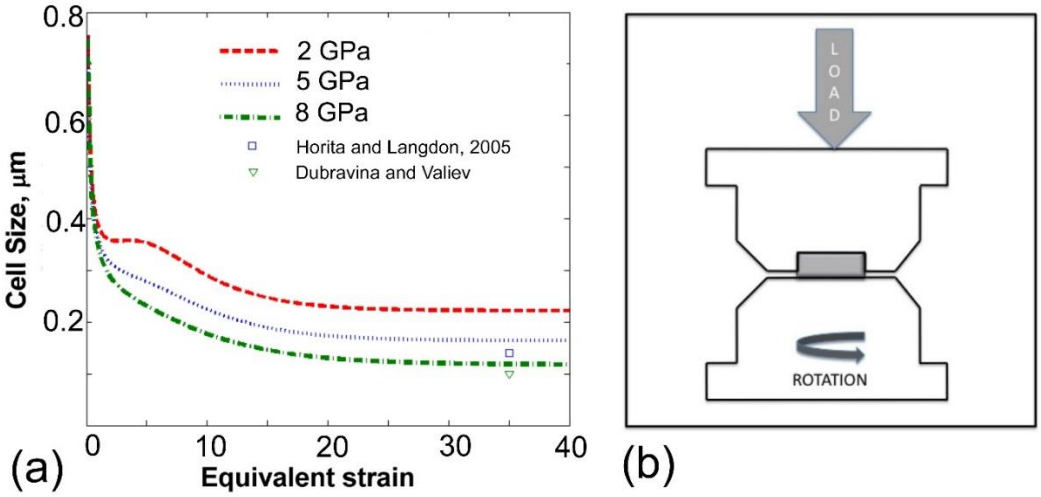

Figure 34. Dislocation cell size variation with the cumulative equivalent strain during high-pressure torsion of copper (a) [384]. The schematic of the process is shown in (b).

The realisation that the details of the strain hardening behaviour in terms of microstructure evolution are important for realistic FEM modelling has motivated a series of studies by Hosseini et al. [272, 437, 438, 498-502] in which FEM modelling was based on dislocation density evolution. They exploited a flow line model originally proposed by Tóth et al. [156] and extended by Hasani et al. [158] which was backed by a two-internal-variable model involving two dislocation densities of the kind described in Section 3.3. It was used to investigate the deformation behaviour of Cu and Al in the route Bc ECAP process with sharp and curved die corners, Figure 3. The strain and strain rate were obtained from the flow line model to inform a modified version of the Estrin-Tóth -Mollinari-Bréchet model [255] for the evolution of a cellular microstructure. The predicted characteristics of the microstructure were found to be in fair agreement with the commonly reported experimental data: (i) the dislocation density for the material pressed in the sharp-corner die was higher than that in the die with a corner curvature; (ii) the dislocation density in processed Al was lower than that in processed Cu; (iii) the cell size in the

processed Cu was predicted to be smaller than that in the processed Al; and (iv) the sharp-corner die produced a finer cell size in both materials than the curved corner die.

Following the success of this modelling approach, that group of authors incorporated constitutive modelling of dislocation hardening into the FEM code which was applied to simulating the groove pressing/repetitive corrugation (GPRC) and repetitive corrugation straightening (RCS) processes [500]. The set of coupled differential equations for the evolution of the cell interiors and the cell walls dislocation densities similar to Eqs. (89) and (90), combined with Eqs. (40), and (86) provide a full constitutive description of dislocation behaviour. To apply this constitutive model to SPD processing, the cumulative strain and the resolved shear strain rate for a particular process, e.g. ECAP, is required. Hosseini and Kazeminezhad [499] calculated these quantities from the flow function results.

A powerful tool to model the deformation behaviour of polycrystalline materials is polycrystal plasticity [68, 94, 503]. A way to incorporate microstructure evolution in the polycrystal plasticity framework is by considering the actual active slip systems with their individual slip rates and the resolved shear stresses that also vary from one slip system to another. For simplicity, it can be assumed that the dislocation cells within a grain are identical and their mechanical response can be characterized by a unique common resolved shear strain rate $\dot{\gamma}_r$. In this didactically simplified way, misorientations between cells within a grain are disregarded, while the orientation of each individual grain is considered. Assuming the shear resistance is the same for all slip systems, $\dot{\gamma}_r$ is derived as follows [504]:

$$\begin{aligned} \dot{\gamma}_r &= M\,\dot{\varepsilon}_{eq} \\ M &= \frac{1}{\dot{\varepsilon}_{eq}} \sum_{n=1}^{N} \dot{\gamma}_{r_n} \end{aligned} \tag{76}$$

where N is the number of slip systems and $\dot{\gamma}_{r_n}$ denotes the strain rate for the n_{th} slip system. The

equivalent (von Mises) strain rate can be calculated via $\dot{\varepsilon}_{eq} = \sqrt{\frac{2}{3}\dot{\varepsilon}_{ij}\dot{\varepsilon}_{ij}}$.

Embedding the two-internal-variable model based on dislocation density evolution [429] in the crystal plasticity framework was considered by Tóth [96] and Shanthraj and Zikry [505]. Hosseini and Kazeminezhad [499] used a similar approach, yet with a specific consideration for the dislocation cell structure. The average dislocation densities within the cell interiors and cell walls as well as the total dislocation density calculated by Hosseini and Kazeminezhad [499] are presented in Figure 35. In agreement with general expectations and experimental observations the model predicts a rapid increase of dislocation density in both cell interiors and cell walls from 10^{13} m^2 and 10^{14} m^2 to 1.54×10^{15} m^{-2} and 5.11×10^{15} m^{-2}, respectively, after 6 ECAP passes. Over the following passes, the calculated dislocation density in cell walls increases continuously at a low rate and reaches a level of 6.29×10^{15} m^{-2} at the end of pressing. This kind of dislocation density evolution was also predicted for Al by McKenzie et al. [222] and reported experimentally by Estrin et al. [473]. In the hybrid model [499] the dislocation density in the cell interior reached a maximum and then dropped slightly with the increasing number of ECAP passes. This characteristic reduction in the dislocation density in the cell interior was attributed to the transformation of cells with low angles of misorientation to fine grains with high angle grain boundaries. This trend was confirmed by the experiments carried out for copper severely deformed by high pressure torsion by Estrin et al. [473].

Modelling of the variation of dislocation density has shown unequivocally that, depending on the material, intensive multiplication and storage of dislocations during SPD occurs up to cumulative imposed strain of 3 to 4. This finding is in excellent agreement with the most known and well documented feature of the SPD processed metals, *viz.* rapid strain hardening during the first ECAP

passes (one to four, depending on the material, tool geometry and processing conditions), followed by saturation or even some small, yet noticeable, reduction of hardness and flow stress.

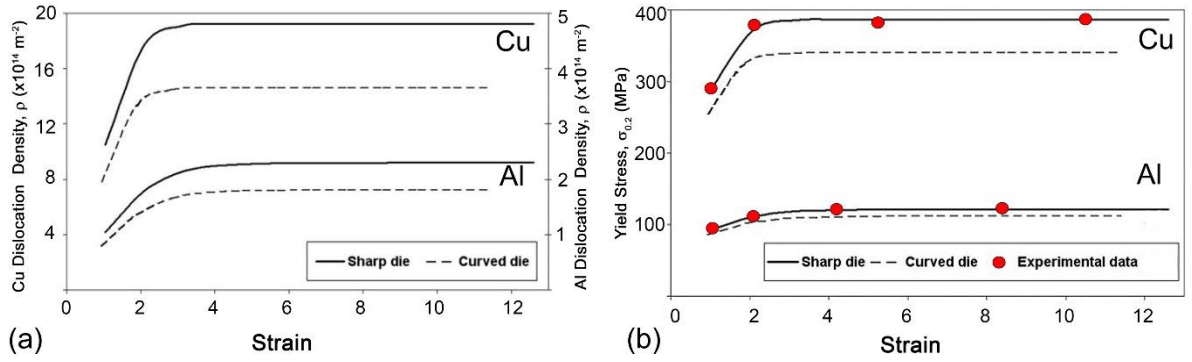

Figure 35. Calculated evolution of the total dislocation density (a) and corresponding flow stress (b) in Cu and Al subjected to different numbers of passes through a sharp-corner and a curved ECAP die (adopted from [498], reprinted with permission).

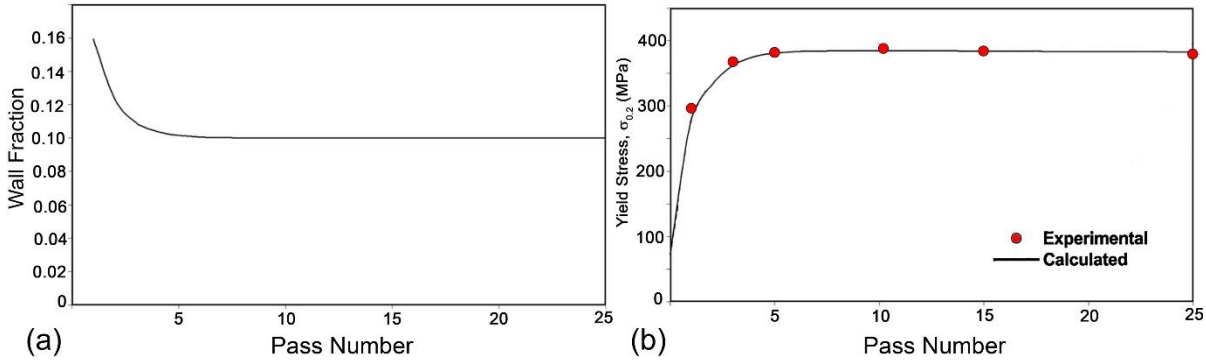

Figure 36. Evolution of (a) the fraction of cell walls and (b) strength as a function of the number of passes in the model by Hosseini and Kazeminezhad (adopted from Hosseini [499], reprinted with permission).

A dislocation density based crystal plasticity formulation in the spirit of Mughrabi's cell wall/cell interior composite model [350] and a finite-element computational method was used by Tóth [96] and Rezvanian et al. [506] in conjunction with the dislocation density evolution approach proposed by Nix et al. [507] and Estrin et al. [255]. Their aim was to investigate grain subdivision into inhomogeneous deformation bands in an aluminium single crystal in cube orientation under large rolling strains.

Evolution equations relating to the dislocation densities in cell interiors and cell walls as well as their dimensions were formulated in line with the above works and coupled to the multiple-slip crystal plasticity formalism. The formation of an inhomogeneous dislocation miscrostructure predicted by Rezvanian et al. is illustrated in Figure 37. The computational analysis clearly shows the non-uniformity of deformation, with localised deformation bands forming and developing with strain. These bands are comprised of two families including relatively wide matrix bands (MBs) and narrow transition bands (TBs) separating MBs, which were initiated and evolved across the thickness of the deforming aluminium crystal. Analysis of slip systems showed that deformation and structure evolution in the TBs was mediated by a combination of four active slip systems with equal activity, while in the MBs two dominant slip systems operated. These different combinations of active slip systems resulted in the microstructures with distinctly different morphologies. The TBs were shown to have a uniform dislocation-cell microstructure, whereas MBs appeared to have a cell block structure with narrower dislocation cells. These predictions were found to be in good agreement with experimental measurements and observations related to formation and evolution of MBs and TBs in cube-oriented single crystals subjected to large strain rolling. The analysis performed in Ref.[506] underscores that models based on dislocation density evolution in conjunction with crystal plasticity can successfully account for the formation of deformation band patterns under large strain processing.

FEM tools based on dislocation density modelling were used for numerical simulation of tube channel pressing (TCP) [508] - a variant of an SPD technique introduced for production of tubes with refined grain structure. The effects of the processing routes, back pressure, and friction were included in the investigation of the deformation behaviour of commercial purity aluminium tubes. Implementing a modified Estrin-Tóth -Molinari-Bréchet constitutive model for large strains [255] in an FEM program allowed evaluating the mechanical response of the material to TCP deformation in fairly accurate agreement with experiment.

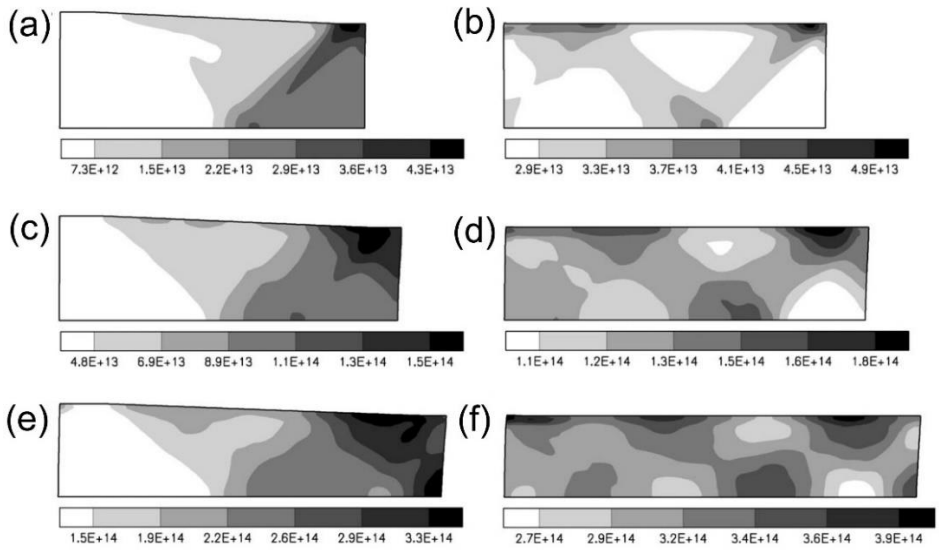

Figure 37. Contour maps of the total stored dislocation density (in units of m/m^3) at different levels of sheet thickness reduction: (a) 0–10%, (b) 10%, (c) 10–20%, (d) 20%, (e) 20–30%, and (f) 30% (from [506], reprinted with permission).

Quite generally, strengthening of tubes by severe plastic deformation is attracting a great deal of attention due to the importance of tubular products for a broad range of engineering applications. FEM simulations provide important assistance in evaluating the behaviour of metallic materials during such processes and the mechanical properties of the tubes strengthened by SPD. Particular examples include the so called Cone-Cone method (CCM) [494] in which a cone-shaped tube is deformed by severe twist under high hydrostatic pressure, and the techniques for producing gradient structures in thin-walled cylindrical tubes, such as High Pressure Tube Twisting (HPTT) [315, 509] and High Pressure Tube Shearing (HPTS) [489]. An important advantage of the latter technique, which is illustrated schematically in Figure 38, is its continuous character, which makes it amenable to large-scale tube manufacturing. FEM simulations of this process were conducted using the QForm software [510]. The results for low carbon steel are shown in Figure 39. The picture on the left is a snapshot that captures a narrow deformation zone (indicated by an arrow) moving along the tube. The picture on the right shows the distribution of the equivalent von Mises strain within the tube wall. In the example seen in Figure

39, the equivalent strain has a value of about 32 at the outer surface and 16 at the inner surface of the tube wall. This gradient of strain does not necessarily translate to a pronounced gradient of microstructure characteristics, as even the lower value of strain is large enough for saturation of microstructure development to have taken place. Thus, reasonably uniform mechanical characteristics can be achieved throughout the entire thickness of the wall. If required, a gradient in hardness and strength can be produced for smaller degrees of shear deformation. FEM simulations provide a very useful means for fine-tuning the processing parameters for the desired outcome in terms of uniformity or deliberately set non-uniformity of microstructure.

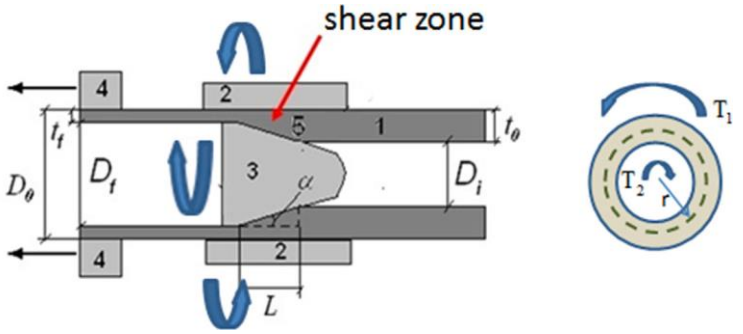

Figure 38. High Pressure Tube Shearing: Tube (1) is continuously drawn through the opening between the die (2) and a mandrel (3) using draw-bench (4). Shear strain is imposed within the thickness of the tube wall by rotation of either the die (2) or the mandrel (3), or both. (From [489], reproduced with permission)

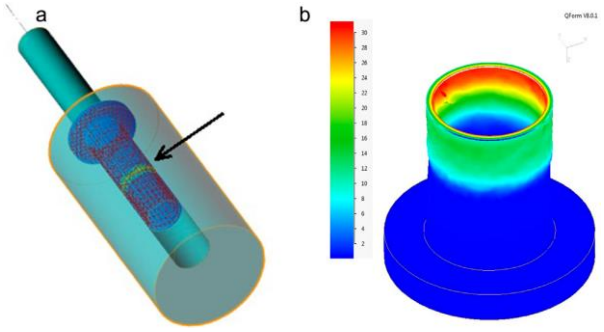

Figure 39. FEM simulation of the room temperature HPTS process for low carbon steel using the QForm software (From [489], reproduced with permission)

Another SPD process that has been studied at length by FEM simulations is twist extrusion (TE). In a series of publications, cf. [511-514], which have been reviewed recently [484], various aspects of TE processing, including the role of friction, die geometry, etc. were investigated by FEM in combination with experimental studies. In particular, these numerical studies helped identifying the limitations associated with the assumption of simple shear that is often made in the TE process modelling.

SPD techniques commonly target large-scale production of bulk UFG materials. Interesting niche applications of SPD processing can be found in manufacturing of parts for microelectronics, micro-electro-mechanical systems (MEMS), and other miniaturised engineering structures. Rosochowska et al. [515] pointed out that successful forming of metallic micro-components requires particularly careful design of the processing route using small-scale tooling, especially considering limited handling capability. They demonstrated that FEM simulations can be helpful in identifying the best process configuration before engaging in expensive experimental trials. Simulations were used to study material flow, the required force, and the tool contact stress in micro-extrusion of a single conical pin. Different process configurations (forward vs. backward extrusion), tool geometries (pin angles) and material models (coarse grained vs. ultrafine grained) were tested to gain a better understanding of the process conditions relevant to microforming. Kim and Nam [516] performed a quantitative FEM simulation and characterisation of the size effects in microscale coining process of copper where the grain size was comparable with the die cavity. In this way, the initial microstructure could be optimised before the actual micro-processing. Another successful exercise in FEM modelling of microforming by cup drawing was presented in Ref. [517]. 3D FEM simulations were carried out using the ABAQUS software package in which the dislocation based constitutive model expressed by Eqs. (89)-(90) was embedded. It was demonstrated that the drawing behaviour of metallic materials, particularly the occurrence of a blank thickness effect, is captured by the model very well. The occurrence of the size effect was shown to be governed by the ratio of the blank thickness to the grain size of the material, as illustrated by Figure 40,

which shows the model prediction and the experimental data for the limit drawing ratio. This quantity is defined as the ratio of the largest blank diameter drawn without failure to the punch diameter, and its calculated dependence on the ratio of the blank thickness to the grain size shows the right kind of trend consistent with experiment.

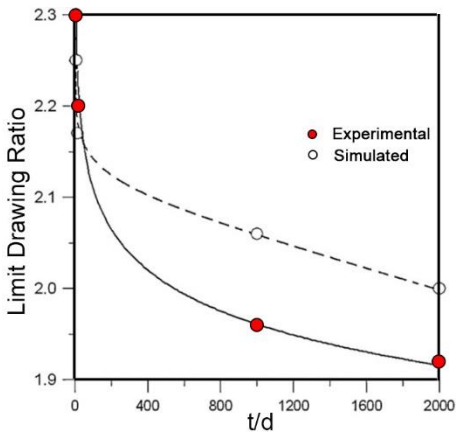

Figure 40. The limit drawing ratio as a function of the thickness *t* to grain size *d* ratio for a blank of ultrafine grained copper (after [517], reproduced with permission).

A metal forming process at microscale, which does not fall in the category of SPD processing in a strict sense, yet has a clear relevance to this group of techniques, is filling of vias for microelectronic devices by the so called forcefill [518]. In this process, aimed at connecting a metallisation level with another circuit level through channels in a semiconducting layer, a metal from a blanket film is forced into the via channels by applied pressure. The metal is in solid state and undergoes a large plastic deformation when filling the vias that commonly have a submicron diameter. A prediction of the process conditions, in terms of the applied pressure and temperature, for efficient via filling with aluminium was made with the aid of FEM simulations employing a commercial software package DEFORM 2D in conjunction with a phenomenological constitutive model having some dislocation underpinning. A useful map in the pressure-temperature plane specifying the regions where efficient via filling occurs was calculated on that basis.

5.2. Softening at large strains and dynamic recrystallisation

Coming back to the variation of strength with the cumulative equivalent strain (or the number of passes) under ECAP, we should mention that the progressive rise of strength with a trend to saturation seen in Figure 33 and accounted for by the two-internal-variable model for copper represents only part of the story. Deformation to still larger strains, beyond the range where monotonic rise of strength was observed, cf. Figure 33, was reported to result in a decrease in strength of copper [176]. This behaviour is illustrated in Figure 41 which shows the results of uniaxial tensile testing of 99.95% pure copper by up to 16 passes via ECAP route Bc. After the very first pass through the die, which corresponds approximately to a strain of 1, a strong increase in strength with a significant decrease in ductility is observed, as shown in Figure 41. With further passes the yield strength σ_{02} and the ultimate tensile stress σ_{UTS} increase and reach a maximum for the specimens subjected to four ECAP passes. This behaviour is similar to that seen in Figure 28 and Figure 33. With further processing beyond four passes, however, both σ_{02} and σ_{UTS} drop. This is believed to be associated with development of inhomogeneous microstructure, as confirmed by TEM observations and XRD measurements of the width of X-ray peak profiles. The total elongation is low (8% to 10%) and remains nearly constant throughout all passes. However, as discussed above in connection with Figure 41, the uniform elongation (i.e. the strain to the onset of necking) increases with the number of passes from 0.75% to up to 2.5%. Qualitatively similar behaviour was observed by Gubicza et al. [27] for several FCC metals, including Ag, Al, Au, Cu, and Ni, deformed to different strains.

As is obvious from Figure 41, we are dealing here with two strain softening effects. The first one is a decrease of the yield strength of copper with pre-straining by ECAP for sufficiently large numbers of passes. The second one is a decrease of stress with strain after a short stage of initial strain hardening under uniaxial tensile deformation of the ECAP-processed material. One possible reason for strain

softening during plastic deformation is dynamic recovery and/or dynamic recrystallisation which is common at high homologous temperatures and/or large strains [519, 520]. The available explanations for the strain softening behaviour observed after severe plastic deformation are diverse and mostly qualitative, although considerable progress has been achieved in understanding the microstructural factors affecting this trend relating it to recovery and dynamic recrystallisation processes [521-523] .

Although the processes of interest - recovery, recrystallisation (and possibly grain growth) - are implicitly hidden in the coefficients of the KME model based on dislocation density evolution (particularly in the parameters k_0 and k_2), the dislocation density tends to saturate, but not to decrease, with strain in the one-internal-variable model [176, 184, 327, 366, 431, 520, 524, 525]. To account for the softening behaviour at large strain, Wei et al. [175] proposed a combined approach where the dislocation density evolution in the spirit of the KME model and the Taylor relation for the friction stress σ_f are complemented with a softening fraction of the flow stress X_S which can be defined as:

$$X_S = \frac{\sigma_f - \sigma}{\sigma_f - \sigma_s} \tag{94}$$

Thus, the strain dependence of the flow stress can be expressed as $\sigma = \sigma_f(\varepsilon) - \left(\sigma_f(\varepsilon) - \sigma_s\right) X_S(\varepsilon)$.

The softening kinetics reflected in the strain dependence of X_S can be described using an Avrami type equation [526] or an empirical relation proposed by McQueen et al. [519] and then modified by Oudin et al. [527] and Wei et al. [175] to

$$X_S = 1 - \exp\left[-r\left(\frac{\varepsilon}{\tilde{\varepsilon}}\right)^q\right] \tag{95}$$

The quantities r and q, together with $\tilde{\varepsilon}$, which is close to the peak strain, are parameters that govern the

softening kinetics and are to be determined by fitting Eq. (95) to the experimental data. Although a satisfactory fit can be obtained for a variety of experimental data, cf. Figure 42, this heuristic approach to strain softening behaviour does not claim to be explanatory. While the form of the intuitively chosen equations is suggested by the theories of dynamic recrystallisation treated as a phase transformation [528-530], this blend of a dislocation-based approach and an empirical one is somewhat artificial. Moreover, the parameters entering Eq. (95) are loosely defined and cannot be related directly to microstructural characteristics of the material.

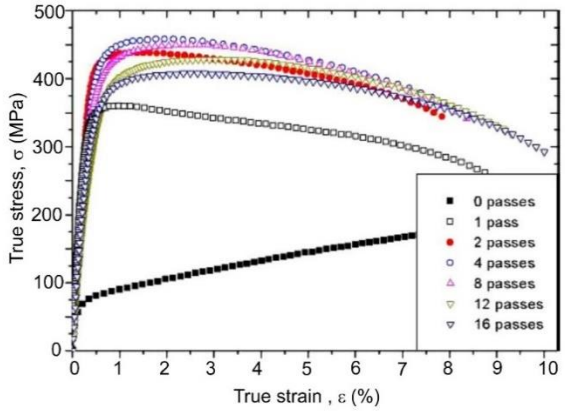

Figure 41. Stress–strain curves obtained by uniaxial tensile tests on pure Cu that has been processed by up to 16 ECAP passes performed at room temperature.

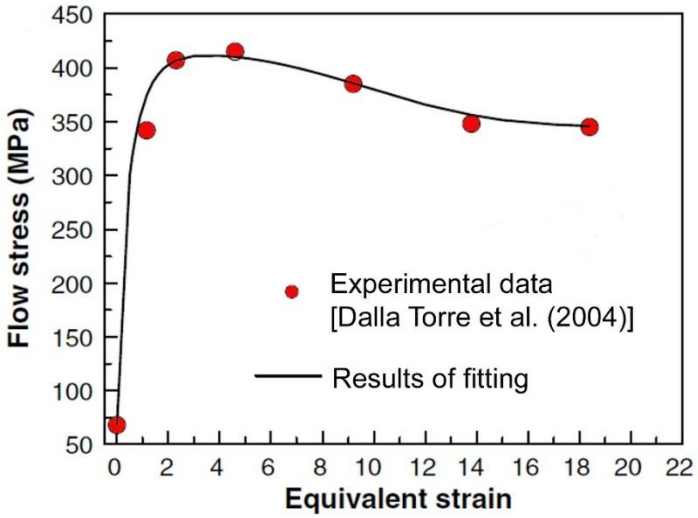

Figure 42. Dependence of the yield strength of pure copper on the pre-strain produced by different numbers of ECAP passes. Adopted from [175] and [176].

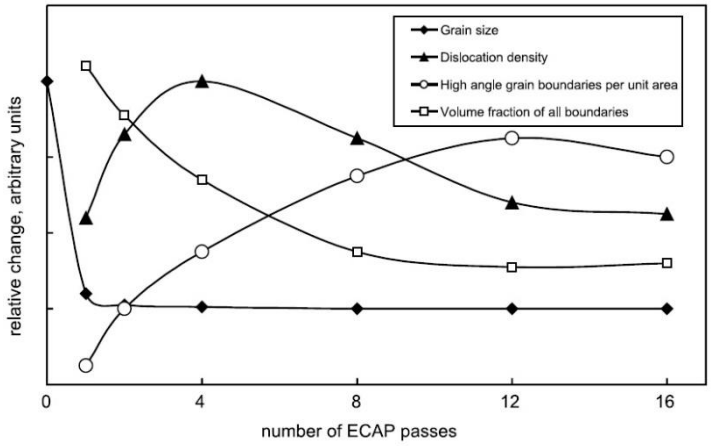

Figure 43. Characteristic evolution of the dominant microstructural parameters for copper with the number of ECAP passes (from [453], reprinted with permission)

A survey of the existing modelling efforts towards predicting the grain size distribution obtained by SPD would be incomplete without a brief remark on the dynamic recrystallisation. Indeed, grain refinement during deformation at high homologous temperatures [529, 531, 532] (or very high strain rates [533]) is often governed by dynamic recrystallisation (DRX). This phenomenon occurs in a deformed material through the nucleation and migration of high-angle grain boundaries that constitute a distinct interface between the previously deformed material and the new fine-grained structure. Once recrystallisation is triggered, the ensuing microstructural changes will affect the dislocation behaviour in the material. The recrystallised microstructure typically comprises residual pre-existing grains with a high dislocation density, newly formed fine grains which are initially dislocation-free, and evolving subgrains. As the average grain size decreases, the volume fraction of grain boundary area rises. The DRX kinetics is usually described by an S-shaped exponential curve for the time dependence of the volume fraction of the recrystallised material:

$$X_{DRX} = 1 - \exp\left[-\left(K_{DRX} / d_0\right) t^{n_{DRX}}\right] \tag{96}$$

where K_{DRX} and n_{DRX} are constants determining the rate of DRX and d_0 is the initial grain size of the non-recrystallised material. With the progress of DRX, the internal boundaries, with their growing total area, will reduce the dislocation mobility. Following this empirical approach, Hallberg et al. [534] described the evolution of the average grain size d from the initial value d_0 to the final saturation one, d_f, as a function of plastic strain

$$d = d_0 - \left(d_0 - d_f\right)\exp\left[-K_X \left\langle \varepsilon_{pl} - \varepsilon_{pl\,c} \right\rangle^{n_X}\right] \tag{97}$$

with another pair of rate-controlling constants K_X and n_X. Here the McCauley brackets $\langle\cdot\rangle$ indicate that no recrystallisation will occur until the critical plastic strain $\varepsilon_{pl\,c}$ is attained, i.e. until $\varepsilon_{pl} > \varepsilon_{pl\,c}$. The strain-dependent average grain size *d* then enters the KME equation for the dislocation density evolution, Eq. (51), as $\langle\lambda\rangle$. The FEM simulations of room-temperature ECAP with the die geometry defined by $\Phi = 90^o$ and $\Psi = 20^o$ showed, Figure 44, that after one pass neither the grain size nor the dislocation density are homogeneously distributed in the 20×20×150 mm^3 Al billet. Largest deviations from homogeneity were observed in the bottom part of the billet. After the second pass, the distribution of both grain size and dislocation density was found to be almost homogeneous. To avoid empirical formulations including loosely defined constants K_{DRX} and n_{DRX} or K_X and n_X, Galindo-Nava and Rivera-Díaz-del-Castillo [530] developed a thermodynamic approach coupled with classical grain nucleation and growth formulations describing the grain size evolution during discontinuous dynamic recrystallisation, which can potentially be incorporated in a more rigorous numerical modelling framework. With the same motivation, Le and Kochmann [535] proposed a thermodynamically based model for the DRX process during SPD, which also provided explicit evolution equations for the grain size and the dislocation density. Despite the simplicity of the model, evaluation of these quantities on its basis showed reasonable (though still only qualitative) agreement with experimental data.

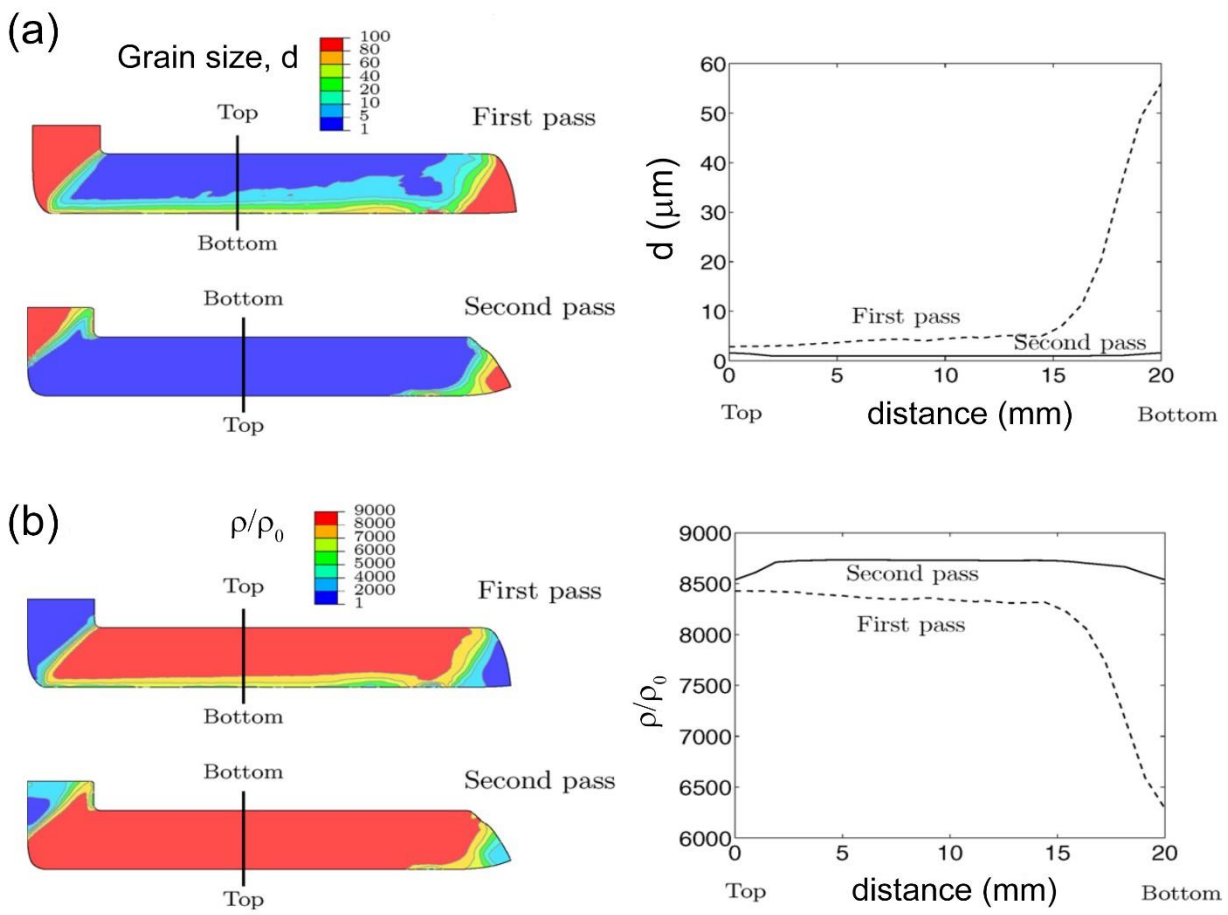

Figure 44. Results showing the average grain size (a) and relative dislocation density (b) distribution across the working Al billet during two ECAP passes via route C. (After Hallberg [534], reproduced with permission.)

6. Phase mixture modelling of nanocrystalline materials

The discussion in the foregoing sections made it clear that most SPD processing techniques produce an ultrafine grained structure that falls short of being qualified as nanocrystalline one. However, modelling of the mechanical behaviour of true nanocrystalline structures – regardless of the way in which it has been produced – is of interest in the context of this review. Here we give a brief account of a model that is well suited to describe this behaviour. It was first proposed in 2000 [536] and was further developed in subsequent work [537-539]. The main features of the model are as follows.

The interior of the grains and the grain boundaries are regarded as two separate phases. It is assumed that plastic strain rate in the grain boundaries is controlled by diffusion fluxes therein and is given by

$$\dot{\varepsilon}_{GB} = \tilde{A}\frac{\Omega}{k_B T}\frac{D_{GB}}{d^2}\sigma_{GB} \tag{98}$$

where σ_{GB} is the stress within the grain boundaries, Ω denotes the atomic volume and $\tilde{A}$ is a constant. This equation resembling the familiar Nabarro-Herring creep equation [540, 541] obtained from semi quantitative considerations [536] was confirmed by molecular dynamic calculations of Yamakov et al. [542] who found the value for the coefficient $\tilde{A}$ for copper to be approximately 55.5. The plastic strain rate in the grain interior (GI) is controlled by an additive combination of dislocation glide and diffusion processes of the Nabarro-Herring and Coble type:

$$\dot{\varepsilon}_{GI} = \dot{\varepsilon}_{disl} + \dot{\varepsilon}_{N-H} + \dot{\varepsilon}_{Coble} \tag{99}$$

with

$$\dot{\varepsilon}_{disl} = \dot{\varepsilon}_0 \left(\frac{|\sigma_{GI}|}{\sigma_0}\right)^m \left(\frac{\rho}{\rho_0}\right)^{-m/2} sign(\dot{\varepsilon}) H(d - d_{crit}) \tag{100}$$

$$\dot{\varepsilon}_{N-H} = 14\frac{\Omega}{k_B T}\frac{D}{d^2}\sigma_{GI} \tag{101}$$

and

$$\dot{\varepsilon}_{Coble} = 14\pi\frac{\Omega}{k_B T}\frac{w}{d}\frac{D_{GB}}{d^2}\sigma_{GI} \tag{102}$$

The Heaviside function $H(d - d_{crit})$ in Eq. (100) accounts for the fact that dislocation glide ceases to contribute to plastic deformation for grain sizes below d_{crit} defined by Eq. (66). In Eq. (102), w denotes the grain boundary thickness, cf. Figure 45. The variation of the dislocation density entering Eq. (100) obeys an evolution equation similar to Eq. (56) with $\langle\lambda\rangle$ identified with the average grain size d.

In the phase-mixture model under consideration, the overall flow stress σ is taken as the weighted sum of the stresses in the grain interiors and grain boundaries:

$$\sigma = (1-f)\sigma_{GI} + f\sigma_{GB} \tag{103}$$

where *f* is the grain size dependent volume fraction of the grain boundaries.

As in the two-internal-variable model considered above, the iso-strain assumption is made. Accordingly, the strain (and strain rate) in the grain interior and the grain boundaries is taken to be the same, as seen in the dashpot-spring diagram in Figure 45, which provides a recipe for the calculation of the flow stress described above. The diagram was augmented by a sequential member associated with gradient terms [543], which were absent in the original model and will be considered below.

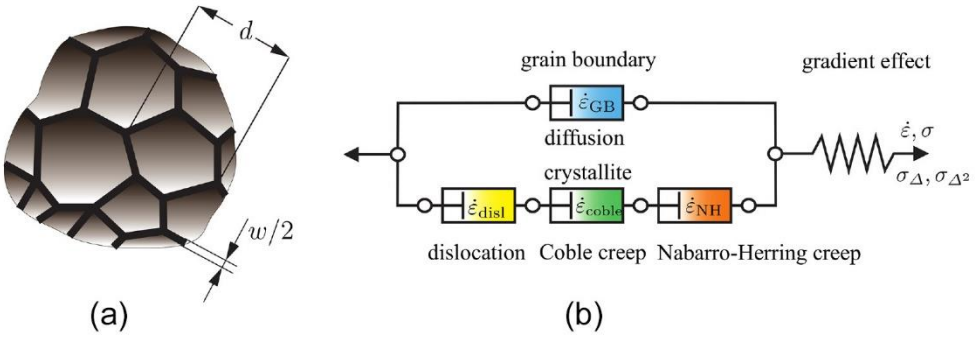

Figure 45. Mechanisms underlying plastic flow in the interior of the grain and the grain boundaries. (a) nanocrystalline material with grain size *d* and grain boundary width *w*. In the phase mixture model a nanocrystalline grain is approximated as being cube-shaped. (b) Rheological interpretation of phase mixture model according to Eq. (99) including a gradient effect. Each dashpot represents a viscoplastic mechanism and the spring accounts for the gradient effects. (After [543], reproduced with permission)

The phase-mixture model has been quite successful with describing the mechanical response of nanocrystalline metals in terms of their strain hardening behaviour and the grain size dependence of the yield stress. An example of the calculated diagram truthfully predicting the Hall-Petch dependence of

the $\sigma_{0.2}$ proof stress of copper and accounting for the 'inverse' Hall-Petch behaviour equally well is given in Figure 46.

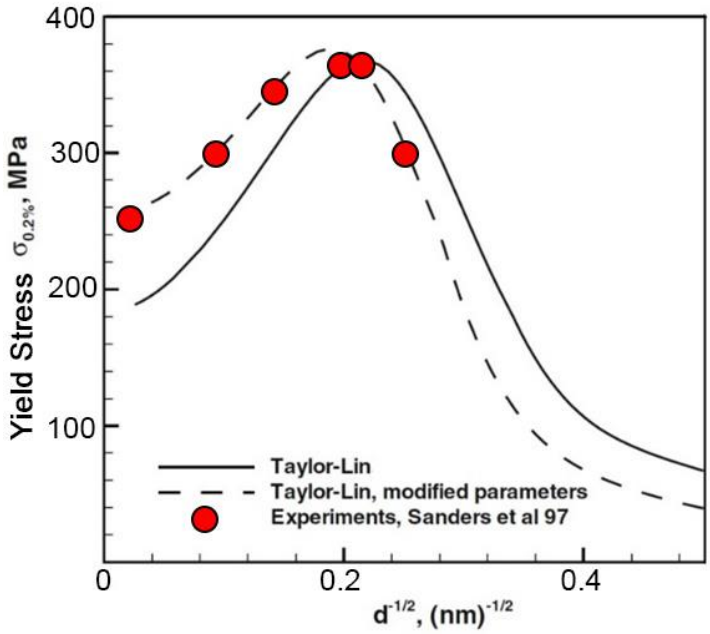

Figure 46. The grain size dependence of the $\sigma_{0.2}$ proof stress of nanocrystalline copper calculated using the phase-mixture model combined with the elastic-viscoplastic (Taylor-Lin) approach [538]. The experimental data by Sanders et al. [544] are shown for comparison.

7. Gradient plasticity for SPD processed materials

While a lot of effort in SPD research went into developments leading to maximising homogeneity of the microstructure of the processed material, there is also great value in processes capable of producing non-uniform, gradient microstructures [545]. In the cited work, an excellent combination of strength and ductility of interstitial-free steel was achieved by surface mechanical attrition treatment (SMAT). This was associated with a microstructure gradient induced by SMAT in a near-surface layer of the material. The benefits of gradient structures were also discussed in a recent work on strengthening thin walled tubes by a process referred to as continuous high pressure tube shearing [489]. Modelling of the mechanical behaviour of such materials calls for new theoretical tools

that account for gradient structures. Of special interest in this regard are gradient plasticity models that are microstructure-based.

A physically based model relating higher (second order) gradient terms to plastic strain incompatibility between the adjoining grains was proposed by Estrin et al. [236, 473]. The model results in an additive second derivative (Laplacian) term in an expression for the flow stress, which is similar in structure to that proposed earlier by Aifantis [335], but has the benefit of providing a link between the coefficient of this term to the grain size. It was shown [473] to account for homogenisation of microstrucure and hardness across a specimen undergoing severe plastic deformation by HPT.

The role of gradient terms in providing a more uniform strain and enabling a more homogeneous strengthening effect of SPD is demonstrated by the measurements of microhardness distribution in a specimen deformed by high pressure torsion. By the very nature of deformation by torsion, the shear strain produced varies from zero to a maximum value with the radial distance from the specimen axis to its rim. However, with the growing twist angle, or the number of revolutions, the microstructure and the microhardness were shown to become more and more uniform throughout a cross-section of an HPT aluminium specimen [546], cf. Figure 47.

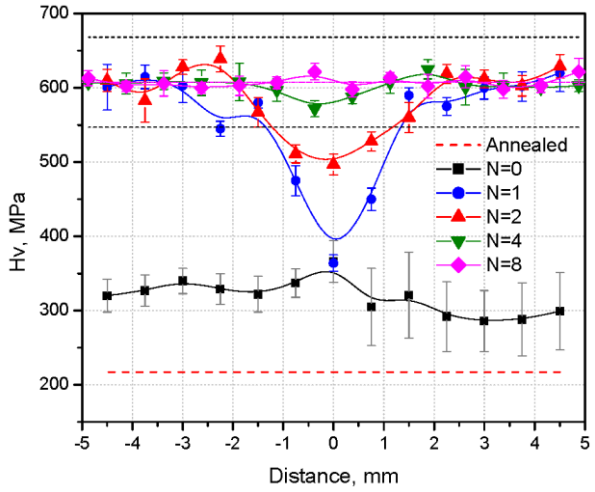

Figure 47. Progressive rise of homogeneity of microhardness in an HPT specimen of aluminium with the number of turns (after A.P. Zhilyaev et al. [547])

This paradox is resolved in terms of the mentioned model by Estrin et al. [473] according to which strain gradients act to equalise the dislocation cell size at different locations within the specimen. This is associated with progressive equalisation of shear stress across an HPT specimen with the growing number of revolutions of the anvil, as illustrated in Figure 48, which shows the variation of the cumulative shear strain with the distance from the HPT specimen axis [473].

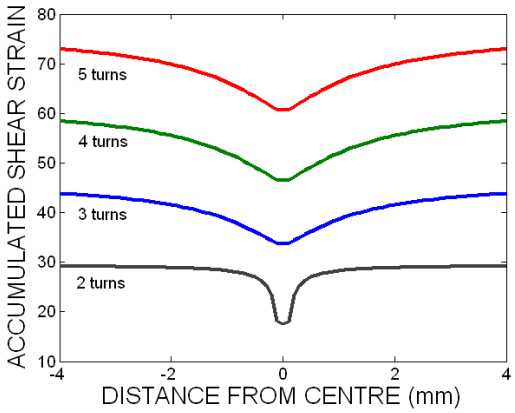

Figure 48. Progressive increase of shear strain uniformity in an HPT specimen of copper with the number of anvil revolutions as calculated using a gradient plasticity model [473].

Another physically sensible variant of gradient plasticity associates a gradient term with mobile dislocation exchange between adjoining regions of the material via dislocation cross slip [284]. Both variants of gradient plasticity were considered in the context of localised strain pattern formation in Mg alloy AZ31 under ECAP deformation [235]. Susceptibility of ECAP processing to strain localisation, particularly due to heat release, was mentioned in Section 2.3, but even without thermomechanical coupling, strain localisation may occur, and gradient plasticity is a suitable way to account for it. Using linear stability analysis, localised strain patterning in the shear zone of the alloy undergoing ECAP deformation was considered for both variants of gradient plasticity theory in conjunction with the two-internal-variable model [254, 255]. In this kind of analysis, conditions for growth of small periodic perturbations of a uniform solution of the constitutive equations with different wave numbers are determined. The temporal and spatial variation of the perturbations are represented by a factor $\exp\left(\eta t + i\xi x\right)$; solutions for which the real part of the 'growth parameter' η is positive correspond to unstable behaviour. This may be the case for various values of the wave number ξ. The one with the largest magnitude (i.e. $\xi = \xi_{max}$ corresponding to a peak in the dispersion curve $\lambda = f(\xi)$) obviously defines the length scale, i.e. the characteristic wave length $\lambda = 2\pi / \xi_{max}$ of the non-uniform strain pattern that develops to become predominant. A comparison between the experimentally observed wave length of the strain localisation patterns with the calculated dispersion curves in Figure 49, demonstrates a very good agreement between the predictions and the measurements done for two different back pressure levels used in ECAP processing.

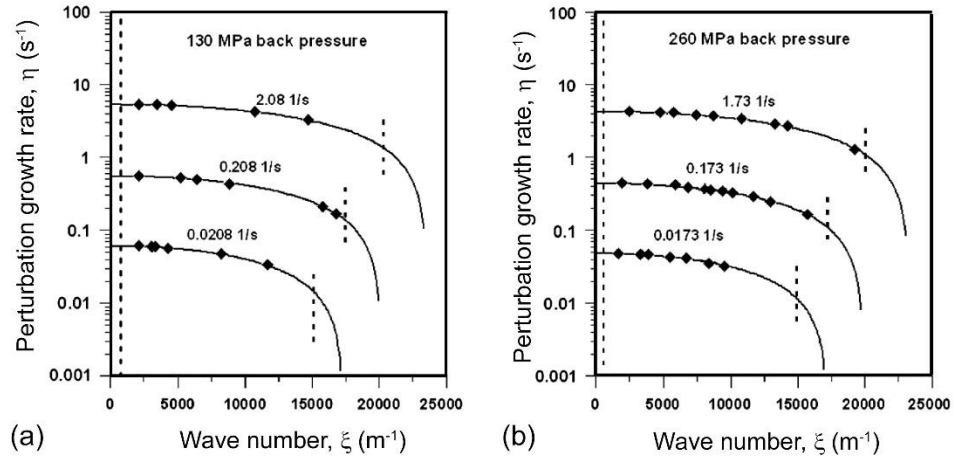

Figure 49. Results of linear stability analysis for strain localisation under ECAP with back pressure of 130 MPa (a) and 260 MPa (b) in magnesium alloy AZ31 [235]. The perturbation growth rate is shown as a function of the wave number. The estimated average shear strain rates in the tests are shown for each curve. The diamonds correspond to the experimentally observed wave numbers and are placed on theoretical curves for the respective strain rates. The vertical dotted line on the left marks the position of the smallest theoretically possible wave number, while the short vertical dashed lines on the right mark the largest possible wave numbers for the respective strain rates. (After [431], reproduced with permission).

In their model of gradient plasticity, Klusemann et al. [543] went beyond the second gradients and extended the phase-mixture model presented in the foregoing section by including a fourth-order gradient. They augmented Eq. (103) for the flow stress with gradient terms in the following form:

$$\sigma = f\sigma_{GB} + (1-f)\sigma_{GI} + h_g\left(l^2\partial_x^2\varepsilon + 2/5 l^4\partial_x^4\varepsilon\right) \quad (104)$$

In the spirit of the Estrin-Mühlhaus model [236], the intrinsic length scale l can be identified with the average grain size; h_g is a numerical parameter whose value controls the magnitude of the gradient effects. Dealing with fourth-order gradients, particularly in the context of FE simulations, is computationally challenging, but a great benefit of the model is that the fourth-order gradient provides a regularisation which results in a stable computational scheme. The analysis based on the model permits efficient treatment of patterning, as was shown in the computational exercises in [543].

8. Simulations of synthesis of architectured materials by SPD techniques

The use of SPD techniques to produce novel hybrid materials heralded as a new paradigm in materials design in [548] is seen as an important emerging direction of research in the area of severe plastic deformation. Indeed, SPD methods can be employed to engineer hybrid (multi-component) materials to a desired inner architecture while simultaneously producing an ultrafine or nanoscale grain structure of the components of a hybrid [464, 549]. This approach to fabrication of architectered hybrid materials was termed 'SPD-induced synthesis' [550, 551]. This nascent area of research is a perfect playground for modelling and numerical simulations, as the variants of thinkable inner architectures of such hybrid materials are sheer countless. Screening of conceived designs and SPD processes leading to hybrids with promising mechanical properties can best be done by numerical simulations, primarily by FEM.

A hybrid design with potentially attractive properties is that with spiral-shaped armour embedded in a massive metallic part ('matrix'). Bouaziz [552] has shown that by embedding a hard spiral-shaped filament in a softer matrix provides the material with enhanced tensile ductility, as the armour gives rise to extra strain-hardening thus delaying the onset of necking. This feature offers a possibility to alleviate a common drawback of UFG materials processed by SPD, *viz.* their low strain hardening capability and the ensuing low ductility. There are various SPD and cognate techniques by which helical armour fibres can be inserted into a massive billet. These include HPT [548], torsion [553], twist extrusion [554], screw rolling [555], and high pressure torsion-extrusion (HPTE) [556] .

By way of example, we present a schematic showing the fabrication of a hybrid material with layered spiral armour architecture [551], Figure 50. SPD-induced synthesis of architectured materials illustrated by Figure 50 involves the following steps. Prior to processing by SPD, inclusions in the form of fibres, solid particles, or powders are embedded in a workpiece. Controlled material fluxes during the SPD process will transform them to produce a desired inner structure of the hybrid material. Knowing

this architecture, one can 'pre-program' the initial distribution of these embedded objects from the targeted final architecture computationally, by solving an inverse problem.

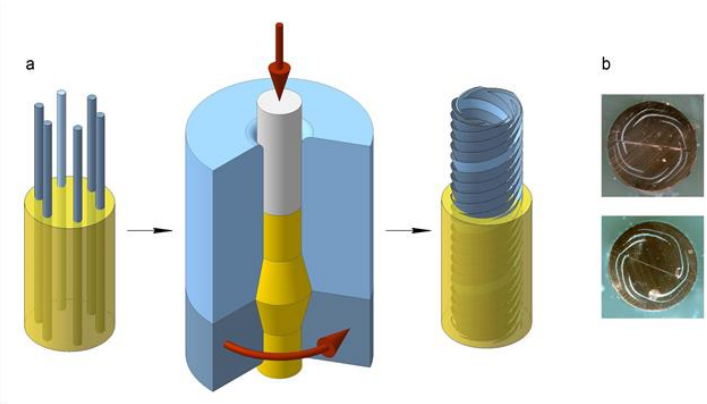

Figure 50. Producing a hybrid material with a spiral layered armour by the HPTE process: (a) initial arrangement of straight armour fibres in a billet that is subjected to HPTE processing and (b) simulated and experimental spiral layered structure in copper armoured with aluminium. (Yellow: Cu matrix; blue: aluminium fibres (transformed to spiral sheets by HPTE). (After [551], reproduced with permission.)

An example of such 'pre-programming' of the initial configuration of reinforcing fibres to produce a desired final architecture is shown in Figure 51 [550]. The SPD process applied is twist extrusion (TE). As seen from Figure 51 that represents the results of FEM simulations using the software package DEFORM 3D, five TE passes have transformed an initially straight copper fibre inserted in a titanium matrix to a helical one. The cumulative strain involved in the process is high enough to impart submicron-scale grain structure on both copper and titanium. In this way, the targeted spiral architecture is achieved with a simultaneous strengthening of both constituents of the hybrid material due to extreme grain refinement.

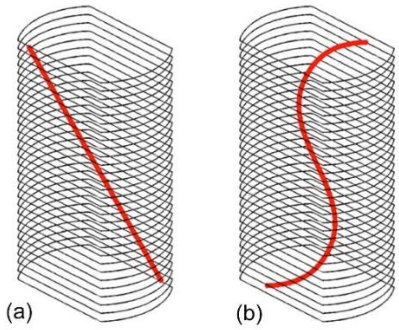

Figure 51. Shape transformation of an inclined straight fibre corresponding to the initial configuration of copper fibres within a titanium matrix (a) to a spiral one (b) after five TE passes (after [550] reproduced with permission).

With the computational tools available, there are practically no limits to the complexity of the targeted inner architecture of a hybrid material. An example of 'pre-programming' the initial embedded structure to obtain a hyperboloid final structure is shown in Figure 52 [550]. On the fabrication side, new additive manufacturing technologies make it possible to produce initial structures with a pre-programmed geometry that may be required for forming hybrid materials with virtually any desired inner architecture. Additional compaction and healing of possible defects in an additively manufactured preform provided by SPD are an extra benefit of this processing strategy.

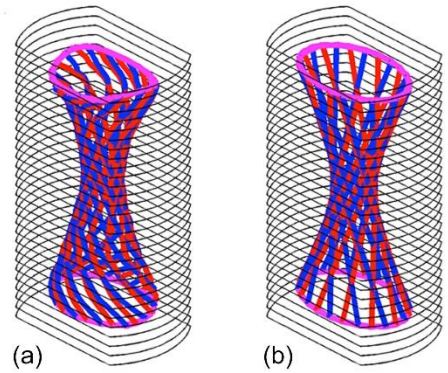

Figure 52. Simulated twist extrusion-based process of fabrication of a hybrid material: (a) 'pre-programmed' billet for obtaining the final hyperboloid structure (b) by four TE passes (simulation by DEFORM 3D, [550].)

9. Texture evolution during SPD processing

The radical grain refinement effect of severe plastic deformation should not be considered in isolation from the variation in the crystallographic texture it may cause. Indeed, the strengthening effect of grain refinement may be negated by unfavourable texture. Hence, predicting texture evolution is an important goal of modelling of SPD processes. That is why already in early work dedicated to simulations of SPD processes of FCC metals, texture evolution was calculated alongside grain refinement. This is exemplified by the work of Baik et al. [257] who employed the dislocation density-based strain hardening model expressed by Eqs. (92) with some modifications [255]. The deformation history calculated by 2D FEM simulation with ABAQUS software was combined with the full constraint Taylor model to compute textures produced by ECAP. A good agreement with the measured textures was achieved. This may appear somewhat surprising, as the model used did not consider grain subdivision that occurs during SPD processing.

An excellent overview of literature on SPD-induced texture development (specifically, for the ECAP process) was provided by Beyerlein and Tóth [94]. At the time the Beyerlein-Tóth report was written, the effect of grain subdivision was not considered in texture simulations associated with severe plastic deformation. Inclusion of the grain subdivision effect in terms of the model [454] described above improved the agreement between the calculated and the experimental texture emerging under SPD processing [108]. Figure 53 shows the results of FEM simulations of texture in the form of a {100} pole figure for micro-extrusion of copper [557] vis-à-vis an experimental pole figure. The simulations were based on polycrystal plasticity modelling (the viscoplastic self-consistent (VPSC) approach) and did include grain subdivision. A good agreement between the computational results and the experimentally measured texture is a testimony to the potential crystal plasticity modelling has in the context of SPD processing – of course, if the grain structure evolution is included in the texture calculations, which entails updating of the grain population throughout the simulation process.

The viscoplastic self-consistent approach mentioned above is a powerful computational technique that permits simultaneous tracing of strain hardening and texture development. It was developed by Molinari et al. [445] and further elaborated for anisotropic materials by Lebensohn and Tomé [558]. In this approach the behaviour of a polycrystalline aggregate is related to the behaviour of a representative ensemble of monocrystalline grains. The components of the local stress $[\sigma]$ and strain rate $[\dot{\varepsilon}]$ tensors in a particular grain are considered to be different from the corresponding macroscopic quantities $[\Sigma]$ and $[\dot{E}]$. The problem is reduced to the calculation of microscopic stresses and strain rates for each grain with explicit account of possible active slip systems. The volume average of these quantities determines the mechanical response of the polycrystalline aggregate. The problem of strain compatibility and stress equilibrium is solved by allowing some local relaxations of both quantities, while keeping their averages equal to their respective macroscopic values. A particular grain is considered as an Eshelby-type inclusion embedded in an equivalent homogeneous medium, whose behaviour is expressed in terms of the volume-weighted average over the ensemble of grains. This yields a relation between the local and the macroscopic quantities in the general form

$$\dot{\varepsilon}_{ij} - \dot{E}_{ij} = \tilde{\alpha} M_{ijkl} \left(\sigma_{kl} - \Sigma_{kl} \right) \tag{105}$$

where $[M]$ is the interaction tensor and $\tilde{\alpha}$ is a constant which parametrises the interaction between an individual grain and the homogeneous equivalent medium, covering the special cases of $\tilde{\alpha} = 0$ for the upper-bound model corresponding to homogenous strain (Taylor limit), $\tilde{\alpha} = 1$ for the tangent self-consistent model, and $\tilde{\alpha} = \infty$ for the lower-bound corresponding to homogeneous stress (Sachs limit).

A constitutive description of slip on multiple slip systems at the level of a grain can be furnished in terms of the dislocation density evolution models of the kind presented in Section 3.3. The complexity

of the problem stems from the need to introduce dislocation densities for each slip system and to consider interactions between dislocations of the different slip systems. This is challenging, but not impossible, as was demonstrated in the mentioned review by by Beyerlein and Tóth [94]. Recently, Ayoub et al. [559] modified the crystal plasticity approach to incorporate the grain boundary sliding mechanism and also account for grain subdivision. Their model provided an accurate prediction of texture evolution and the mechanical response of the magnesium alloy AZ31B at different temperatures and strain rates.

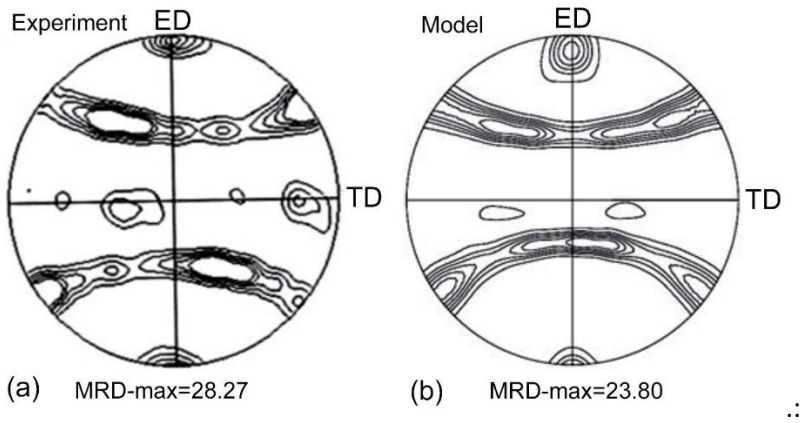

Figure 53 Experimental (left) and predicted (right) {100} pole figure for micro-extruded UFG copper. Isolevels shown are 1.2, 2.0, 2.5, 3.0, 3.5, 4, 8, 12, 20, 30; also shown is the texture intensity in terms of the multiples of random distribution (MRD) (after [557], reproduced with permission).

It is believed that crystal plasticity modelling, which has been championed by Lebensohn and Tomé, cf., e.g. [558], and advanced by Molinari and Tóth [96, 497, 560], Skrotzki et al. [561], Beyerlein and Tóth [94], Horstemeyer et al. [562], Roters et al. [78], and others, offers the most suitable platform for texture simulations for polycrystalline materials. This applies to modelling of the SPD processes and the mechanical properties of ultrafine-grained materials produced by SPD technology. As mentioned above, in numerical simulations of the SPD processes their specifics, notably progressive grain fragmentation, needs to be accounted for by updating the representative grain population.

Conclusion

In this article, we attempted to overview the extensive literature on the modelling and computational aspects of severe plastic deformation processing. Starting from phenomenological models common in solid mechanics, we took the reader through the various modelling approaches. Certainly, our preferred taste for mechanism-related and microstructure based models was obvious in this exposé. We hope to have convinced the reader that this type of modelling has substantial benefits over the more phenomenological approaches that are still common in solid mechanics literature. The entirety of the models available provide a useful toolkit for both analytical work and numerical simulations, which can be employed 'on demand', depending on the specifics of the SPD-related problem to be solved and the detail to which the microstructu information is required. Examples of the use of these modelling approaches to particular SPD processes were given and practical advice on the suitability of one or the other model was offered.

If, from the various elements presented in this overview, we were to construct an 'ideal' model to predict the material behaviour and the load on the tooling in a given SPD process, along with the microstructure, texture, and the mechanical properties of the processed material under subsequent service conditions, our model of choice would be as follows. We would certainly opt for a crystal plasticity model of the Lebensohn-Tomé kind [94, 563], but would include a provision for grain subdivision as proposed in Ref. [557]. The description of strain hardening for individual slip systems of a crystallite would be motivated by a two-internal-variable model presented in Section 3.3. Such a model would have sufficient flexibility to monitor the microstructure and texture development, yet would be robust enough to be handled within a commercial FEM code with a facility for implementing a constitutive material model through a user interface. If no microstructural detail is needed for a particular application, a simple phenomenological constitutive description, such as the Voce [177],

Johnson-Cook [287], or Armstrong-Zerilli [288] model, can be used instead. We would certainly advise against the use of oversimplified models of the Ludwik or Ludwik-Hollomon type, as they do not capture the essential feature of large strain processing, *viz.* a trend to stress saturation. Regardless of the choice of constitutive model, our preference would definitely be for a full 3D FEM simulation.

It is hoped that through this paper we helped eliminating a blind spot in the review literature on severe plastic deformation, provided the reader with a compendium of suitable modelling tools, and offered an outlook on possible future directions of analytical and computational work on SPD modelling.

Acknowledgements

The authors would like to thank Ronald Armstrong, Swantje Bargmann, Yan Beygelzimer, Hyoung Seop Kim, Benjamin Klusemann, Roman Kulagin, Rimma Lapovok, Vincent Lemiale, Sebastian Mercier, Alain Molinari, Andrey Molotnikov, Laszlo Tóth , Yuntian Zhu, and Igor Yasnikov for stimulating discussions. AV wishes to acknowledge financial support from the Russian Science Foundation through the grant-in-aid No.15-19-30025 and the State Assignment, contract #3.3881.2017/4.6. YE acknowledges research funding received from the Ministry of Education and Science of the Russian Federation through grant #14.A12.31.0001 to the National University of Science and Technology “MISIS” where part of this work was conducted.

References

[1] Valiev RZ, Estrin Y, Horita Z, Langdon TG, Zehetbauer MJ, Zhu YT. Producing bulk ultrafine-grained materials by severe plastic deformation. Journal of Metals. 2006;58:33-9.
[2] Valiev RZ, Islamgaliev RK, Alexandrov IV. Bulk nanostructured materials from severe plastic deformation. Progress in Materials Science. 2000;45:103-89.
[3] Valiev RZ, Langdon TG. Principles of equal-channel angular pressing as a processing tool for grain refinement. Progress in Materials Science. 2006;51:881-981.
[4] Estrin Y, Vinogradov A. Extreme grain refinement by severe plastic deformation: A wealth of challenging science. Acta Materialia. 2013;61:782-817.
[5] Bridgman PW. The Tensile Properties of Several Special Steels and Certain Other Materials under Pressure. Journal of Applied Physics. 1946;17:201-12.

[6] Carreker RP, Hibbard WR. Tensile deformation of high-purity copper as a function of temperature, strain rate, and grain size. Acta Metallurgica. 1953;1:656-&.
[7] Kawasaki M, Lee H-J, Jang J-i, Langdon TG. Strengthening of metals through severe plastic deformation. Reviews on Advanced Materials Science. 2017;48:13-24.
[8] Armstrong RW. 60 years of Hall-Petch: Past to present nano-scale connections. Materials Transactions. 2014;55:2-12.
[9] Armstrong RW. Plasticity: grain size effects III. Reference Module in Materials Science and Materials Engineering: Elsevier; 2016.
[10] Langer JS. Yielding transitions and grain-size effects in dislocation theory. Physical Review E. 2017;95.
[11] Gleiter H. On the structure of grain boundaries in metals. Materials Science and Engineering. 1982;52:91-131.
[12] Gleiter H. Nanocrystalline materials. Progress in Materials Science. 1989;33:223-315.
[13] Hansen N. Plastic Behavior of Metals: Large Strains. In: Buschow KHJ, Cahn RW, Flemings CR, Ilschner B, Kramer EJ, Mahajan S, et al., editors. Encyclopedia of Materials: Science and Technology (Second Edition). Oxford: Elsevier; 2001. p. 7040-50.
[14] Hansen N. Hall–Petch relation and boundary strengthening. Scripta Materialia. 2004;51:801-6.
[15] Chokshi AH, Kottada RS. The deformation characteristics of nanocrystalline metals. Transactions of the Indian Institute of Metals. 2005;58:939-50.
[16] Li Z, Hou C, Huang M, Ouyang C. Strengthening mechanism in micro-polycrystals with penetrable grain boundaries by discrete dislocation dynamics simulation and Hall–Petch effect. Computational Materials Science. 2009;46:1124-34.
[17] Lyu H, Taheri-Nassaj N, Zbib HM. A multiscale gradient-dependent plasticity model for size effects. Philosophical Magazine. 2016;96:1883-908.
[18] Zontsika NA, Abdul-Latif A, Ramtani S. Pertinence of the Grain Size on the Mechanical Strength of Polycrystalline Metals. Journal of Engineering Materials and Technology. 2017;139:021017--10.
[19] Armstrong RW, Balasubramanian N. Unified Hall-Petch description of nano-grain nickel hardness, flow stress and strain rate sensitivity measurements. AIP Advances. 2017;7:085010.
[20] Eshelby JD, Frank FC, Nabarro FRN. XLI. The equilibrium of linear arrays of dislocations. The London, Edinburgh, and Dublin Philosophical Magazine and Journal of Science. 1951;42:351-64.
[21] Cheng S, Spencer JA, Milligan WW. Strength and tension/compression asymmetry in nanostructured and ultrafine-grain metals. Acta Materialia. 2003;51:4505-18.
[22] Estrin Y, Kim HS, Nabarro FRN. A comment on the role of Frank-Read sources in plasticity of nanomaterials. Acta Materialia. 2007;55:6401-7.
[23] Estrin Y, Mecking H. A unified phenomenological description of work hardening and creep based on one-parameter models. Acta Metallurgica. 1984;32:57-70.
[24] Gubicza J, Chinh NQ, Szommer P, Vinogradov A, Langdon TG. Microstructural characteristics of pure gold processed by equal-channel angular pressing. Scripta Materialia. 2007;56:947-50.
[25] Balogh L, Ungar T, Zhao Y, Zhu YT, Horita Z, Xu C, et al. Influence of stacking-fault energy on microstructural characteristics of ultrafine-grain copper and copper-zinc alloys. Acta Materialia. 2008;56:809-20.
[26] Vinogradov A, Maruyama M, Hashimoto S. On the role of dislocation hardening in the monotonic and cyclic strength of severely plastically deformed metals. Scripta Materialia. 2009;61:817-20.
[27] Gubicza J, Chinh NQ, Lábár JL, Dobatkin S, Hegedüs Z, Langdon TG. Correlation between microstructure and mechanical properties of severely deformed metals. Journal of Alloys and Compounds. 2009;483:271-4.
[28] Vinogradov A, Maruyama M, Kaneko Y, Hashimoto S. Effect of dislocation hardening on monotonic and cyclic strength of severely deformed copper. Philosophical Magazine. 2012;92:666-89.

[29] Starink MJ, Cheng X, Yang S. Hardening of pure metals by high-pressure torsion: A physically based model employing volume-averaged defect evolutions. Acta Materialia. 2013;61:183-92.
[30] Jóni B, Schafler E, Zehetbauer M, Tichy G, Ungár T. Correlation between the microstructure studied by X-ray line profile analysis and the strength of high-pressure-torsion processed Nb and Ta. Acta Materialia. 2013;61:632-42.
[31] Chen Y, Gao N, Sha G, Ringer SP, Starink MJ. Microstructural evolution, strengthening and thermal stability of an ultrafine-grained Al–Cu–Mg alloy. Acta Materialia. 2016;109:202-12.
[32] Starink MJ. Dislocation versus grain boundary strengthening in SPD processed metals: Non-causal relation between grain size and strength of deformed polycrystals. Materials Science and Engineering: A. 2017;705:42-5.
[33] Osakada K. History of plasticity and metal forming analysis. Journal of Materials Processing Technology. 2010;210:1436-54.
[34] McDowell DL. A perspective on trends in multiscale plasticity. International Journal of Plasticity. 2010;26:1280-309.
[35] Edalati K, Horita Z. A review on high-pressure torsion (HPT) from 1935 to 1988. Materials Science and Engineering: A. 2016;652:325-52.
[36] Cottrell A. Theory of Crystal Dislocations. London, Glasgow; printed in Belgium: Blackie & Son; 1965.
[37] Mura T, American Society of Mechanical Engineers. Applied Mechanics Division. Mathematical theory of dislocations. New York,: American Society of Mechanical Engineers; 1969.
[38] Hirth JP, Lothe J. Theory of dislocations. 2nd ed. New York: Wiley; 1982.
[39] Nabarro FRN. Theory of crystal dislocations. Oxford: Clarendon Press; 1967.
[40] Friedel J. Dislocations. [1st English ed. Oxford, New York,: Pergamon Press;; 1964.
[41] Kubin L, Oxford University Press. Dislocations, mesoscale simulations and plastic flow. Oxford series on materials modelling 5. Oxford: Oxford University Press,; 2013. p. 1 online resource.
[42] Yip S. Handbook of materials modeling. Dordrecht ; [London]: Springer; 2005.
[43] Tadmor EB, Miller RE. Modeling materials: Continuum, atomistic and multiscale techniques: Cambridge University Press; 2011.
[44] Tadmor EB, Miller RE, Elliott RS. Continuum mechanics and thermodynamics: From fundamental concepts to governing equations: Cambridge University Press; 2011.
[45] Li J. Atomistic Calculation of Mechanical Behavior. In: Yip S, editor. Handbook of Materials Modeling: Springer Netherlands; 2005. p. 773-92.
[46] Kaxiras E, Yip S. Introduction: Atomistic Nature of Materials. In: Yip S, editor. Handbook of Materials Modeling: Springer Netherlands; 2005. p. 451-8.
[47] Jones RE, Weinberger CR, Coleman SP, Tucker GJ. Introduction to Atomistic Simulation Methods. In: Weinberger CR, Tucker GJ, editors. Multiscale Materials Modeling for Nanomechanics. Cham: Springer International Publishing; 2016. p. 1-52.
[48] Van der Giessen E, Needleman A. Discrete Dislocation Plasticity. In: Yip S, editor. Handbook of Materials Modeling: Springer Netherlands; 2005. p. 1115-31.
[49] Zbib HM, Khraishi TA. Dislocation Dynamics. In: Yip S, editor. Handbook of Materials Modeling: Springer Netherlands; 2005. p. 1097-114.
[50] Vladimirov VI, Romanov AE. Disclinations in Crystalline Solids. Amsterdam, North Holland1991. p. p.191.
[51] Groma I, Bak, oacute, B. Dislocation Patterning: From Micro- to Mesoscale Description. Physical Review Letters. 2000;84:1487.
[52] Groma I, Bako B. Linking different scales: discrete, self-consistent field, and stochastic dislocation dynamics. Materials Science and Engineering A. 2001;309-310:356-9.
[53] Groma I, Balogh P. Investigation of dislocation pattern formation in a two-dimensional self-consistent field approximation. Acta Materialia. 1999;47:3647-54.

[54] Hähner P. Stochastic dislocation patterning during cyclic plastic deformation. Applied Physics A: Materials Science & Processing. 1996;63:45-55.
[55] Teodosiu C. Large plastic deformation of crystalline aggregates. Wien etc.: Springer; 1997.
[56] Argon AS. Strengthening mechanisms in crystal plasticity. Oxford: Oxford University Press; 2008.
[57] Chakrabarty J. Applied plasticity. 2nd ed. ed. New York: Springer; 2010.
[58] Gil Sevillano J, van Houtte P, Aernoudt E. Large strain work hardening and textures. Progress in Materials Science. 1980;25:69-134.
[59] Walgraef D, Aifantis EC. On the formation and stability of dislocation patterns-II: Two-dimensional considerations. International Journal of Engineering Science. 1985;23:1359-64.
[60] Walgraef D, Aifantis EC. Dislocation patterning in fatigued metals as a result of dynamical instabilities. Journal of Applied Physics. 1985;58:688-91.
[61] Walgraef D, Aifantis EC. On the formation and stability of dislocation patterns-I: One-dimensional considerations. International Journal of Engineering Science. 1985;23:1351-8.
[62] Walgraef D, Aifantis EC. On the formation and stability of dislocation patterns-III: Three-dimensional considerations. International Journal of Engineering Science. 1985;23:1365-72.
[63] Hähner P. A theory of dislocation cell formation based on stochastic dislocation dynamics. Acta Materialia. 1996;44:2345-52.
[64] Hähner P, Zaiser M. Dislocation dynamics and work hardening of fractal dislocation cell structures. Materials Science and Engineering A. 1999;272:443-54.
[65] Panin VE, Grinyaev YV, Elsukova TF, Ivanchin AG. Structural levels of deformation in solids. Russian Physics Journal. 1982;25:479-97.
[66] Estrin Y. Syntheses: Playing scales - a brief summary. 1999;7:747-51.
[67] Raabe D. Computational materials science the simulation of materials, microstructures and properties. Weinheim etc.: Wiley-VCH; 1998.
[68] Roters F, Eisenlohr P, Hantcherli L, Tjahjanto DD, Bieler TR, Raabe D. Overview of constitutive laws, kinematics, homogenization and multiscale methods in crystal plasticity finite-element modeling: Theory, experiments, applications. Acta Materialia. 2010;58:1152-211.
[69] Curtin WA, Ronald EM. Atomistic/continuum coupling in computational materials science. Modelling and Simulation in Materials Science and Engineering. 2003;11:R33.
[70] Shilkrot LE, Miller RE, Curtin WA. Coupled Atomistic and Discrete Dislocation Plasticity. Physical Review Letters. 2002;89:025501.
[71] Horstemeyer MF. Multiscale modeling: A review. Practical Aspects of Computational Chemistry: Methods, Concepts and Applications: Springer Netherlands; 2010. p. 87-135.
[72] Horstemeyer MF. Mesoscale/Macroscale Computational Methods. In: Yip S, editor. Handbook of Materials Modeling: Springer Netherlands; 2005. p. 1071-5.
[73] Pippan R, Gumbsch P. Multiscale modelling of plasticity and fracture by means of dislocation mechanics. Courses and lectures ; no 522. Wien New York: Springer Verlag; 2010. p. 394 p.
[74] Weygand D, Mrovec M, Hochrainer T, Gumbsch P. Multiscale Simulation of Plasticity in bcc Metals. Annual Review of Materials Research: Annual Reviews Inc.; 2015. p. 369-90.
[75] Koester A, Ma A, Hartmaier A. Atomistically informed crystal plasticity model for body-centered cubic iron. Acta Materialia. 2012;60:3894-901.
[76] Blanckenhagen Bv, Gumbsch P, Arzt E. Dislocation sources in discrete dislocation simulations of thin-film plasticity and the Hall-Petch relation. Modelling and Simulation in Materials Science and Engineering. 2001;9:157.
[77] Raabe D, Sachtleber M, Zhao Z, Roters F, Zaefferer S. Micromechanical and macromechanical effects in grain scale polycrystal plasticity experimentation and simulation. Acta Materialia. 2001;49:3433-41.

[78] Roters F, Eisenlohr P, Bieler TR, Raabe D. Crystal plasticity finite element methods in materials science and engineering. Weinheim: Wiley-Vch; 2010.
[79] Phillips R. Crystals, defects and microstructures : modeling across scales. Cambridge ; New York: Cambridge University Press; 2001.
[80] Tadmor EB, Ortiz M, Phillips R. Quasicontinuum analysis of defects in solids. Philosophical Magazine A. 1996;73:1529-63.
[81] The Minerals M, Materials S. Modeling Across Scales: A Roadmapping Study for Connecting Materials Models and Simulations Across Length and Time Scales. Warrendale, PA: TMS; 2015.
[82] Lemaitre J, Chaboche J-L. Mechanics of solid materials. Repr. 2000, transferred to digital printing 2002 ed. Cambridge: Cambridge University Press; 2002.
[83] Bower AF. Applied mechanics of solids. Boca Raton: CRC Press; 2010.
[84] Zienkiewicz OC, Cheung YK. The finite element method in structural and continuum mechanics: numerical solution of problems in structural and continuum mechanics. London, New York etc.: McGraw-Hill; 1967.
[85] Zienkiewicz OC, Taylor RL. The finite element method for solid and structural mechanics. 6th ed. Oxford ; Burlington, MA: Elsevier Butterworth-Heinemann; 2005.
[86] Prathap G. The finite element method in structural mechanics : principles and practice of design of field-consistent elements for structural and solid mechanics. Dordrecht ; Boston: Kluwer Academic; 1993.
[87] Landau LD, Lifshitz EM. Theory of elasticity. 2d English ed. Oxford, New York,: Pergamon Press; 1970.
[88] Kosevich AM. Crystal Dislocations and Theory of Elasticity. In: Nabarro FRN, editor. Dislocations in Solids: North-Holland, Amsterdam; 1979. p. 33.
[89] Kobayashi So, Oh S-I, Altan T. Metal forming and the finite-element method. New York: Oxford University Press; 1989.
[90] Nowick AS, Berry BS. Anelastic Relaxation in Crystalline Solids. New York, USA: Academic Press 1972.
[91] Zaïri F, Aour B, Gloaguen JM, Naït-Abdelaziz M, Lefebvre JM. Numerical modelling of elastic–viscoplastic equal channel angular extrusion process of a polymer. Computational Materials Science. 2006;38:202-16.
[92] Kamrani M, Levitas VI, Feng B. FEM simulation of large deformation of copper in the quasi-constrain high-pressure-torsion setup. Materials Science and Engineering: A. 2017;705:219-30.
[93] Cerri E, De Marco PP, Leo P. FEM and metallurgical analysis of modified 6082 aluminium alloys processed by multipass ECAP: Influence of material properties and different process settings on induced plastic strain. Journal of Materials Processing Technology. 2009;209:1550-64.
[94] Beyerlein IJ, Tóth LS. Texture evolution in equal-channel angular extrusion. Progress in Materials Science. 2009;54:427-510.
[95] Anand L. Single-crystal elasto-viscoplasticity: application to texture evolution in polycrystalline metals at large strains. Computer Methods in Applied Mechanics and Engineering. 2004;193:5359-83.
[96] Tóth LS. Modelling of strain hardening and microstructural evolution in equal channel angular extrusion. Computational Materials Science. 2005;32:568-76.
[97] Acharya A, Beaudoin AJ. Grain-size effect in viscoplastic polycrystals at moderate strains. Journal of the Mechanics and Physics of Solids. 2000;48:2213-30.
[98] Aoyagi Y, Tsuru T, Shimokawa T. Crystal plasticity modeling and simulation considering the behavior of the dislocation source of ultrafine-grained metal. International Journal of Plasticity. 2013.
[99] Aoyagi Y, Shizawa K. Multiscale crystal plasticity modeling based on geometrically necessary crystal defects and simulation on fine-graining for polycrystal. International Journal of Plasticity. 2007;23:1022-40.

[100] Narutani T, Takamura J. Grain-size strengthening in terms of dislocation density measured by resistivity. Acta Metallurgica et Materialia. 1991;39:2037-49.
[101] Beaudoin AJ, Acharya A, Chen SR, Korzekwa DA, Stout MG. Consideration of grain-size effect and kinetics in the plastic deformation of metal polycrystals. Acta Materialia. 2000;48:3409-23.
[102] Beaudoin AJ, Acharya A. A model for rate-dependent flow of metal polycrystals based on the slip plane lattice incompatibility. Materials Science and Engineering: A. 2001;309–310:411-5.
[103] Arsenlis A, M. Parks D, Becker R, V. Bulatov V. On the evolution of crystallographic dislocation density in non-homogeneously deforming crystals. Journal of the Mechanics and Physics of Solids. 2004;52:1213-46.
[104] Asaro RJ, Needleman A. Overview no. 42 Texture development and strain hardening in rate dependent polycrystals. Acta Metallurgica. 1985;33:923-53.
[105] Tóth LS. Texture Evolution in Severe Plastic Deformation by Equal Channel Angular Extrusion. Advanced Engineering Materials. 2003;5:308-16.
[106] Kalidindi SR, Donohue BR, Li S. Modeling texture evolution in equal channel angular extrusion using crystal plasticity finite element models. International Journal of Plasticity. 2009;25:768-79.
[107] Tóth LS, Estrin Y, Lapovok R, Gu C. A model of grain fragmentation based on lattice curvature. Acta Materialia. 2010;58:1782-94.
[108] Gu CF, Tóth LS. Texture development and grain refinement in non-equal-channel angular-pressed Al. Scripta Materialia. 2012;67:33-6.
[109] Humphreys J, Bate P. Gradient plasticity and deformation structures around inclusions. Scripta Materialia. 2003;48:173-8.
[110] Aifantis EC. Update on a class of gradient theories. Mechanics of Materials. 2003;35:259-80.
[111] Aifantis EC. Mechanics aspects in micro- and nano-scales. New York, NY, United States: Publ by ASME; 1992. p. 1-3.
[112] Fleck NA, Hutchinson JW. Strain Gradient Plasticity. In: John WH, Theodore YW, editors. Advances in Applied Mechanics: Elsevier; 1997. p. 295-361.
[113] Fleck NA, Muller GM, Ashby MF, Hutchinson JW. Strain gradient plasticity: Theory and experiment. Acta Metallurgica et Materialia. 1994;42:475-87.
[114] Nye JF. Some geometrical relations in dislocated crystals. Acta Metallurgica. 1953;1:153-62.
[115] Zhang X, Aifantis K. Interpreting the internal length scale in strain gradient plasticity. Reviews on Advanced Materials Science. 2015;41:72-83.
[116] Needleman A, Van Der Giessen E. Discrete dislocation and continuum descriptions of plastic flow. Materials Science and Engineering A. 2001;309-310:1-13.
[117] Hiratani M, Zbib HM. Stochastic Dislocation Dynamics for Dislocation-Defects Interaction: A Multiscale Modeling Approach. Journal of Engineering Materials and Technology. 2002;124:335-41.
[118] Deshpande VS, Needleman A, Van der Giessen E. Finite strain discrete dislocation plasticity. Journal of the Mechanics and Physics of Solids. 2003;51:2057-83.
[119] Kubin LP, Fressengeas C, Ananthakrishna G. Chapter 57 Collective behaviour of dislocations in plasticity. In: Duesbery FRNNaMS, editor. Dislocations in Solids: Elsevier; 2002. p. 101-92.
[120] Zepeda-Ruiz LA, Stukowski A, Oppelstrup T, Bulatov VV. Probing the limits of metal plasticity with molecular dynamics simulations. Nature. 2017;advance online publication.
[121] Srinivasan R, Cherukuri B, Chaudhury PK. Scaling up of equal channel angular pressing (ECAP) for the production of forging stock. Nanomaterials by Severe Plastic Deformation. 2006;503-504:371-8.
[122] Orlov D, Raab G, Lamark TT, Popov M, Estrin Y. Improvement of mechanical properties of magnesium alloy ZK60 by integrated extrusion and equal channel angular pressing. Acta Materialia. 2011;59:375-85.
[123] Raab GJ, Valiev RZ, Lowe TC, Zhu YT. Continuous processing of ultrafine grained Al by ECAP-Conform. Materials Science and Engineering A. 2004;382:30-4.

[124] Jin YG, Baek HM, Im Y-T, Jeon BC. Continuous ECAP process design for manufacturing a microstructure-refined bolt. Materials Science and Engineering: A. 2011;530:462-8.
[125] Jin YG, Baek HM, Hwang SK, Im Y-T, Jeon BC. Continuous high strength aluminum bolt manufacturing by the spring-loaded ECAP system. Journal of Materials Processing Technology. 2012;212:848-55.
[126] Valiev RZ, Zhilyaev AP, Langdon TG. Bulk nanostructured materials : fundamentals and applications2014.
[127] Rosochowski A, Olejnik L. Finite element simulation of severe plastic deformation processes. Proceedings of the Institution of Mechanical Engineers Part L-Journal of Materials-Design and Applications. 2007;221:187-96.
[128] Medeiros Nd, Moreira LP, Bressan JD, Lins JFC, Gouvêa JPd. Sensitivity analysis of the ECAE process via 2k experiments design. Matéria (Rio de Janeiro). 2010;15:208-17.
[129] Segal VM, Reznikov VI, Drobyshevkiy AE, Kopylov VI. Plastic Metal Working by Simple Shear. Russian Metall. 1981:99.
[130] Segal VM. Severe plastic deformation: simple shear versus pure shear. Materials Science and Engineering A. 2002;338:331-44.
[131] Segal VM. Slip line solutions, deformation mode and loading history during equal channel angular extrusion. Materials Science and Engineering A. 2003;345:36-46.
[132] Khoddam S, Hodgson PD, Zarei-Hanzaki A, Yan Foon L. A simple model for material's strengthening under high pressure torsion. Materials & Design. 2016;99:335-40.
[133] Khoddam S. A detailed model of high pressure torsion. Materials Science and Engineering: A. 2017;683:256-63.
[134] Kleiber M. Incremental finite element modelling in non-linear solid mechanics. Chichester, England: E. Horwood Halsted Press; 1989.
[135] Kim HS. Evaluation of Strain Rate During Equal-channel Angular Pressing. Journal of Materials Research. 2002;17:172-9.
[136] Iwahashi Y, Horita Z, Nemoto M, Langdon TG. The process of grain refinement in equal-channel angular pressing. Acta Materialia. 1998;46:3317-31.
[137] Alkorta J, Gil Sevillano J. A comparison of FEM and upper-bound type analysis of equal-channel angular pressing (ECAP). Journal of Materials Processing Technology. 2003;141:313-8.
[138] Paydar MH, Reihanian M, Ebrahimi R, Dean TA, Moshksar MM. An upper-bound approach for equal channel angular extrusion with circular cross-section. Journal of Materials Processing Technology. 2008;198:48-53.
[139] Luis-Perez CJ, Luri-Irigoyen R, Gaston-Ochoa D. Finite element modelling of an Al-Mn alloy by equal channel angular extrusion (ECAE). Journal of Materials Processing Technology. 2004;153-54:846-52.
[140] Luis Pérez CJ, Luri R. Comparative analysis of actual processing conditions in ECAE between FEM and both analytical and experimental results. Materials and Manufacturing Processes. 2011;26:1147-56.
[141] Eivani AR, Karimi Taheri A. An upper bound solution of ECAE process with outer curved corner. Journal of Materials Processing Technology. 2007;182:555-63.
[142] Eivani AR, Taheri AK. A new method for estimating strain in equal channel angular extrusion. Journal of Materials Processing Technology. 2007;183:148-53.
[143] Luis Pérez CJ. On the correct selection of the channel die in ECAP processes. Scripta Materialia. 2004;50:387-93.
[144] Luis Pérez CJ, Luri R. Study of the ECAE process by the upper bound method considering the correct die design. Mechanics of Materials. 2008;40:617-28.
[145] Luri R, Luis CJ, Leon J, Sebastian MA. A new configuration for equal channel angular extrusion dies. Journal of Manufacturing Science and Engineering-Transactions of the Asme. 2006;128:860-5.

[146] Luri R, Luis CJ. Study of ECAE process by using FEM. Advances in Materials Processing Technologies. 2006;526:193-8.
[147] Luri R, Luis Pérez CJ. Modeling of the processing force for performing ECAP of circular cross-section materials by the UBM. International Journal of Advanced Manufacturing Technology. 2012;58:969-83.
[148] Luri R, Luis Pérez CJ. Analysis and modelling by finite element method of the equal channel angular extrusion pressure. Proceedings of the Institution of Mechanical Engineers, Part B: Journal of Engineering Manufacture. 2010;224:925-35.
[149] Şimşir C, Karpuz P, Gür CH. Quantitative analysis of the influence of strain hardening on equal channel angular pressing process. Computational Materials Science. 2010;48:633-9.
[150] Segal VM. Materials processing by simple shear. Materials Science and Engineering A. 1995;197:157-64.
[151] Segal VM, Reznikov VI, Kopylov VI, Pavlik DA, Malyshev VF. Processes of Plastic Structure Formation of Metals (in Russian). Minsk, Belarus: Nauka i Tehnika; 1994.
[152] Iwahashi Y, Wang J, Horita Z, Nemoto M, Langdon TG. Principle of equal-channel angular pressing for the processing of ultra-fine grained materials. Scripta Materialia. 1996;35:143-6.
[153] Goforth RE, Hartwig KT, Cornwell LR. Severe Plastic Deformation of Materials by Equal Channel Angular Extrusion (ECAE). In: Lowe T, Valiev R, editors. Investigations and Applications of Severe Plastic Deformation: Springer Netherlands; 2000. p. 3-12.
[154] Milind TR, Date PP. Analytical and finite element modeling of strain generated in equal channel angular extrusion. International Journal of Mechanical Sciences. 2012;56:26-34.
[155] Aida T, Matsuki K, Horita Z, Langdon TG. Estimating the equivalent strain in equal-channel angular pressing. Scripta Materialia. 2001;44:575-9.
[156] Tóth LS, Arruffat Massion R, Germain L, Baik SC, Suwas S. Analysis of texture evolution in equal channel angular extrusion of copper using a new flow field. Acta Materialia. 2004;52:1885-98.
[157] Panigrahi A, Scheerbaum N, Chekhonin P, Scharnweber J, Beausir B, Hockauf M, et al. Effect of back pressure on material flow and texture in ECAP of aluminum. IOP Conference Series: Materials Science and Engineering. 2014;63:012153.
[158] Hasani A, Tóth LS, Beausir B. Principles of nonequal channel angular pressing. Journal of Engineering Materials and Technology, Transactions of the ASME. 2010;132:0310011-9.
[159] Beyerlein IJ, Tomé CN. Analytical modeling of material flow in equal channel angular extrusion (ECAE). Materials Science and Engineering: A. 2004;380:171-90.
[160] Bridgman PW. Effects of high shearing stress combined with high hydrostatic pressure. Physical Review. 1935;48:825-47.
[161] Bridgman PW. Shearing Phenomena at High Pressure of Possible Importance for Geology. The Journal of Geology. 1936;44:653-69.
[162] Dieter GE. Mechanical metallurgy. ed. 3 ed. New York a. o.: McGraw-Hill; 1986.
[163] Pippan R, Scheriau S, Hohenwarter A, Hafok M. Advantages and limitations of HPT: a review. In: Estrin YMHJ, editor. 4th International Conference on Nanomaterials by Severe Plastic Deformation. Goslar, GERMANY: Trans Tech Publications Ltd; 2008. p. 16-21.
[164] Beygelzimer Y, Kulagin R, Toth LS, Ivanisenko Y. The self-similarity theory of high pressure torsion. Beilstein J Nanotechnology. 2016;7:1267-77.
[165] Onaka S. Appropriateness of the hencky equivalent strain as the quantity to represent the degree of severe plastic deformation. Materials Transactions. 2012;53:1547-8.
[166] Jonas JJ, Ghosh C, Toth LS. The equivalent strain in high pressure torsion. Materials Science and Engineering: A. 2014;607:530-5.
[167] Beygelzimer Y, Toth LS, Jonas JJ. Some Physical Characteristics of Strain Hardening in Severe Plastic Deformation. Advanced Engineering Materials. 2015;17:1783-91.

[168] Kim HS, Seo MH, Hong SI. Plastic deformation analysis of metals during equal channel angular pressing. Journal of Materials Processing Technology. 2001;113:622-6.
[169] Yamaguchi D, Horita Z, Nemoto M, Langdon TG. Significance of adiabatic heating in equal-channel angular pressing. Scripta Materialia. 1999;41:791-6.
[170] Yamaguchi D, Horita Z, Fujinami T, Nemoto M, Langdon TG. Factors affecting grain refinement in equal-channel angular pressing. Aluminium Alloys: Their Physical and Mechanical Properties, Pts 1-3. 2000;331-3:607-12.
[171] Berbon P, Furukawa M, Horita Z, Nemoto M, Langdon T. Influence of pressing speed on microstructural development in equal-channel angular pressing. Metall and Mat Trans A. 1999;30:1989-97.
[172] Antolovich SD, Armstrong RW. Plastic strain localization in metals: origins and consequences. Progress in Materials Science. 2014;59:1-160.
[173] Komura S, Horita Z, Nemoto M, Langdon TG. Influence of stacking fault energy on microstructural development in equal-channel angular pressing. Journal of Materials Research. 1999;14:4044-50.
[174] Horita Z, Fujinami T, Nemoto M, Langdon T. Equal-channel angular pressing of commercial aluminum alloys: Grain refinement, thermal stability and tensile properties. Metall and Mat Trans A. 2000;31:691-701.
[175] Wei W, Wei KX, Fan GJ. A new constitutive equation for strain hardening and softening of fcc metals during severe plastic deformation. Acta Materialia. 2008;56:4771-9.
[176] Dalla Torre F, Lapovok R, Sandlin J, Thomson PF, Davies CHJ, Pereloma EV. Microstructures and properties of copper processed by equal channel angular extrusion for 1-16 passes. Acta Materialia. 2004;52:4819-32.
[177] Voce E. The relationship between stress and strain for homogeneous deformation. Journal of the Institute of Metals. 1948;74:537-62.
[178] Panin VE, Likhachev VA, Grinyaev YV. Structural Levels of Deformation of Solids (in Russian). Novosibirsk, Russia: Nauka Publishers; 1985.
[179] Wetscher F, Vorhauer A, Pippan R. Strain hardening during high pressure torsion deformation. Materials Science and Engineering A. 2005;410:213-6.
[180] Csanádi T, Chinh NQ, Gubicza J, Langdon TG. Plastic behavior of fcc metals over a wide range of strain: Macroscopic and microscopic descriptions and their relationship. Acta Materialia. 2011;59:2385-91.
[181] Mecking H, Lücke K. Quantitative analyse der bereich III-verfestigung von silber-einkristallen. Acta Metallurgica. 1969;17:279-89.
[182] Kocks UF. Laws for work-hardening and low-temperature creep. Journal of Engineering Materials and Technology-Transactions of the Asme. 1976;98:76-85.
[183] Mecking H. Description of hardening curves of fcc single- and polycrystals. In: Thompson AW, editor. Work hardening in tension and fatigue: proceedings of a symposium, Cincinnati, Ohio, November 11, 1975 The Metallurgical Society of AIME; 1977. p. 67-90.
[184] Kocks UF, Mecking H. Physics and phenomenology of strain hardening: the FCC case. Progress in Materials Science. 2003;48:171-273.
[185] Chinh NQ, Horvath G, Horita Z, Langdon TG. A new constitutive relationship for the homogeneous deformation of metals over a wide range of strain. Acta Materialia. 2004;52:3555-63.
[186] Chinh NQ, Illy J, Horita Z, Langdon TG. Using the stress–strain relationships to propose regions of low and high temperature plastic deformation in aluminum. Materials Science and Engineering: A. 2005;410–411:234-8.
[187] Prangnell PB, Harris C, Roberts SM. Finite element modelling of equal channel angular extrusion. Scripta Materialia. 1997;37:983-9.

[188] Valberg HS. Applied metal forming : including FEM analysis. Cambridge: Cambridge University Press; 2010.
[189] Segal VM. Equal channel angular extrusion: from macromechanics to structure formation. Materials Science and Engineering A. 1999;271:322-33.
[190] DeLo DP, Semiatin SL. Finite-element modeling of nonisothermal equal-channel angular extrusion. Metall and Mat Trans A. 1999;30:1391-402.
[191] Semiatin SL, DeLo DP, Shell EB. The effect of material properties and tooling design on deformation and fracture during equal channel angular extrusion. Acta Materialia. 2000;48:1841-51.
[192] Li S, Bourke MAM, Beyerlein IJ, Alexander DJ, Clausen B. Finite element analysis of the plastic deformation zone and working load in equal channel angular extrusion. Materials Science and Engineering A. 2004;382:217-36.
[193] Son I-H, Lee J-H, Im Y-T. Finite element investigation of equal channel angular extrusion with back pressure. Journal of Materials Processing Technology. 2006;171:480-7.
[194] Dumoulin S, Roven HJ, Werenskiold JC, Valberg HS. Finite element modeling of equal channel angular pressing: Effect of material properties, friction and die geometry. Materials Science and Engineering: A. 2005;410–411:248-51.
[195] Krallics G, Budilov IN, Alexandrov IV, Raab GI, Zhernakov VS, Valiev RZ. Computer Simulation of Equal-Channel Angular Pressing of Tungsten by Means of the Finite Element Method. Nanomaterials by Severe Plastic Deformation: Wiley-VCH Verlag GmbH & Co. KGaA; 2005. p. 271-7.
[196] Bowen JR, Gholinia A, Roberts SM, Prangnell PB. Analysis of the billet deformation behaviour in equal channel angular extrusion. Materials Science and Engineering A. 2000;287:87-99.
[197] Oruganti RK, Subramanian PR, Marte JS, Gigliotti MF, Amancherla S. Effect of friction, backpressure and strain rate sensitivity on material flow during equal channel angular extrusion. Materials Science and Engineering A. 2005;406:102-9.
[198] Suo T, Li Y, Guo Y, Liu Y. The simulation of deformation distribution during ECAP using 3D finite element method. Materials Science and Engineering: A. 2006;432:269-74.
[199] Kim HS, Seo MH, Hong SI. Finite element analysis of equal channel angular pressing of strain rate sensitive metals. Journal of Materials Processing Technology. 2002;130-131:497-503.
[200] Djavanroodi F, Ebrahimi M. Effect of die channel angle, friction and back pressure in the equal channel angular pressing using 3D finite element simulation. Materials Science and Engineering: A. 2010;527:1230-5.
[201] Ono M, Mizufune H, Narita M. Development of semicontinuous 4-stage ECAE method. In: Yanagimoto NKHNJ, editor. Proceedings of the 7th International Conference on Technology of Plasticity. Yokohama, Japan,: Japan Society for Technology of Plasticity; 2002. p. 1249–54
[202] Raab GI. Plastic flow at equal channel angular processing in parallel channels. Materials Science and Engineering: A. 2005;410–411:230-3.
[203] Rosochowski A, Olejnik L. Numerical and physical modelling of plastic deformation in 2-turn equal channel angular extrusion. Journal of Materials Processing Technology. 2002;125–126:309-16.
[204] Nagasekhar AV, Tick-Hon Y. Optimal tool angles for equal channel angular extrusion of strain hardening materials by finite element analysis. Computational Materials Science. 2004;30:489-95.
[205] Suo T, Li YL, Deng Q, Liu YY. Optimal pressing route for continued equal channel angular pressing by finite element analysis. Materials Science and Engineering A. 2007;466:166-71.
[206] Srinivasan R. Computer simulation of the equichannel angular extrusion (ECAE) process. Scripta Materialia. 2001;44:91-6.
[207] Djavanroodi F, Omranpour B, Ebrahimi M, Sedighi M. Designing of ECAP parameters based on strain distribution uniformity. Progress in Natural Science: Materials International. 2012;22:452-60.
[208] Yang F, Saran A, Okazaki K. Finite element simulation of equal channel angular extrusion. Journal of Materials Processing Technology. 2005;166:71-8.

[209] Toth LS, Lapovok R, Hasani A, Gu CF. Non-equal channel angular pressing of aluminum alloy. Scripta Materialia. 2009;61:1121-4.
[210] Nagasekhar AV, Yoon SC, Tick-Hon Y, Kim HS. An experimental verification of the finite element modelling of equal channel angular pressing. Computational Materials Science. 2009;46:347-51.
[211] Nagasekhar AV, Tick-Hon Y, Li S, Seow HP. Effect of acute tool-angles on equal channel angular extrusion/pressing. Materials Science and Engineering A. 2005;410:269-72.
[212] Nagasekhar AV, Kim HS. Analysis of T-Shaped Equal Channel Angular Pressing using the Finite Element Method. Metals and Materials International. 2008;14:565-8.
[213] Nagasekhar AV, Kim HS. Plastic deformation characteristics of cross-equal channel angular pressing. Computational Materials Science. 2008;43:1069-73.
[214] Balasundar I, Raghu T. Effect of friction model in numerical analysis of equal channel angular pressing process. Materials & Design. 2010;31:449-57.
[215] Suh J-Y, Kim H-S, Park J-W, Chang J-Y. Finite element analysis of material flow in equal channel angular pressing. Scripta Materialia. 2001;44:677-81.
[216] Park J-W, Suh J-Y. Effect of die shape on the deformation behavior in equal-channel angular pressing. Metall and Mat Trans A. 2001;32:3007-14.
[217] Kim HS. Finite element analysis of equal channel angular pressing using a round corner die. Materials Science and Engineering A. 2001;315:122-8.
[218] Kim HS, Hong SI, Seo MH. Effects of strain hardenability and strain-rate sensitivity on the plastic flow and deformation homogeneity during equal channel angular pressing. Journal of Materials Research. 2001;16:856-64.
[219] Kim HS. Finite-Element Method Simulation of Severe Plastic-Deformation Methods. Bulk Nanostructured Materials: Wiley-VCH Verlag GmbH & Co. KGaA; 2009. p. 137-63.
[220] Kim HS. Finite element analysis of deformation behaviour of metals during equal channel multi-angular pressing. Materials Science and Engineering A. 2002;328:317-23.
[221] Zuyan L, Gang L, Wang ZR. Finite element simulation of a new deformation type occurring in changing-channel extrusion. Journal of Materials Processing Technology. 2000;102:30-2.
[222] Mckenzie PWJ, Lapovok R, Estrin Y. The influence of back pressure on ECAP processed. AA 6016: Modeling and experiment. Acta Materialia. 2007;55:2985-93.
[223] Lapovok R. The positive role of back-pressure in equal channel angular extrusion. Nanomaterials by Severe Plastic Deformation. 2006;503-504:37-44.
[224] Lapovok R. The role of back-pressure in equal channel angular extrusion. Journal of Materials Science. 2005;40:341-6.
[225] Ouyang JH, Sasaki S. Unlubricated friction and wear behavior of low-pressure plasma-sprayed ZrO2 coating at elevated temperatures. Ceramics International. 2001;27:251-60.
[226] Kang F, Wang JT, Su YL, Xia KN. Finite element analysis of the effect of back pressure during equal channel angular pressing. Journal of Materials Science. 2007;42:1491-500.
[227] Lee DN. An upper-bound solution of channel angular deformation. Scripta Materialia. 2000;43:115-8.
[228] Chung SW, Somekawa H, Kinoshita T, Kim WJ, Higashi K. The non-uniform behavior during ECAE process by 3-D FVM simulation. Scripta Materialia. 2004;50:1079-83.
[229] Edalati K, Yamamoto A, Horita Z, Ishihara T. High-pressure torsion of pure magnesium: Evolution of mechanical properties, microstructures and hydrogen storage capacity with equivalent strain. Scripta Materialia. 2011;64:880-3.
[230] Kim WJ, Namgung JC, Kim JK. Analysis of strain uniformity during multi-pressing in equal channel angular extrusion. Scripta Materialia. 2005;53:293-8.
[231] Leo P, Cerri E, De Marco PP, Roven HJ. Properties and deformation behaviour of severe plastic deformed aluminium alloys. Journal of Materials Processing Technology. 2007;182:207-14.

[232] Alexandrov IV, Budilov IN, Krallics G, Kim HS, Yoon SC, Smolyakov AA, et al. Simulation of equal-channel angular extrusion pressing. Nanomaterials by Severe Plastic Deformation. 2006;503-504:201-8.
[233] Semiatin SL, Jones JJ. Formability and workability of metals : plastic instability and flow localization. Metals Park, Ohio: American Society for Metals; 1984.
[234] Semiatin SL, Staker MR, Jonas JJ. Plastic instability and flow localization in shear at high rates of deformation. Acta Metallurgica. 1984;32:1347-54.
[235] Lapovok R, Toth LS, Molinari A, Estrin Y. Strain localisation patterns under equal-channel angular pressing. Journal of the Mechanics and Physics of Solids. 2009;57:122-36.
[236] Estrin Y, Mühlhaus HB. From micro- to macroscale, gradient models of plasticity. Proceedings of the International Conference on Engineering Mathematics. In: Yuen D, editor. IEAust. AEMC Sydney, Australia1996. p. 161-5.
[237] Mahallawy NE, Shehata FA, Hameed MAE, Aal MIAE, Kim HS. 3D FEM simulations for the homogeneity of plastic deformation in Al-Cu alloys during ECAP. Materials Science and Engineering A. 2010;527:1404-10.
[238] Figueiredo RB, Pinheiro IP, Aguilar MTP, Modenesi PJ, Cetlin PR. The finite element analysis of equal channel angular pressing (ECAP) considering the strain path dependence of the work hardening of metals. Journal of Materials Processing Technology. 2006;180:30-6.
[239] Kim HS, Seo MH, Hong SI. On the die corner gap formation in equal channel angular pressing. Materials Science and Engineering: A. 2000;291:86-90.
[240] Semiatin SL, DeLo DP, Segal VM, Goforth RE, Frey ND. Workability of commercial-purity titanium and 4340 steel during equal channel angular extrusion at cold-working temperatures. Metall and Mat Trans A. 1999;30:1425-35.
[241] Semiatin SL, DeLo DP. Equal channel angular extrusion of difficult-to-work alloys. Materials & Design. 2000;21:311-22.
[242] Horn T, Silbermann C, Frint P, Wagner M, Ihlemann J. Strain Localization during Equal-Channel Angular Pressing Analyzed by Finite Element Simulations. Metals. 2018;8:55.
[243] Valiev R. Nanostructuring of metals by severe plastic deformation for advanced properties. Nature Materials. 2004;3:511-6.
[244] Furukawa M, Iwahashi Y, Horita Z, Nemoto M, Langdon TG. The shearing characteristics associated with equal-channel angular pressing. Materials Science and Engineering A. 1998;257:328-32.
[245] Azushima A, Kopp R, Korhonen A, Yang DY, Micari F, Lahoti GD, et al. Severe plastic deformation (SPD) processes for metals. CIRP Annals - Manufacturing Technology. 2008;57:716-35.
[246] Teodosiu C, Hu Z. Evolution of the intragranular microstructure at moderate and large strains: modelling and computational significance. In: Shen S-F, Dawson P, editors. Simulation of Materials Processing: Theory, Methods and Applications Proceedings of the 5th international conference NUMIFORM'95, Ithaca, New York, 18-21 June 1995. Rotterdam: A.A. ; 1995. p. 173-82.
[247] Peeters B, Seefeldt M, Teodosiu C, Kalidindi SR, Van Houtte P, Aernoudt E. Work-hardening/softening behaviour of b.c.c. polycrystals during changing strain paths: I. An integrated model based on substructure and texture evolution, and its prediction of the stress–strain behaviour of an IF steel during two-stage strain paths. Acta Materialia. 2001;49:1607-19.
[248] Li S, Hoferlin E, Bael AV, Houtte PV, Teodosiu C. Finite element modeling of plastic anisotropy induced by texture and strain-path change. International Journal of Plasticity. 2003;19:647-74.
[249] Wen W, Borodachenkova M, Tomé CN, Vincze G, Rauch EF, Barlat F, et al. Mechanical behavior of low carbon steel subjected to strain path changes: Experiments and modeling. Acta Materialia. 2016;111:305-14.
[250] Figueiredo RB, Aguilar MTP, Cetlin PR. Finite element modelling of plastic instability during ECAP processing of flow-softening materials. Materials Science and Engineering: A. 2006;430:179-84.

[251] Lee SC, Ha SY, Kim KT, Hwang SM, Huh LM, Chung HS. Finite element analysis for deformation behavior of an aluminum alloy composite containing SiC particles and porosities during ECAP. Materials Science and Engineering A. 2004;371:306-12.
[252] Lapovok R. Damage evolution under severe plastic deformation. International Journal of Fracture. 2002;115:159-72.
[253] Li SY, Beyerlein IJ, Necker CT, Alexander DJ, Bourke M. Heterogeneity of deformation texture in equal channel angular extrusion of copper. Acta Materialia. 2004;52:4859-75.
[254] Toth LS, Molinari A, Estrin Y. Strain Hardening at Large Strains as Predicted by Dislocation Based Polycrystal Plasticity Model. Journal of Engineering Materials and Technology. 2002;124:71-7.
[255] Estrin Y, Tóth LS, Molinari A, Bréchet Y. A dislocation-based model for all hardening stages in large strain deformation. Acta Materialia. 1998;46:5509-22.
[256] Baik SC, Estrin Y, Kim HS, Hellmig RJ. Dislocation density-based modeling of deformation behavior of aluminium under equal channel angular pressing. Materials Science and Engineering A. 2003;351:86-97.
[257] Baik SC, Estrin Y, Hellmig RJ, Jeong HT, Brokmeier HG, Kim HS. Modeling of texture evolution in copper under equal channel angular pressing. Zeitschrift Fur Metallkunde. 2003;94:1189-98.
[258] Baik SC, Estrin Y, Kim HS, Jeong HT, Hellmig RJ. Calculation of deformation behavior and texture evolution during equal channel angular pressing of IF steel using dislocation based modeling of strain hardening. Textures of Materials, Pts 1 and 2. 2002;408-4:697-702.
[259] Bratov V, Borodin EN. Comparison of dislocation density based approaches for prediction of defect structure evolution in aluminium and copper processed by ECAP. Materials Science and Engineering: A. 2015;631:10-7.
[260] Nagasekhar AV, Tick-Hon Y, Li S, Seow HP. Stress and strain histories in equal channel angular extrusion/pressing. Materials Science and Engineering A. 2006;423:143-7.
[261] Lee DJ, Yoon EY, Lee SH, Kang SY, Kim HS. Finite element analysis for compression behavior of high pressure torsion processing. Reviews on Advanced Materials Science. 2012;31:25-30.
[262] Lee DJ, Yoon EY, Ahn D-H, Park BH, Park HW, Park LJ, et al. Dislocation density-based finite element analysis of large strain deformation behavior of copper under high-pressure torsion. Acta Materialia. 2014;76:281-93.
[263] Chung SW, Kim WJ, Kohzu M, Higashi K. The effect of ram speed on mechanical and thermal properties in ECAE process simulation. Materials Transactions. 2003;44:973-80.
[264] Belytschko T, Krongauz Y, Organ D, Fleming M, Krysl P. Meshless methods: An overview and recent developments. Computer Methods in Applied Mechanics and Engineering. 1996;139:3-47.
[265] Lu P, Zhao G, Guan Y, Wu X. Bulk metal forming process simulation based on rigid-plastic/viscoplastic element free Galerkin method. Materials Science and Engineering: A. 2008;479:197-212.
[266] Yanjin G, Guoqun Z, Ping L. Numerical study of equal-channel angular pressing based on the element-free Galerkin method. International Journal of Materials Research. 2012;103:1361-75.
[267] Monaghan JJ. An introduction to SPH. Computer Physics Communications. 1988;48:89-96.
[268] Cleary PW, Prakash M, Ha J, Stokes N, Scott C. Smooth particle hydrodynamics: Status and future potential. Prog Comput Fluid Dyn. 2007;7:70-90.
[269] Tan H, Nairn JA. Hierarchical, adaptive, material point method for dynamic energy release rate calculations. Computer Methods in Applied Mechanics and Engineering. 2002;191:2123-37.
[270] Fagan T, Das R, Lemiale V, Estrin Y. Modelling of equal channel angular pressing using a mesh-free method. Journal of Materials Science. 2012;47:4514-9.
[271] Lemiale V, Nairn J, Hurmane A. Material point method simulation of equal channel angular pressing involving large plastic strain and contact through sharp corners. CMES Comput Model Eng Sci. 2010;70:41-66.

[272] Kazeminezhad M, Hosseini E. Modeling of induced empirical constitutive relations on materials with FCC, BCC, and HCP crystalline structures: Severe plastic deformation. International Journal of Advanced Manufacturing Technology. 2010;47:1033-9.
[273] Medeiros N, Lins JFC, Moreira LP, Gouvea JP. The role of the friction during the equal channel angular pressing of an IF-steel billet. Mat Sci Eng a-Struct. 2008;489:363-72.
[274] Marchand A, Duffy J. An experimental study of the formation process of adiabatic shear bands in a structural steel. Journal of the Mechanics and Physics of Solids. 1988;36:251-83.
[275] Bever MB, Holt DL, Titchener AL. The stored energy of cold work. Progress in Materials Science. 1973;17:5-177.
[276] Stainier L. Mechanically Generated Heat. In: Hetnarski R, editor. Encyclopedia of Thermal Stresses: Springer Netherlands; 2014. p. 2958-64.
[277] Farren WS, Taylor GI. The Heat Developed during Plastic Extension of Metals. Proceedings of the Royal Society of London Series A. 1925;107:422-51.
[278] Taylor GI, Quinney H. The Latent Energy Remaining in a Metal after Cold Working. Proceedings of the Royal Society of London Series A, Containing Papers of a Mathematical and Physical Character (1905-1934). 1934;143:307-26.
[279] Benzerga AA, Bréchet Y, Needleman A, Van der Giessen E. The stored energy of cold work: Predictions from discrete dislocation plasticity. Acta Materialia. 2005;53:4765-79.
[280] Poliak EI, Jonas JJ. A one-parameter approach to determining the critical conditions for the initiation of dynamic recrystallization. Acta Materialia. 1996;44:127-36.
[281] Hansen N, Vandermeer RA. Recovery, Recrystallization, and Grain Growth. In: Wyder FBLL, editor. Encyclopedia of Condensed Matter Physics. Oxford: Elsevier; 2005. p. 116-24.
[282] Mishin OV, Godfrey A, Juul Jensen D, Hansen N. Recovery and recrystallization in commercial purity aluminum cold rolled to an ultrahigh strain. Acta Materialia. 2013;61:5354-64.
[283] Yamasaki T, Miyamoto H, Mimaki T, Vinogradov A, S.Hashimoto. Corrosion Fatigue of Ultra-Fine Grain Copper Fabricated by Severe Plastic Deformation. Ultrafine grain metals II TMS:USA; 2002. p. 361-70.
[284] Estrin Y, Kubin LP. Plastic instabilities: phenomenology and theory. Materials Science and Engineering: A. 1991;137:125-34.
[285] Kubin LP, Spiesser P, Estrin Y. Computer simulation of the low temperature instability of plastic flow. Acta Metallurgica. 1982;30:385-94.
[286] Rogers HC. Adiabatic Plastic Deformation. Annual Review of Materials Science. 1979;9:283-311.
[287] Johnson GR, Cook WH. Fracture characteristics of three metals subjected to various strains, strain rates, temperatures and pressures. Engineering Fracture Mechanics. 1985;21:31-48.
[288] Zerilli FJ, Armstrong RW. Dislocation-mechanics-based constitutive relations for material dynamics calculations. Journal of Applied Physics. 1987;61:1816-25.
[289] Vinogradov A, Kaneko Y, Kitagawa K, Hashimoto S, Stolyarov V, Valiev R. Cyclic response of ultrafine-grained copper at constant plastic strain amplitude. Scripta Materialia. 1997;36:1345-51.
[290] Vinogradov A, Hashimoto S. Multiscale phenomena in fatigue of ultra-fine grain materials - an overview. Materials Transactions Jim. 2001;42:74-84.
[291] Mason JJ, Rosakis AJ, Ravichandran G. On the strain and strain rate dependence of the fraction of plastic work converted to heat: an experimental study using high speed infrared detectors and the Kolsky bar. Mechanics of Materials. 1994;17:135-45.
[292] Hodowany J, Ravichandran G, Rosakis AJ, Rosakis P. Partition of plastic work into heat and stored energy in metals. Experimental Mechanics. 2000;40:113-23.
[293] Oliferuk W, Maj M. Stress–strain curve and stored energy during uniaxial deformation of polycrystals. European Journal of Mechanics - A/Solids. 2009;28:266-72.

[294] Kostina A, Iziumova A, Plekhov O. Energy dissipation and storage in iron under plastic deformation (experimental study and numerical simulation). Frattura ed Integrità Strutturale. 2014;27:28-37.
[295] Rosakis P, Rosakis AJ, Ravichandran G, Hodowany J. A thermodynamic internal variable model for the partition of plastic work into heat and stored energy in metals. Journal of the Mechanics and Physics of Solids. 2000;48:581-607.
[296] Estrin Y, Kubin LP. Criterion for thermomechanical instability of low temperature plastic deformation. Scripta Metallurgica. 1980;14:1359-64.
[297] Tsagrakis I, Aifantis EC. On the Effect of Strain Gradient on Adiabatic Shear Banding. Metallurgical and Materials Transactions A: Physical Metallurgy and Materials Science. 2014.
[298] Korn M, Lapovok R, Böhner A, Höppel HW, Mughrabi H. Bimodal grain size distributions in UFG materials produced by SPD - Their evolution and effect on the fatigue and monotonic strength properties. Kovove Materialy. 2011;49:51-63.
[299] Rybin VV. Bolshie Plasticheskie Deformacii i Razrushenie Metallov. Moscow, Russia: Metallurgiya; 1986.
[300] Huang X, Winther G. Dislocation structures. Part I. Grain orientation dependence. Philosophical Magazine. 2007;87:5189-214.
[301] Winther G, Huang X. Dislocation structures. Part II. Slip system dependence. Philosophical Magazine. 2007;87:5215-35.
[302] Hughes DA, Hansen N, Bammann DJ. Geometrically necessary boundaries, incidental dislocation boundaries and geometrically necessary dislocations. Scripta Materialia. 2003;48:147-53.
[303] Hansen N, Barlow CY. 17 - Plastic Deformation of Metals and Alloys. In: Hono DEL, editor. Physical Metallurgy (Fifth Edition). Oxford: Elsevier; 2014. p. 1681-764.
[304] Kozlov EV, Zhdanov AN, Popova NA, Pekarskaya EE, Koneva NA. Subgrain structure and internal stress fields in UFG materials: problem of Hall-Petch relation. Materials Science and Engineering A-Structural Materials Properties Microstructure and Processing. 2004;387-89:789-94.
[305] Koneva NA, Kozlov EV. Deformation-induced ordering of dislocation structures. Materials Science and Engineering A-Structural Materials Properties Microstructure and Processing. 2004;387-89:64-6.
[306] Pantleon W. The evolution of disorientations for several types of boundaries. Materials Science and Engineering: A. 2001;319:211-5.
[307] Pantleon W. Disorientations in dislocation structures. Materials Science and Engineering: A. 2005;400:118-24.
[308] Zhilyaev AP, Swaminathan S, Pshenichnyuk AI, Langdon TG, McNelley TR. Adiabatic heating and the saturation of grain refinement during SPD of metals and alloys: Experimental assessment and computer modeling. Journal of Materials Science. 2013;48:4626-36.
[309] Zhilyaev AP, Garcia-Infanta JM, Carreno F, Langdon TG, Ruano OA. Particle and grain growth in an Al-Si alloy during high-pressure torsion. Scripta Materialia. 2007;57:763-5.
[310] Shaw MC. Metal cutting principles. 2nd ed. New York ; Oxford: Oxford University Press; 2005.
[311] Kim HS. Prediction of Temperature Rise in Equal Channel Angular Pressing. MATERIALS TRANSACTIONS. 2001;42:536-8.
[312] Kuhlmann-Wilsdorf D, Duesbery FRNNaMS. Chapter 59 The LES theory of solid plasticity. Dislocations in Solids: Elsevier; 2002. p. 211-342.
[313] Kuhlmann-Wilsdorf D. The theory of dislocation-based crystal plasticity. Philosophical Magazine A. 1999;79:955 - 1008.
[314] Sauzay M, Kubin LP. Scaling laws for dislocation microstructures in monotonic and cyclic deformation of fcc metals. Progress in Materials Science. 2011;56:725-84.
[315] Pougis A, Tóth LS, Bouaziz O, Fundenberger JJ, Barbier D, Arruffat R. Stress and strain gradients in high-pressure tube twisting. Scripta Materialia. 2012;66:773-6.

[316] Li JCM, Chou YT. The role of dislocations in the flow stress grain size relationships. Metallurgical and Materials Transactions B. 1970;1:1145.
[317] Thompson AW, Baskes MI, Flanagan WF. The dependence of polycrystal work hardening on grain size. Acta Metallurgica. 1973;21:1017-28.
[318] Ashby MF. The deformation of plastically non-homogeneous materials. Philosophical Magazine. 1970;21:399-424.
[319] Li JCM. Petch relation and grain boundary sources. Trans Metall Soc AIME. 1963;277:239-47.
[320] Kato M, Fujii T, Onaka S. Dislocation bow-out model for yield stress of ultra-fine grained materials. Materials Transactions. 2008;49:1278-83.
[321] Gryaznov VG, Gutkin MY, Romanov AE, Trusov LI. On the yield stress of nanocrystals. J Mater Sci. 1993;28:4359-65.
[322] Armstrong RW, Rodriguez P. Flow stress/strain rate/grain size coupling for fcc nanopolycrystals. Philosophical Magazine. 2006;86:5787-96.
[323] Kopylov VI, Chyvil'deev VN. The limit of grain refinement on equal cannel angular deformation. Metally. 2004:22-35.
[324] Gottstein G. Integral materials modeling : towards physics-based through-process models. Weinheim: Wiley-VCH ; Chichester : John Wiley [distributor]; 2007.
[325] Cottrell A. Dislocations and Plastic Flow in Crystals. Oxford: Clarendon Press; 1953.
[326] Zehetbauer MJ, Estrin Y. Modeling of Strength and Strain Hardening of Bulk Nanostructured Materials. Bulk Nanostructured Materials: Wiley-VCH Verlag GmbH & Co. KGaA; 2009. p. 109-36.
[327] Mecking H, Kocks UF. Kinetics of flow and strain-hardening. Acta Metallurgica. 1981;29:1865-75.
[328] Mandelbrot BB. The fractal geometry of nature. Updated and augm. ed. New York: W.H. Freeman; 1983.
[329] Onsager L. Reciprocal Relations in Irreversible Processes. I. Physical Review. 1931;37:405-26.
[330] Onsager L. Reciprocal Relations in Irreversible Processes. II. Physical Review. 1931;38:2265-79.
[331] Prigogine I. Introduction to thermodynamics of irreversible processes. 2d, rev. ed. New York,: Interscience Publishers; 1961.
[332] Bridgman PW. The Thermodynamics of Plastic Deformation and Generalized Entropy. Reviews of Modern Physics. 1950;22:56.
[333] Kubin LP, Estrin Y, Canova G. Dislocation Patterns and Plastic Instabilities. In: Walgraef D, Ghoniem NM, editors. Patterns, Defects and Materials Instabilities: Springer Netherlands; 1990. p. 277-301.
[334] Aifantis EC. Deformation and failure of bulk nanograined and ultrafine-grained materials. Materials Science and Engineering: A. 2009;503:190-7.
[335] Aifantis EC. The physics of plastic deformation. International Journal of Plasticity. 1987;3:211-47.
[336] Ziegler H. An introduction to thermomechanics. 2d rev. ed. Amsterdam ; New York: North-Holland Pub. Co. ;; 1983.
[337] Ziegler H, Eidgenössische Technische Hochschule. Some extremum principles in irreversible thermodynamics, with application to continuum mechanics. Zürich,: Swiss Federal Institute of Technology; 1962.
[338] Drucker DC. Some implications of work hardening and ideal plasticity. Quarterly of Applied Mathematics. 1950;7:411–8.
[339] Hill R. The mathematical theory of plasticity. Oxford,: Clarendon Press; 1950.
[340] Rabotnov IUN, Novozhilov VV. Mechanics of deformable solids and structures. Moskva: Mashinostroenie; 1975.
[341] Ghoniem NM, Tong SH, Sun LZ. Parametric dislocation dynamics: A thermodynamics-based approach to investigations of mesoscopic plastic deformation. Physical Review B. 2000;61:913.
[342] Langer JS, Bouchbinder E, Lookman T. Thermodynamic theory of dislocation-mediated plasticity. Acta Materialia. 2010;58:3718-32.

[343] Langer JS. Statistical thermodynamics of strain hardening in polycrystalline solids. Physical Review E. 2015;92:032125.
[344] Vinogradov A, Yasnikov IS, Estrin Y. Evolution of Fractal Structures in Dislocation Ensembles during Plastic Deformation. Physical Review Letters. 2012;108:205504.
[345] Huang M, Rivera-Díaz-Del-castillo PEJ, Bouaziz O, Zwaag SVD. Predicting the strength and ductility of ultrafine grained interstitial free steels using irreversible thermodynamics. Buenos Aires2008. p. 805-12.
[346] Huang M, Rivera-Díaz-del-Castillo PEJ, Bouaziz O, van der Zwaag S. Irreversible thermodynamics modelling of plastic deformation of metals. Materials science and technology. 2008;24:495-500.
[347] Mughrabi H. The α-factor in the Taylor flow-stress law in monotonic, cyclic and quasi-stationary deformations: Dependence on slip mode, dislocation arrangement and density. Current Opinion in Solid State and Materials Science. 2016;20:411-20.
[348] Zaiser M. Scale invariance in plastic flow of crystalline solids. Advances in Physics. 2006;55:185-245.
[349] Mughrabi H. Implications of Linera relationships between local and macroscopic Flow Stresses in the Composite Model. Journal of Materials Research. 2006;97:594-6.
[350] Mughrabi H. Dislocation wall and cell structures and long-range internal-stresses in deformed metal crystals. Acta Metallurgica. 1983;31:1367-79.
[351] Holt DL. Dislocation Cell Formation in Metals. Journal of Applied Physics. 1970;41:3197-201.
[352] Kocks UF, Argon AS, Ashby MF. Thermodynamics and kinetics of slip. Progress in Materials Science. 1975;19:1-281.
[353] Hansen N, Kuhlmann-Wilsdorf D. Low energy dislocation structures due to unidirectional deformation at low temperatures. Materials Science and Engineering. 1986;81:141-61.
[354] Marthinsen K, Nes E. A general model for metal plasticity. Materials Science and Engineering: A. 1997;234–236:1095-8.
[355] Nes E. Modelling of work hardening and stress saturation in FCC metals. Progress in Materials Science. 1997;41:129-93.
[356] Estrin Y. Unified constitutive laws of plastic deformation. San Diego ; London: Academic Press; 1996.
[357] Alexandrov IV, Chembarisova RG. Development and application of the dislocation model for analysis of the microstructure evolution and deformation behavior of metals subjected to severe plastic deformation. Reviews on Advanced Materials Science. 2007;16:51-72.
[358] Caillard D, Martin J-L. Thermally activated mechanisms in crystal plasticity. Amsterdam: Pergamon; 2003.
[359] Klepaczko J. Thermally activated flow and strain rate history effects for some polycrystalline f.c.c. metals. Materials Science and Engineering. 1975;18:121-35.
[360] Malygin GA. Dislocation density evolution equation and strain-hardening of fcc crystals. Physica Status Solidi A-Applied Research. 1990;119:423-36.
[361] Bergström Y. Reviews on Powder Metallurgy and Physical Ceramics. 1973;2:79.
[362] Gottstein G, Argon AS. Dislocation theory of steady state deformation and its approach in creep and dynamic tests. Acta Metallurgica. 1987;35:1261-71.
[363] Starink MJ, Qiao XG, Zhang J, Gao N. Predicting grain refinement by cold severe plastic deformation in alloys using volume averaged dislocation generation. Acta Materialia. 2009;57:5796-811.
[364] Holmedal B. On the basic relation between mean free slip length and work hardening of metals. Philosophical Magazine. 2015;95:2817-30.
[365] Hahner P, Bay K, Zaiser M. Fractal Dislocation Patterning During Plastic Deformation. Physical Review Letters. 1998;81:2470.

[366] Yasnikov IS, Vinogradov A, Estrin Y. Revisiting the Considère criterion from the viewpoint of dislocation theory fundamentals. Scripta Materialia. 2014;76:37-40.
[367] Yasnikov IS, Estrin Y, Vinogradov A. What governs ductility of ultrafine-grained metals? A microstructure based approach to necking instability. Acta Materialia. 2017;141:18-28.
[368] Torre D, Pereloma EV, Davies CHJ. Strain rate sensitivity and apparent activation volume measurements on equal channel angular extruded Cu processed by one to twelve passes. Scripta Materialia. 2004;51:367-71.
[369] Dao M, Lu L, Shen YF, Suresh S. Strength, strain-rate sensitivity and ductility of copper with nanoscale twins. Acta Materialia. 2006;54:5421-32.
[370] Vinogradov A, Yasnikov IS, Matsuyama H, Uchida M, Kaneko Y, Estrin Y. Controlling strength and ductility: Dislocation-based model of necking instability and its verification for ultrafine grain 316L steel. Acta Materialia. 2016;106:295-303.
[371] Vinogradov A. Mechanical properties of ultrafine-grained metals: new challenges and perspectives. Advanced Engineering Materials. 2015;17:1710-22.
[372] Essmann U, Mughrabi H. Annihilation of dislocations during tensile and cyclic deformation and limits of dislocation densities. Philosophical Magazine A. 1979;40:731-56.
[373] Blum W. Role of Dislocation Annihilation during Steady-State Deformation. physica status solidi (b). 1971;45:561-71.
[374] Rivera-Díaz-del-Castillo PEJ, Huang M. Dislocation annihilation in plastic deformation: I. Multiscale irreversible thermodynamics. Acta Materialia. 2012;60:2606-14.
[375] Galindo-Nava EI, Rivera-Díaz-del-Castillo PEJ. Modelling plastic deformation in BCC metals: Dynamic recovery and cell formation effects. Materials Science and Engineering: A. 2012;558:641-8.
[376] Galindo-Nava EI, Rivera-Díaz-del-Castillo PEJ. Thermostatistical modelling of hot deformation in FCC metals. International Journal of Plasticity. 2013;47:202-21.
[377] Galindo-Nava EI, Sietsma J, Rivera-Díaz-del-Castillo PEJ. Dislocation annihilation in plastic deformation: II. Kocks–Mecking Analysis. Acta Materialia. 2012;60:2615-24.
[378] Huang M, Rivera-Díaz-del-Castillo PEJ, Bouaziz O, van der Zwaag S. Modelling plastic deformation of metals over a wide range of strain rates using irreversible thermodynamics. IOP Conference Series: Materials Science and Engineering. 2009;3:012006.
[379] Bonneville J, Escaig B. Cross-slipping process and the stress-orientation dependence in pure copper. Acta Metallurgica. 1979;27:1477-86.
[380] Vinogradov AY, Stolyarov VV, Hashimoto S, Valiev RZ. Cyclic behavior of ultrafine-grain titanium produced by severe plastic deformation. Materials Science and Engineering A. 2001;318:163-73.
[381] Patlan V, Higashi K, Kitagawa K, Vinogradov A, Kawazoe M. Cyclic response of fine grain 5056 Al-Mg alloy processed by equal-channel angular pressing. Materials Science and Engineering A. 2001;319:587-91.
[382] Patlan V, Vinogradov A, Higashi K, Kitagawa K. Overview of fatigue properties of fine grain 5056 Al-Mg alloy processed by equal-channel angular pressing. Materials Science and Engineering A. 2001;300:171-82.
[383] Vinogradov A, Yasnikov IS, Estrin Y. Irreversible thermodynamics approach to plasticity: dislocation density based constitutive modelling. Materials Science and Technology. 2015;31:1664-72.
[384] Molotnikov A. Application of Strain Gradient Plasticity Modelling to High Pressure Torsion. Materials Science Forum. 2008;584-586:1051-6.
[385] Kumar KS, Van Swygenhoven H, Suresh S. Mechanical behavior of nanocrystalline metals and alloys. Acta Materialia. 2003;51:5743-74.
[386] Wolf D, Yamakov V, Phillpot SR, Mukherjee A, Gleiter H. Deformation of nanocrystalline materials by molecular-dynamics simulation: relationship to experiments? Acta Materialia. 2005;53:1-40.

[387] Van Swygenhoven H, Derlet PM, Frøseth AG. Nucleation and propagation of dislocations in nanocrystalline fcc metals. Acta Materialia. 2006;54:1975-83.
[388] Chang L, Zhou C-Y, Li J, He X-H. Investigation on tensile properties of nanocrystalline titanium with ultra-small grain size. Computational Materials Science. 2018;142:135-44.
[389] Höppel HW, Zhou ZM, Mughrabi H, Valiev RZ. Microstructural study of the parameters governing coarsening and cyclic softening in fatigued ultrafine-grained copper. Philosophical Magazine A. 2002;82:1781 - 94.
[390] Höppel HW, Mughrabi H, Vinogradov A. Fatigue Properties of Bulk Nanostructured Materials: Wiley-VCH Verlag GmbH & Co. KGaA; 2009.
[391] Miyamoto H, Fushimi J, Mimaki T, Vinogradov A, Hashimoto S. Dislocation structures and crystal orientations of copper single crystals deformed by equal-channel angular pressing. Materials Science and Engineering A. 2005;405:221-32.
[392] Miyamoto H, Fushimi J, Mimaki T, Vinogradov A, Hashimoto S. The effect of the initial orientation on microstructure development of copper single crystals subjected to equal-channel angular pressing. In: Horita Z, editor. Nanomaterials by Severe Plastic Deformation2006. p. 799-804.
[393] Rybin VV. Large Plastic Deformations and Fracture of Metals: Metallurgiya, Moscow; 1986.
[394] Rybin VV. Physical model of the phenomenon of loss of mechanical stability and necking. hys Met Metallogr. 1977;44:149.
[395] Klemm R. Zyklische Plastizität von mikro- und submikrokristallinem Nickel: Technische Universität Dresden; 2004.
[396] Mughrabi H, Höppel HW. Cyclic deformation and fatigue properties of very fine-grained metals and alloys. International Journal of Fatigue. 2010;32:1413-27.
[397] Polyakova VV, Semenova IP, Valiev RZ, Vinogradov A. (in preparation).
[398] Estrin Y, Braasch H, Brechet Y. A dislocation density based constitutive model for cyclic deformation. JEngMaterTechASME. 1996;118:441-57.
[399] Bouaziz O, Estrin Y, Bréchet Y, Embury JD. Critical grain size for dislocation storage and consequences for strain hardening of nanocrystalline materials. Scripta Materialia. 2010;63:477-9.
[400] Schafler E, Pippan R. Effect of thermal treatment on microstructure in high pressure torsion (HPT) deformed nickel. Materials Science and Engineering A. 2004;387-89:799-804.
[401] Hebesberger T, Stuwe HP, Vorhauer A, Wetscher F, Pippan R. Structure of Cu deformed by high pressure torsion. Acta Materialia. 2005;53:393-402.
[402] Pippan R, Wetscher F, Hafok M, Vorhauer A, Sabirov I. The limits of refinement by severe plastic deformation. Advanced Engineering Materials. 2006;8:1046-56.
[403] Reichert B, Estrin Y. Steel Res Intl. 2007;78:791-7.
[404] Baufeld B, Petukhov BV, Bartsch M, Messerschmidt U. Transition of mechanisms controlling the dislocation motion in cubic ZrO2 below 700°C. Acta Materialia. 1998;46:3077-85.
[405] Lee S, Estrin Y, De Cooman BC. Effect of the strain rate on the TRIP-TWIP transition in austenitic Fe-12 pct Mn-0.6 pct C TWIP Steel. Metallurgical and Materials Transactions A: Physical Metallurgy and Materials Science. 2014;45:717-30.
[406] Petukhov BV. Phenomenological description of material plasticity in the region of transition from the kink mechanism of dislocation motion to the mechanism of their local pinning. Crystallogr Rep. 1996;41:181-8.
[407] Dour G, Estrin Y. Dislocation Motion in Crystals With a High Peierls Relief: A Unified Model Incorporating the Lattice Friction and Localized Obstacles. Journal of Engineering Materials and Technology. 2002;124:7-12.
[408] Cheng GM, Jian WW, Xu WZ, Yuan H, Millett PC, Zhu YT. Grain Size Effect on Deformation Mechanisms of Nanocrystalline bcc Metals. Materials Research Letters. 2013;1:26-31.

[409] Dunlop JW, Bréchet YJM, Legras L, Estrin Y. Dislocation density-based modelling of plastic deformation of Zircaloy-4. Materials Science and Engineering: A. 2007;443:77-86.
[410] Ahn D-H, Kim HS, Estrin Y. A semi-phenomenological constitutive model for hcp materials as exemplified by alpha titanium. Scripta Materialia. 2012;67:121-4.
[411] Bouaziz O, Guelton N. Modelling of TWIP effect on work-hardening. Materials Science and Engineering: A. 2001;319–321:246-9.
[412] Allain S, Chateau JP, Bouaziz O. A physical model of the twinning-induced plasticity effect in a high manganese austenitic steel. Materials Science and Engineering: A. 2004;387–389:143-7.
[413] Bouaziz O, Allain S, Scott C. Effect of grain and twin boundaries on the hardening mechanisms of twinning-induced plasticity steels. Scripta Materialia. 2008;58:484-7.
[414] Gil Sevillano J. Geometrically necessary twins and their associated size effects. Scripta Materialia. 2008;59:135-8.
[415] Sevillano JS. An alternative model for the strain hardening of FCC alloys that twin, validated for twinning-induced plasticity steel. Scripta Materialia. 2009;60:336-9.
[416] Bouaziz O, Allain S, Scott CP, Cugy P, Barbier D. High manganese austenitic twinning induced plasticity steels: A review of the microstructure properties relationships. Current Opinion in Solid State and Materials Science. 2011;15:141-68.
[417] Armstrong RW, Worthington PJ. A Constitutive Relation for Deformation Twinning in Body Centered Cubic Metals. In: Rohde RW, Butcher BM, Holland JR, Karnes CH, editors. Metallurgical Effects at High Strain Rates. Boston, MA: Springer US; 1973. p. 401-14.
[418] Meyers MA, Vöhringer O, Lubarda VA. The onset of twinning in metals: a constitutive description. Acta Materialia. 2001;49:4025-39.
[419] Wu XL, Youssef KM, Koch CC, Mathaudhu SN, Kecskés LJ, Zhu YT. Deformation twinning in a nanocrystalline hcp Mg alloy. Scripta Materialia. 2011;64:213-6.
[420] Beyerlein IJ, Capolungo L, Marshall PE, McCabe RJ, Tomé CN. Statistical analyses of deformation twinning in magnesium. Philosophical Magazine. 2010;90:2161-90.
[421] Zhu YT, Liao XZ, Wu XL. Deformation twinning in nanocrystalline materials. Progress in Materials Science. 2012;57:1-62.
[422] Ueno H, Kakihata K, Kaneko Y, Hashimoto S, Vinogradov A. Nanostructurization assisted by twinning during equal channel angular pressing of metastable 316L stainless steel. Journal of Materials Science. 2011:1-8.
[423] Lu L, Chen X, Huang X, Lu K. Revealing the Maximum Strength in Nanotwinned Copper. Science. 2009;323:607-10.
[424] Liu MP, Roven HJ, Yu YD. Deformation twins in ultrafine grained commercial aluminum. International Journal of Materials Research. 2007;98:184-90.
[425] Wu XL, Ma E. Dislocations and twins in nanocrystalline Ni after severe plastic deformation: the effects of grain size. Materials Science and Engineering: A. 2008;483:84-6.
[426] Vinogradov A, Vasilev E, Merson D, Estrin Y. A Phenomenological Model of Twinning Kinetics Advanced Engineering Materials. 2017;19:1600092-n/a.
[427] Fátima Vaz M, Fortes MA. Grain size distribution: The lognormal and the gamma distribution functions. Scripta Metallurgica. 1988;22:35-40.
[428] Zehetbauer M, Seumer V. Cold work hardening in stages IV and V of F.C.C. metals—I. Experiments and interpretation. Acta Metallurgica et Materialia. 1993;41:577-88.
[429] Kubin LP, Estrin Y. Evolution of dislocation densities and the critical conditions for the Portevin-Le Châtelier effect. Acta Metallurgica et Materialia. 1990;38:697-708.
[430] Prinz FB, Argon AS. The evolution of plastic resistance in large strain plastic flow of single phase subgrain forming metals. Acta Metallurgica. 1984;32:1021-8.

[431] Zehetbauer M. Cold work hardening in stages IV and V of F.C.C. metals—II. Model fits and physical results. Acta Metallurgica et Materialia. 1993;41:589-99.
[432] Nes E, Marthinsen K. Modeling the evolution in microstructure and properties during plastic deformation of f.c.c.-metals and alloys – an approach towards a unified model. Materials Science and Engineering: A. 2002;322:176-93.
[433] Malygin GA. Kinetic mechanism of the formation of fragmented dislocation structures upon large plastic deformations. Physics of the Solid State. 2002;44:2072-9.
[434] Estrin Y, Kubin LP. Local strain hardening and nonuniformity of plastic deformation. Acta Metallurgica. 1986;34:2455-64.
[435] Les P, Zehetbauer Mj. Evolution of Microstructural Parameters in Large Strain Deformation: Description by Zehetbauer's Model. Key Engineering Materials. 1994;97-97:335-40.
[436] Zehetbauer MJ, Stüwe HP, Vorhauer A, Schafler E, Kohout J. The Role of Hydrostatic Pressure in Severe Plastic Deformation. Nanomaterials by Severe Plastic Deformation: Wiley-VCH Verlag GmbH & Co. KGaA; 2005. p. 433-46.
[437] Hosseini E, Kazeminezhad M. Integration of physically based models into FE analysis: Homogeneity of copper sheets under large plastic deformations. Computational Materials Science. 2010;48:166-73.
[438] Hosseini E, Kazeminezhad M. A new microstructural model based on dislocation generation and consumption mechanisms through severe plastic deformation. Computational Materials Science. 2011;50:1123-35.
[439] Argon AS, Haasen P. A new mechanism of work hardening in the late stages of large strain plastic flow in F.C.C. and diamond cubic crystals. Acta Metallurgica et Materialia. 1993;41:3289-306.
[440] Lemiale V, Estrin Y, Kim HS, O'Donnell R. Grain refinement under high strain rate impact: A numerical approach. Computational Materials Science. 2010;48:124-32.
[441] Martin JW. Precipitation hardening. 2nd ed. Oxford: Butterworth-Heinemann; 1998.
[442] Nembach E. Particle strengthening of metals and alloys. New York etc.: Wiley; 1997.
[443] Estrin Y. Constitutive modelling of creep of metallic materials: Some simple recipes. Materials Science and Engineering: A. 2007;463:171-6.
[444] Rösler J, Arzt E. A new model-based creep equation for dispersion strengthened materials. Acta Metallurgica et Materialia. 1990;38:671-83.
[445] Molinari A, Canova GR, Ahzi S. A self consistent approach of the large deformation polycrystal viscoplasticity. Acta Metallurgica. 1987;35:2983-94.
[446] Mercier S, Molinari A, Berbenni S, Berveiller M. Comparison of different homogenization approaches for elastic–viscoplastic materials. Modelling and Simulation in Materials Science and Engineering. 2012;20:024004.
[447] Ardeljan M, Beyerlein IJ, Knezevic M. A dislocation density based crystal plasticity finite element model: Application to a two-phase polycrystalline HCP/BCC composites. Journal of the Mechanics and Physics of Solids. 2014;66:16-31.
[448] Estrin Y, Kim H. Modelling microstructure evolution towards ultrafine crystallinity produced by severe plastic deformation. Journal of Materials Science. 2007;42:9092-6.
[449] Alexandrov IV, Chembarisova RG, Sitdikov VD. Analysis of the deformation mechanisms in bulk ultrafine grained metallic materials. Materials Science and Engineering: A. 2007;463:27-35.
[450] Pantleon W. Formation of Disorientations in Dislocation Structures during Plastic Deformation. Solid State Phenomena. 2002;87:73-92.
[451] Estrin Y, Tóth L, Bréchet Y, Kim HS. Modelling of the Evolution of Dislocation Cell Misorientation under Severe Plastic Deformation. Materials Science Forum. 2006;503-504.
[452] Hughes DA, Hansen N. Microstructure and strength of nickel at large strains. Acta Materialia. 2000;48:2985-3004.

[453] Maier HJ, Gabor P, Gupta N, Karaman I, Haouaoui M. Cyclic stress-strain response of ultrafine grained copper. International Journal of Fatigue. 2006;28:243-50.
[454] Tóth LS, Beausir B, Gu CF, Estrin Y, Scheerbaum N, Davies CHJ. Effect of grain refinement by severe plastic deformation on the next-neighbor misorientation distribution. Acta Materialia. 2010;58:6706-16.
[455] Kratochvíl J, Kružík M, Sedláček R. A model of ultrafine microstructure evolution in materials deformed by high-pressure torsion. Acta Materialia. 2009;57:739-48.
[456] Seefeldt M, Delannay L, Peeters B, Kalidindi SR, Van Houtte P. A disclination-based model for grain subdivision. Materials Science and Engineering A. 2001;319-321:192-6.
[457] Zhang Y, Tao NR, Lu K. Mechanical properties and rolling behaviors of nano-grained copper with embedded nano-twin bundles. Acta Materialia. 2008;56:2429-40.
[458] Lu K, Lu L, Suresh S. Strengthening Materials by Engineering Coherent Internal Boundaries at the Nanoscale. Science. 2009;324:349-52.
[459] Olivares FH, Gil Sevillano J. A quantitative assessment of forest-hardening in f.c.c. metals. Acta Metallurgica. 1987;35:631-41.
[460] Gil Sevillano J, Aernoudt E. Low energy dislocation structures in highly deformed materials. Materials Science and Engineering. 1987;86:35-51.
[461] Zhang HW, Huang X, Hansen N. Evolution of microstructural parameters and flow stresses toward limits in nickel deformed to ultra-high strains. Acta Materialia. 2008;56:5451-65.
[462] Pippan R, Scheriau S, Taylor A, Hafok M, Hohenwarter A, Bachmaier A. Saturation of Fragmentation During Severe Plastic Deformation. Annual Review of Materials Research. 2010;40:319-43.
[463] Huang Y. Steady state and a general scale law of deformation. 1 ed: Institute of Physics Publishing; 2017.
[464] Bachmaier A, Pippan* R. Generation of metallic nanocomposites by severe plastic deformation. International Materials Reviews. 2013;58:41-62.
[465] Tomé C, Canova GR, Kocks UF, Christodoulou N, Jonas JJ. The relation between macroscopic and microscopic strain hardening in F.C.C. polycrystals. Acta Metallurgica. 1984;32:1637-53.
[466] Lee DJ, Kim HS. Finite element analysis for the geometry effect on strain inhomogeneity during high-pressure torsion. Journal of Materials Science. 2014;49:6620-8.
[467] Borodachenkova M, Wen W, Pereira AMdB. High-Pressure Torsion: Experiments and Modeling. In: Cabibbo M, editor. Severe Plastic Deformation Techniques. Rijeka: InTech; 2017. p. Ch. 04.
[468] Yoon SC, Seo MH, Krishnaiah A, Kim HS. Finite element analysis of rotary-die equal channel angular pressing. Materials Science and Engineering: A. 2008;490:289-92.
[469] Rosochowski A, Rodiet R, Lipinski P. Finite element simulation of cyclic extrusion-compression. In: M. Pietrzyk JK, and J. Majta, editor. Metal forming 2000 Krakow, Poland: A. A. Balkema, Rotterdam, Brookfield; 2000. p. 253–9
[470] Kim HS. Finite element analysis of high pressure torsion processing. Journal of Materials Processing Technology. 2001;113:617-21.
[471] Figueiredo RB, Pereira PHR, Aguilar MTP, Cetlin PR, Langdon TG. Using finite element modeling to examine the temperature distribution in quasi-constrained high-pressure torsion. Acta Materialia. 2012;60:3190-8.
[472] Figueiredo RB, Cetlin PR, Langdon TG. Using finite element modeling to examine the flow processes in quasi-constrained high-pressure torsion. Materials Science and Engineering A. 2011;528:8198-204.
[473] Estrin Y, Molotnikov A, Davies CHJ, Lapovok R. Strain gradient plasticity modelling of high-pressure torsion. Journal of the Mechanics and Physics of Solids. 2008;56:1186-202.

[474] Zhou W, Lin J, Dean TA, Wang L. Feasibility studies of a novel extrusion process for curved profiles: Experimentation and modelling. International Journal of Machine Tools and Manufacture. 2018;126:27-43.
[475] Pardis N, Ebrahimi R. Deformation behavior in Simple Shear Extrusion (SSE) as a new severe plastic deformation technique. Materials Science and Engineering: A. 2009;527:355-60.
[476] Bagherpour E, Ebrahimi R, Qods F. An analytical approach for simple shear extrusion process with a linear die profile. Materials & Design. 2015;83:368-76.
[477] Sheikh H, Ebrahimi R, Bagherpour E. Crystal plasticity finite element modeling of crystallographic textures in simple shear extrusion (SSE) process. Materials & Design. 2016;109:289-99.
[478] Mohebbi MS, Akbarzadeh A. Constitutive equation and FEM analysis of incremental cryo-rolling of UFG AA 1050 and AA 5052. Journal of Materials Processing Technology. 2018;255:35-46.
[479] List G, Sutter G, Bi XF, Molinari A, Bouthiche A. Strain, strain rate and velocity fields determination at very high cutting speed. Journal of Materials Processing Technology. 2013;213:693-9.
[480] Sevier M, Yang HTY, Lee S, Chandrasekar S. Severe plastic deformation by machining characterized by finite element simulation. Metallurgical and Materials Transactions B-Process Metallurgy and Materials Processing Science. 2007;38:927-38.
[481] Sevier M, Yang HTY, Moscoso W, Chandrasekar S. Analysis of severe plastic deformation by large strain extrusion machining. Metallurgical and Materials Transactions a-Physical Metallurgy and Materials Science. 2008;39A:2645-55.
[482] Lee JW, Park JJ. Numerical and experimental investigations of constrained groove pressing and rolling for grain refinement. Journal of Materials Processing Technology. 2002;130–131:208-13.
[483] Rosochowski A, Olejnik L. Incremental Equal Channel Angular Pressing for Grain Refinement. Materials Science Forum. 2011;674:19-28.
[484] Beygelzimer Y, Kulagin R, Estrin Y, Tóth LS, Kim HS, Latypov MI. Twist Extrusion as a Potent Tool for Obtaining Advanced Engineering Materials: A Review. Advanced Engineering Materials. 2017;19.

[485] Khoddam S, Farhoumand A, Hodgson PD. Upper-bound analysis of axi-symmetric forward spiral extrusion. Mechanics of Materials. 2011;43:684-92.
[486] Salehi Seyed M, Serajzadeh S. A new upper bound solution for the analysis of the twist extrusion process with an elliptical die cross-section. Proc Inst Mech Eng Part C J Mech Eng Sci. 2009;223:1975-81.
[487] Lapovok R, Pougis A, Lemiale V, Orlov D, Tóth L, Estrin Y. Severe plastic deformation processes for thin samples. Journal of Materials Science. 2010;45:4554-60.
[488] Lapovok R, Estrin Y, Djugum R, Lerk A. Severe plastic deformation processes with friction induced shear. 2011. p. 25-30.
[489] Lapovok R, Qi Y, Ng HP, Tóth LS, Estrin Y. Gradient Structures in Thin-Walled Metallic Tubes Produced by Continuous High Pressure Tube Shearing Process. Advanced Engineering Materials.1700345-n/a.
[490] Faraji G, Babaei A, Mashhadi MM, Abrinia K. Parallel tubular channel angular pressing (PTCAP) as a new severe plastic deformation method for cylindrical tubes. Materials Letters. 2012;77:82-5.
[491] Zangiabadi A, Kazeminezhad M. Development of a novel severe plastic deformation method for tubular materials: Tube Channel Pressing (TCP). Materials Science and Engineering: A. 2011;528:5066-72.
[492] Farshidi MH, Kazeminezhad M. The effects of die geometry in tube channel pressing: Severe plastic deformation. Proc Inst Mech Eng Part L J Mat Des Appl. 2016;230:263-72.
[493] Babaei A, Jafarzadeh H, Esmaeili F. Tube Twist Pressing (TTP) as a New Severe Plastic Deformation Method. Transactions of the Indian Institute of Metals. 2017.

[494] Bouaziz O, Estrin Y, Kim HS. A New Technique for Severe Plastic Deformation: The Cone–Cone Method. Advanced Engineering Materials. 2009;11:982-5.
[495] Joo S-H, Kim H. Comparison of deformation and microstructural evolution between equal channel angular pressing and forward extrusion using the dislocation cell mechanism-based finite element method. J Mater Sci. 2010;45:4705-10.
[496] Baik SC, Hellmig RJ, Estrin Y, Kim HS. Modeling of deformation behavior of copper under equal channel angular pressing. Zeitschrift Fur Metallkunde. 2003;94:754-60.
[497] Molinari A, Tóth LS. Tuning a self consistent viscoplastic model by finite element results—I. Modeling. Acta Metallurgica et Materialia. 1994;42:2453-8.
[498] Hosseini E, Kazeminezhad M. The effect of ECAP die shape on nano-structure of materials. Computational Materials Science. 2009;44:962-7.
[499] Hosseini E, Kazeminezhad M. A hybrid model on severe plastic deformation of copper. Computational Materials Science. 2009;44:1107-15.
[500] Hosseini E, Kazeminezhad M. Implementation of a constitutive model in finite element method for intense deformation. Materials & Design. 2011;32:487-94.
[501] Hosseini E, Kazeminezhad M, Mani A, Rafizadeh E. On the evolution of flow stress during constrained groove pressing of pure copper sheet. Computational Materials Science. 2009;45:855-9.
[502] Kazeminezhad M, Hosseini E. Coupling kinetic dislocation model and Monte Carlo algorithm for recrystallized microstructure modeling of severely deformed copper. Journal of Materials Science. 2008;43:6081-6.
[503] Beyerlein IJ, Lebensohn RA, Tomé CN. Modeling texture and microstructural evolution in the equal channel angular extrusion process. Materials Science and Engineering A. 2003;345:122-38.
[504] Roters F, Raabe D, Gottstein G. Work hardening in heterogeneous alloys—a microstructural approach based on three internal state variables. Acta Materialia. 2000;48:4181-9.
[505] Shanthraj P, Zikry MA. Dislocation density evolution and interactions in crystalline materials. Acta Materialia. 2011;59:7695-702.
[506] Rezvanian O, Zikry MA, Rajendran AM. Microstructural modeling of grain subdivision and large strain inhomogeneous deformation modes in f.c.c. crystalline materials. Mechanics of Materials. 2006;38:1159-69.
[507] Nix W, Gibeling J, Hughes D. Time-dependent deformation of metals. Metall and Mat Trans A. 1985;16:2215-26.
[508] Zangiabadi A, Kazeminezhad M. Computation on new deformation routes of tube channel pressing considering back pressure and friction effects. Computational Materials Science. 2012;59:174-81.
[509] Tóth LS, Arzaghi M, Fundenberger JJ, Beausir B, Bouaziz O, Arruffat-Massion R. Severe plastic deformation of metals by high-pressure tube twisting. Scripta Materialia. 2009;60:175-7.
[510] QForm. Software for Metal Forming Simulation.
[511] Latypov MI, Alexandrov IV, Beygelzimer YE, Lee S, Kim HS. Finite element analysis of plastic deformation in twist extrusion. Computational Materials Science. 2012;60:194-200.
[512] Latypov MI, Lee M-G, Beygelzimer Y, Kulagin R, Kim HS. Simple shear model of twist extrusion and its deviations. Metals and Materials International. 2015;21:569-79.
[513] Beygelzimer Y, Kulagin R, Latypov MI, Varyukhin V, Kim HS. Off-axis twist extrusion for uniform processing of round bars. Metals and Materials International. 2015;21:734-40.
[514] Chen C, Beygelzimer Y, Toth LS, Estrin Y, Kulagin R. Tensile Yield Strength of a Material Preprocessed by Simple Shear. Journal of Engineering Materials and Technology. 2016;138:031010--4.
[515] Rosochowska M, Rosochowski A, Olejnik L. FE simulation of micro-extrusion of a conical pin. International Journal of Material Forming. 2010;3:423-6.
[516] Kim HS, Nam JS. Quantitative modeling and characterization of the size effects in microscale coining process of copper. Precision Engineering. 2018;51:490-8.

[517] Molotnikov A, Lapovok R, Gu CF, Davies CHJ, Estrin Y. Size effects in micro cup drawing. Materials Science and Engineering: A. 2012;550:312-9.
[518] Estrin Y, Kim HS, Kovler M, Berler G, Shaviv R, Rabkin E. Modeling of aluminum via filling by forcefill. Journal of Applied Physics. 2003;93:5812-5.
[519] McQueen HJ, Yue S, Ryan ND, Fry E. Hot working characteristics of steels in austenitic state. Journal of Materials Processing Technology. 1995;53:293-310.
[520] Huang C, Hawbolt EB, Chen X, Meadowcroft TR, Matlock DK. Flow stress modeling and warm rolling simulation behavior of two Ti–Nb interstitial-free steels in the ferrite region. Acta Materialia. 2001;49:1445-52.
[521] Shih MH, Yu CY, Kao PW, Chang CP. Microstructure and flow stress of copper deformed to large plastic strains. Scripta Materialia. 2001;45:793-9.
[522] Li YJ, Valiev R, Blum W. Deformation kinetics of ultrafine-grained Cu and Ti. Materials Science and Engineering: A. 2005;410–411:451-6.
[523] Mazilkin AA, Straumal BB, Rabkin E, Baretzky B, Enders S, Protasova SG, et al. Softening of nanostructured Al-Zn and Al-Mg alloys after severe plastic deformation. Acta Materialia. 2006;54:3933-9.
[524] Estrin Y, Mecking H. A Unified Constitutive Model with Dislocation Densities as Internal Variables. In: Boehler J-P, Khan A, editors. Anisotropy and Localization of Plastic Deformation: Springer Netherlands; 1991. p. 385-8.
[525] Estrin Y. 2 - Dislocation-Density-Related Constitutive Modeling. In: Krausz AS, Krausz K, editors. Unified Constitutive Laws of Plastic Deformation. San Diego: Academic Press; 1996. p. 69-106.
[526] Kong LX, Hodgson PD, Wang B. Development of constitutive models for metal forming with cyclic strain softening. Journal of Materials Processing Technology. 1999;89-90:44-50.
[527] Oudin A, Hodgson PD, Barnett MR. EBSD analysis of a Ti-IF steel subjected to hot torsion in the ferritic region. Materials Science and Engineering: A. 2008;486:72-9.
[528] Porter DA, Easterling KE, Sherif MY. Phase transformations in metals and alloys. 3rd ed. Boca Raton, FL: CRC Press; 2009.
[529] Sakai T, Belyakov A, Kaibyshev R, Miura H, Jonas JJ. Dynamic and post-dynamic recrystallization under hot, cold and severe plastic deformation conditions. Progress in Materials Science. 2014;60:130-207.
[530] Galindo-Nava EI, Rivera-Díaz-del-Castillo PEJ. Grain size evolution during discontinuous dynamic recrystallization. Scripta Materialia. 2014;72:1-4.
[531] Sakai T, Jonas JJ. Overview no. 35 Dynamic recrystallization: Mechanical and microstructural considerations. Acta Metallurgica. 1984;32:189-209.
[532] Kaibyshev OA, Kaibyshev R, Salishchev G. Formation of Submicrocrystalline Structure in Materials during Dynamic Recrystallization. Materials Science Forum. 1993;113-115:423-8.
[533] Murr LE, Pizana C. Dynamic recrystallization: The dynamic deformation regime. 4th Symposium on the Dynamic Behavior of Materials held at the 2007 TMS Annual Meeting and Exhibition. Orlando, FL: Minerals Metals Materials Soc; 2007. p. 2611-28.
[534] Hallberg H, Wallin M, Ristinmaa M. Modeling of continuous dynamic recrystallization in commercial-purity aluminum. Materials Science and Engineering: A. 2010;527:1126-34.
[535] Le KC, Kochmann DM. A simple model for dynamic recrystallization during severe plastic deformation. Archive of Applied Mechanics. 2008;79:579.
[536] Kim HS, Estrin Y, Bush MB. Plastic deformation behaviour of fine-grained materials. Acta Materialia. 2000;48:493-504.
[537] Kim HS, Estrin Y, Bush MB. Constitutive modelling of strength and plasticity of nanocrystalline metallic materials. Materials Science and Engineering: A. 2001;316:195-9.

[538] Mercier S, Molinari A, Estrin Y. Grain size dependence of strength of nanocrystalline materials as exemplified by copper: an elastic-viscoplastic modelling approach. Journal of Materials Science. 2007;42:1455-65.
[539] Kim HS, Estrin Y. Strength and strain hardening of nanocrystalline materials. Materials Science and Engineering: A. 2008;483:127-30.
[540] Mukherjee AK. An examination of the constitutive equation for elevated temperature plasticity. Materials Science and Engineering: A. 2002;322:1-22.
[541] Langdon TG. An analysis of flow mechanisms in high temperature creep and superplasticity. Materials Transactions. 2005;46:1951-6.
[542] Yamakov V, Wolf D, Phillpot SR, Gleiter H. Grain-boundary diffusion creep in nanocrystalline palladium by molecular-dynamics simulation. Acta Materialia. 2002;50:61-73.
[543] Klusemann B, Bargmann S, Y. E. Fourth-order strain-gradient phase mixture model for nanocrystalline fcc materials. Modelling and Simulation in Materials Science and Engineering. 2016;24:085016.
[544] Sanders PG, Eastman JA, Weertman JR. Elastic and tensile behavior of nanocrystalline copper and palladium. Acta Materialia. 1997;45:4019-25.
[545] Wu XL, Jiang P, Chen L, Zhang JF, Yuan FP, Zhu YT. Synergetic Strengthening by Gradient Structure. Materials Research Letters. 2014;2:185-91.
[546] Zhilyaev AP, Langdon TG. Using high-pressure torsion for metal processing: Fundamentals and applications. Progress in Materials Science. 2008;53:893-979.
[547] Zhilyaev AP, Oh-ishi K, Langdon TG, McNelley TR. Microstructural evolution in commercial purity aluminum during high-pressure torsion. Materials Science and Engineering A. 2005;410:277-80.
[548] Bouaziz O, Kim HS, Estrin Y. Architecturing of Metal-Based Composites with Concurrent Nanostructuring: A New Paradigm of Materials Design. Advanced Engineering Materials. 2013;15:336-40.
[549] Raabe D, Choi, P.-P., .Li, Y., Kostka, A., Sauvage, X., Lecouturier, F., Hono, K., Kirchheim, R., Pippan, R. Embury, D. Metallic composites processed via extreme deformation: Toward the limits of strength in bulk materials. MRS Bulletin. 2010;35:982-91.
[550] Beygelzimer Y, Estrin Y, Kulagin R. Synthesis of Hybrid Materials by Severe Plastic Deformation: A New Paradigm of SPD Processing. Advanced Engineering Materials. 2015;17:1853-61.
[551] Beygelzimer Y, Kulagin R, Estrin Y. Severe Plastic Deformation as a Way to Produce Architectured Materials. In: Estrin Y, Dunlop J, Brechet Y, Fratzl P, Dendievel R, editors. Architectured Materials: Springer 2018.
[552] Bouaziz O. Geometrically induced strain hardening. Scripta Materialia. 2013;68:28-30.
[553] Khoddam S, Estrin Y, Kim HS, Bouaziz O. Torsional and compressive behaviours of a hybrid material: Spiral fibre reinforced metal matrix composite. Materials & Design. 2015;85:404-11.
[554] Latypov MI, Beygelzimer Y, Kulagin R, Varyukhin V, Kim HS. Toward architecturing of metal composites by twist extrusion. Materials Research Letters. 2015;3:161-8.
[555] Diez M, Kim H-E, Serebryany V, Dobatkin S, Estrin Y. Improving the mechanical properties of pure magnesium by three-roll planetary milling. Materials Science and Engineering: A. 2014;612:287-92.
[556] Ivanisenko Y, Kulagin R, Fedorov V, Mazilkin A, Scherer T, Baretzky B, et al. High Pressure Torsion Extrusion as a new severe plastic deformation process. Materials Science and Engineering: A. 2016;664:247-56.
[557] Gu CF, Tóth LS, Lapovok R, Davies CHJ. Texture evolution and grain refinement of ultrafine-grained copper during micro-extrusion. Philosophical Magazine. 2011;91:263-80.
[558] Lebensohn RA, Tomé CN. A Self-Consistent Anisotropic Approach for the Simulation of Plastic-Deformation and Texture Development of Polycrystals - Application to Zirconium Alloys. Acta Metallurgica Et Materialia. 1993;41:2611-24.

[559] Ayoub G, Rodrigez AK, Shehadeh M, Kridlia G, Young JP, Zbib H. Modeling the rate and temperature dependent behavior and texture evolution of the Mg AZ31B alloy TRC sheets. Philosophical Magazine. (in press).
[560] Tóth LS, Molinari A. Tuning a self consistent viscoplastic model by finite element results—II. Application to torsion textures. Acta Metallurgica et Materialia. 1994;42:2459-66.
[561] Skrotzki W, Scheerbaum N, Oertel CG, Arruffat-Massion R, Suwas S, Toth LS. Microstructure and texture gradient in copper deformed by equal channel angular pressing. Acta Materialia. 2007;55:2013-24.
[562] Horstemeyer MF, Potirniche GP, Marin EB. Crystal Plasticity. In: Yip S, editor. Handbook of Materials Modeling: Springer Netherlands; 2005. p. 1133-49.
[563] Lebensohn RA, Tomй CN. A self-consistent anisotropic approach for the simulation of plastic deformation and texture development of polycrystals: Application to zirconium alloys. Acta Metallurgica et Materialia. 1993;41:2611-24.